Investigating the Effect of Salts and Small Molecule on Dissociation and Association Kinetics of the DNA Processivity Clamps using Fluorescence Techniques

by

Anirban Purohit

A Thesis Presented in Partial Fulfillment
of the Requirements for the Degree
Doctor of Philosophy

Approved May 2020 by the
Graduate Supervisory Committee:

Marcia Levitus, Chair
Wade Van Horn
Yan Liu

ARIZONA STATE UNIVERSITY

August 2020

ABSTRACT

In this study, the stability of two protein homo-oligomers, the β clamp (homodimer) from *E. coli* and the Proliferation Cell Nuclear Antigen (PCNA) from the yeast cell, were characterized. These clamps open through one interface by another protein called clamp loader, which helps it to encircle the DNA template strand. The β clamp protein binds with DNA polymerase and helps it to slide through the template strand and prevents its dissociation from the template strand. The questions need to be to answered in this research are, whether subunit stoichiometry contributes to the stability of the clamp proteins and how does the clamp loader open up the clamp, does it have to exert force on the clamp or does it take advantage of the dynamic behavior of the interface?

The x-ray crystallography structure of the β clamp suggests that there are oppositely charged amino acid pairs present at the interface of the dimer. They can form strong electrostatic interactions between them. However, for Proliferation Cell Nuclear Antigen (PCNA), there are no such charged amino acids present at its interface. High sodium chloride (NaCl) concentrations were used to disrupt the electrostatic interactions at the interface. The role of charged pairs in the clamp interface was characterized by measuring the apparent diffusion times (τ_{app}) with fluorescence correlation spectroscopy (FCS). However, the dissociation of the Proliferation Cell Nuclear Antigen (PCNA) trimer does not depend on sodium chloride (NaCl) concentration.

In the next part of my thesis, potassium glutamate (KGlu) and glycine betaine (GB) were used to investigate their effect on the stability of both clamp proteins. FCS experiments with labeled β clamp and Proliferation Cell Nuclear Antigen (PCNA) were performed containing different concentrations of potassium glutamate and glycine betaine in the

solution, showed that the apparent diffusion time (τ_{app}) increases with potassium glutamate and glycine betaine concentrations, which indicate clamps are forming higher-order oligomers. Solute molecules get excluded from the protein surface when the binding affinity of the protein surface for water molecules is more than solutes (potassium glutamate, and glycine betaine), which has a net stabilizing effect on the protein structure.

DEDICATION

To my parents, for their endless love, support and encouragement

ACKNOWLEDGMENTS

I would like to thank my parents and my elder brother for their continuous support throughout my life.

I would like to thank my wife, Arpita, as she has always stood by me through my bad and good days and helped me to make the correct decisions.

I would like to thank my advisor Prof. Marcia Levitus for allowing me to research in her laboratory and her continuous guidance and mentoring throughout my Ph.D. program.

I would like to say thanks to the past and present lab members: Dr. Jennifer Binder, Dr. Elana Stennet, Dr. Monika Ciuba, Dr. Andrew Serban, Dr. Bryan Donaphon, Nikita Kumari and Kaitlyn Parrott for being helpful.

I would like to thank our collaborator Dr.Linda Bloom, at the University of Florida for providing protein samples to us.

I would like to say thanks to my committee members Dr. Yan Liu and Dr. Wade Van Horn, for their valuable advice on my research.

TABLE OF CONTENTS

Page

CHAPTER Page

CHAPTER Page

CHAPTER Page

LIST OF TABLES

LIST OF FIGURES

Figure Page

PREFACE

This dissertation will cover the research projects I've done in the last six years under the guidance of Prof. Marcia Levitus at Arizona State University. In chapter one, The significance of DNA processivity clamps in biochemical pathways both in *E. coli* and yeast cells is discussed. The crystallographic structures of two clamp proteins, homodimeric β clamp from *E. coli* and homotrimeric PCNA from yeast cell are explained in details. We explored the interface interactions with fluorescently labeled protein samples prepared in Dr. Bloom's lab at the University of Florida. I discussed this in detail in the experimental strategy section in chapter one.

Chapter two will be on the techniques we used in this project. We mostly used two techniques, including time-correlated single-photon counting and fluorescence correlation spectroscopy (FCS), in this project, and we designed our experiments accordingly. I described the principle of the time-correlated single-photon counting technique and how we used this technique in our project. We have a home-built FCS set up in our lab. I also discussed the components of the FCS setup and the alignment check of the instrument in this chapter.

In chapter two, I explained the FCS data analysis using a mathematical treatment developed by Dr. Levitus and David Kanno. I discussed how we calculated equilibrium dissociation constant (K_d) and kinetic rate constants (k_d, k_a) for dimer-monomer equilibrium kinetics.

We designed a few FCS experiments to assess the stability of β-dimer mutants in solution disrupting the interface stability, with titrating in NaCl or changing the pH of the borate buffer solution from 7 to 10. Three different clamp protein samples were synthesized by mutating out a hydrophilic residue (Ser-109), hydrophobic residue (Ile-305), or charged

residue (Arg-103) with Cys residue and labeled with TMR (tetramethyl rhodamine). Each protein sample contains a single fluorophore in each β-monomer. These data can be found in chapter three. NaCl was chosen because it does not show any stabilizing or destabilizing effect on a protein structure. However, it only minimizes electrostatic interactions between oppositely charged amino acids. We observed that Arg103 plays a vital role in maintaining the stability of the clamp protein. The supplemental section of this thesis covers the supplemental information from the research work discussed in chapter three.

In chapter four, I've discussed my current research work, where we investigated the salt specific effect of potassium glutamate (KGlu) and glycine betaine (GB) on the clamp stability. KGlu is the most abundant metabolite present in *E. coli* cytoplasm. GB is a zwitterionic compound that acts as an osmoprotectant. When *E. coli* cells are allowed to grow in the high extracellular solutes, GB concentration increases in the cell. We observed that in the presence of KGlu and GB, both β clamp and PCNA from clamp assembly instead of dissociating into monomers. The size of the clamp assembly increases when we increase protein concentration. We used the FCS technique to investigate this clamp assembly formation by measuring apparent diffusion times (τ_{app}). The biological relevance of this phenomenon is still not clear. However, we speculated a few scenarios by correlating our experimental data with the information available in the literature.

The future directions of this research are explained in chapter five.

CHAPTER 1

INTRODUCTION

1.1 Biological importance of β clamp and PCNA

Sliding clamps encircle DNA and tether DNA polymerase III enzyme to the template strand, which enhances the processivity of nucleotide polymerization. The core polymerase requires the processivity clamp to glide through the template DNA strand. Only the catalytic core of the DNA polymerase enzyme III gives replication rate 20 nucleotides/s, whereas, with the clamp, the replication rate goes up to 750 nucleotides/s[1]. The sliding clamp also plays an essential role in DNA metabolism and maturation of Okazaki fragment. In our study, we characterized two DNA processivity clamps. The first, *E. coli* sliding clamp which is a homodimer that consists of six globular domains. The second, PCNA, comes from yeast and is a homotrimer.

1.2 Crystallographic Structures of β clamp and PCNA

The available crystal structures of β clamp have 2.5 Å and 1.8 Å resolutions[2]. It is composed of two monomers in a head to tail arrangement forming two interfaces. Each monomer contains three domains with similar tertiary structures. In each domain, the outer layer of the clamp is composed of two four-stranded antiparallel β sheets. These β sheets provide the scaffold to support the other two α helices present in the inner layer. There is a hydrophobic cleft located between domain II and domain III of β clamp, which interacts with DNA polymerase III. The outer diameter of the ring is ~ 80 Å, and the inner diameter is ~ 35 Å, as depicted in Figure 1.1**.**

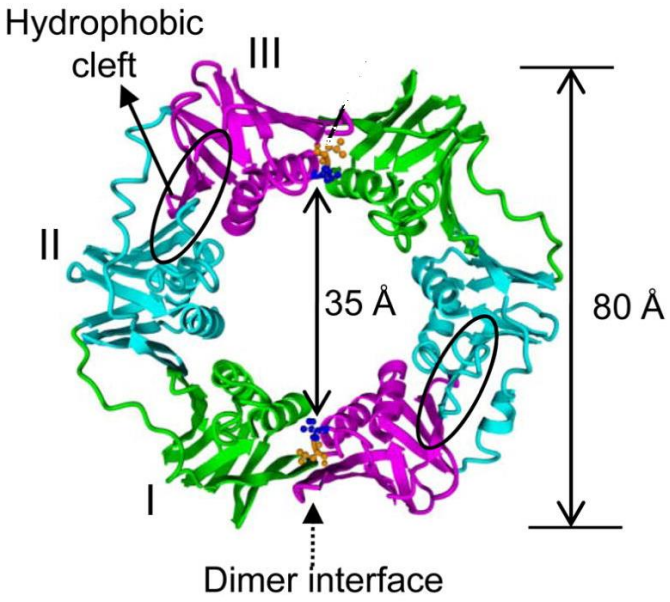

Figure 1.1 X-ray crystallography structure of the β clamp[2] (PDB: 1MMI). It is a homodimer. Each monomer contains three domains (cyan, green and magenta), and a hydrophobic cleft is present between domain II and domain III, which acts as a binding site for DNA polymerase.

It can comfortably accommodate double-stranded DNA. In the previous study by Fang et al., they had shown domain I is more dynamic compared to other domains. The dimer interface of the β clamp may open spontaneously as domain I dissociate from domain III. Another study had shown that β clamp forms a stable complex with DNA with a lifetime[3] of ~100 - 170 mins at 37 ºC, and dissociation of 1 nM clamp dimer in solution takes 48 h. These observations support the fact that the amino acid interactions at the interface of the dimer play a significant role in dimer stability.

On the other hand, the crystal structure of PCNA was determined by Kong et al. in 1992. It has a similar structure as a β clamp, but it has three monomers in it. The inner diameter of PCNA is ~34 Å, which is sufficient to accommodate B type DNA. The trimeric ring of

PCNA has six-fold symmetry as each domain contains two α helices, and they are supported by a continuous layer of nine β sheets from outside, as Figure 1.2.

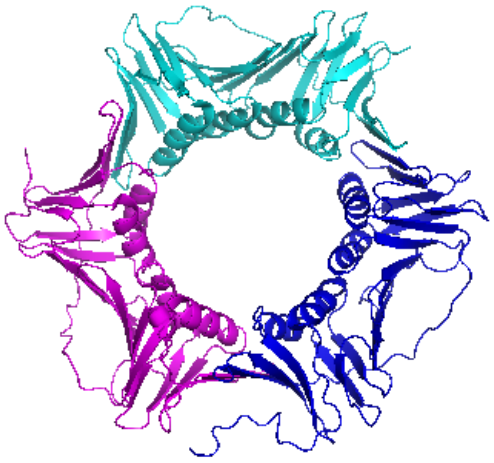

Figure 1.2 X-ray crystallography structure of PCNA. It is a homotrimer (Cyan, Magenta, and blue). The middle part of the ring has enough space to accommodate a DNA template strand. (PDB: 3JA9)

1.3 β clamp enhances processivity of DNA replication in E. coli

The charge distribution on the ring is asymmetric. There is a strong negative electrostatic potential in the outer surface and a net positive electrostatic potential in the central cavity. The negative charge on the surface may prevent nonspecific interaction with DNA. During DNA replication, a clamp loader helps clamp to load on to the DNA template strand, and when the process is over, it unloads the clamp from DNA. The clamp in the closed conformation is highly stable; hence, the role of the clamp loader is to stabilize the open conformation of the ring to allow loading on to the template strand. The mechanism of opening the clamp through one interface by clamp loader has been studied extensively[4]. The clamp loader is a member of the AAA+ family of ATPase enzymes, which utilizes ATP binding and hydrolysis to carry out a biochemical process. It consists of seven subunits (three γ subunit and one copy each of δ, δ', χ and ψ)[4]. ATP binding by clamp

loader drives a conformational change in clamp loader, which helps in opening clamp through one interface. DNA binding triggers ATP hydrolysis and lets the clamp released from the clamp-DNA complex. The schematic diagram[5] of this biochemical process explained in Figure 1.3. It has been concluded from the pre-steady-state kinetic experiment that clamp binding occurs before clamp opening, which indicates that clamp loader doesn't bind the open conformation; instead, it opens the clamp. Therefore, the clamp interface must be destabilized by the clamp loader to carry out this whole process.

1.4 PCNA enhances the processivity of DNA replication in Yeast/Human cell

On the other hand, for eukaryotic cells, PCNA, a homotrimeric ring-shaped protein, plays a significant role in DNA replication, repair, and chromatin assembly[6,7,8]. When PCNA binds with DNA, the positively charged central cavity stabilizes the PCNA-DNA complex. The lifetime of the PCNA-DNA complex is determined at approximately 35 minutes[9]. Hence, loading and unloading of PCNA on the DNA template strand require higher precision. RFC (replication factor C), a pentameric protein, acts as a clamp loader in the loading and unloading process[10,11,12]. Experimental results suggest that spiral-shaped RFC complex assembles in the presence of ATP help to open the trimeric ring through one interface to accommodate the template DNA strand. Upon DNA binding, opened PCNA ring twists and closes after ATP hydrolysis, followed by dissociation of RFC[13,14]. Once the replication process is over, PCNA needs to be released, PCNA needs to be released from the DNA strand to avoid recruitment of inappropriate replication enzymes. It is still not clear which subunit of RFC helps to unload PCNA from the DNA strand[15-17]. Another study showed that PCNA unloading is mediated by ATAD5-RLC (RFC like complexes) in human cells[18]. It is reported that the depletion of ATAD5 triggers the accumulation of

PCNA on the DNA strand showing its importance in PCNA unloading. These findings imply the functional importance of ATAD5-RLC[19,20]. However, there have been no studies to prove ATAD5-RLC is involved in a biochemical process to release PCNA from the DNA strand. It has also been reported that the ligation of Okazaki fragments is required for PCNA unloading from replicated chromatin in a yeast cells[21,22]. Premature unloading of PNA should be inhibited to prevent obstruction in DNA replication. It is found in-vitro that a protein called Fen1 inhibits PCNA unloading with the help of another protein called Elg1-RLC through its binding to PCNA. It is reported that Fen1-PCNA interactions are likely to hinder the access of ATAD5-RLC to PCNA[23,24]. This helps to maintain the balance of the PCNA loading-unloading process.

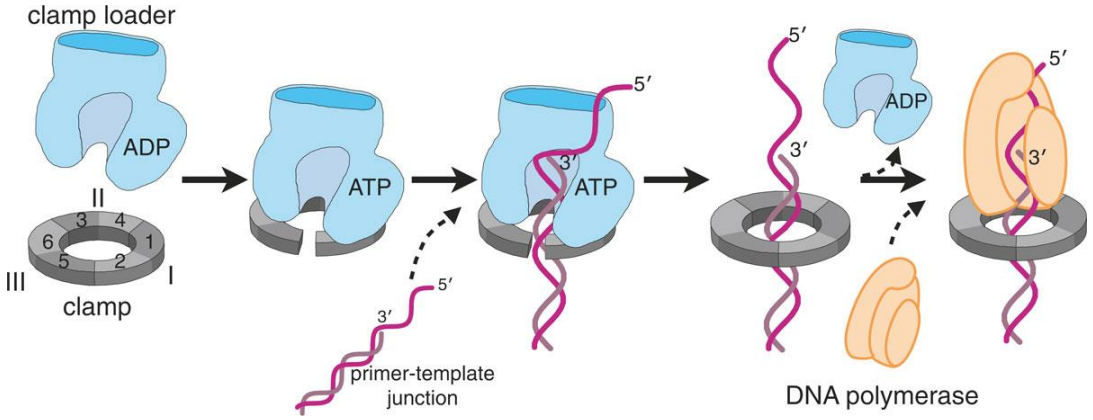

Figure 1.3 The clamp loader opens up the clamp through one interface in the presence of ATP. The clamp loader dissociates from the clamp after ATP hydrolysis and helps it to encircle the double-stranded DNA. The clamp protein increases the processivity of DNA polymerase. (from **ref 4**)

1.5 Clamp stability

The previous studies[2] predicted from hydrogen-exchange mass spectrometry that *E. coli* β clamp has a highly dynamic interface. However, no study was conducted to conclude that these interfaces are dynamic in solution, and fluctuations in the interface would play an important role in clamp opening. The clamp loader might be taking advantage of the

dynamic nature of the clamp interface to open it up during DNA replication. In this work, the primary focus is to characterize the factors which would destabilize the interface of the clamp. Solution stability and intrinsic stability of these two proteins were previously studied by Dr. Binder from our lab[25]. Solution stability is dictated by the dissociation constants of these clamps, which is an equilibrium measurement that depends on the concentrations of the species in solution. On the other hand, the intrinsic stability is related to the lifetime of the closed ring, which is given by the inverse of the dissociation rate constant, a kinetic parameter. These two are related, but they are different. It is established from Dr. Binder's study that β clamp is more stable than PCNA in low salt concentration. The solution stabilities for these two clamps differ by three orders of magnitude, but we attribute that difference to the association rate constants, which are very different. This is reasonable because a dimeric clamp needs to bring together two components, whereas the trimeric clamp needs to bring together three. However, the stabilities of these clamps would only be 1/3 different, because PCNA can dissociate through interfaces in 3 possible ways, and instead, we see one order of magnitude difference in lifetimes[25]. Hence, we argue that a better way to compare the stabilities of these clamps is to compare the lifetimes of the closed rings or the intrinsic stabilities, which differ by only one order of magnitude. We also argue that there must be some differences between the interfaces of these two clamps. However, we predicted from the crystallography structure of the β clamp that three pairs of charged amino acids (Arg103-Glu304, Arg105-Glu303, and Lys74-Glu301) might be forming salt bridge interactions at the dimer interface which are absent in case of PCNA. Dr. Binder showed that at high NaCl concentration, clamp dimer dissociates into monomers, which also indicates that charged amino acids are playing an essential role in

dimer stabilization. To determine what factors contribute to the stability of the dimer interfaces in closed conformation of the clamp and how interface dynamics contribute to the formation of open conformation, we used high NaCl to destabilize the dimer and characterized the role of electrostatic interactions in stabilizing the clamp interface. The equilibrium dissociation constant of the dimer changes with NaCl concentration. It was observed that mutation of a charged amino acid at the interface (Arg 103) weakens the interface significantly, whereas effects are negligible when a hydrophilic (Ser 109) or a hydrophobic (Ile 305) were mutated out. For this study, we used labeled protein samples received from our collaborator at the University of Florida. To express mutated and labeled protein samples, they knocked out desired amino acid residues and incorporate cysteine residues by using site-directed mutagenesis. This is a standard biochemical procedure to prepare genetically modified protein samples[26]. It is easier to label cysteine residue with Tetramethylrhodamine (TMR-maleimide) dye molecule because Cys has a reactive thiol group in its structure. However, to avoid undesired labeling, the native Cys residues were knocked out at first. It is known from the crystal structure of the clamp that native Cys333 and Cys260 are susceptible to undesired labeling. Hence, these two amino acid residues were mutated out with serine. Although there are other native Cys residues present in the clamp protein, they are inside in bulk and not prone to undesired tagging. Since the structure of Cysteine and Serine are quite similar except Cys has a thiol group, whereas serine has a hydroxyl group, it did not cause any significant change in the protein's structure and function. TMR was selected for labeling because the excitation wavelength for this dye is between 540 - 550 nm, and the laser source we have in our lab is a green laser of the wavelength of 532 nm. The molecular weight of TMR-maleimide dye is 482 Dalton, and

the maleimide group can form a covalent bond with the thiol group of a cysteine residue. The protein samples are labeled differently. One is singly labeled, which means one TMR dye at each interface. Singly labeled samples are fluorescent. We monitored the clamp dissociation and association through a subunit exchange experiment by taking advantage of the change in fluorescence intensity from H-dimer(non-fluorescent) to single labeled protein (fluorescent).

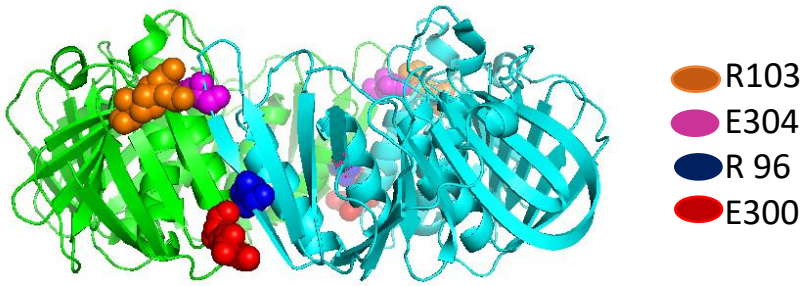

Figure 1.4 The oppositely charged amino acids are present at the interface of the dimer. Arginine is a positively charged amino acid, and glutamate is a negatively charged amino acid. These charged amino acids form strong electrostatic interactions in the dimer interface.

1.6 H dimer

On the other hand, doubly labeled samples have two TMR dye molecules at each interface, forming an H dimer. These doubly labeled samples are non-fluorescent. According to exciton theory, when the transition dipole moments of two fluorophores come parallel to each other, they quench their fluorescence. It has been studied that TMR can form an H dimer even at very low concentrations. When two TMR dye molecules form an H dimer, we see a significant change in the excitation spectrum. Although free TMR dye shows

maximum intensity around 550 nm and there is a shoulder peak at 520 nm when it forms an H dimer, the intensity of 520 nm goes higher than that of 550 nm.

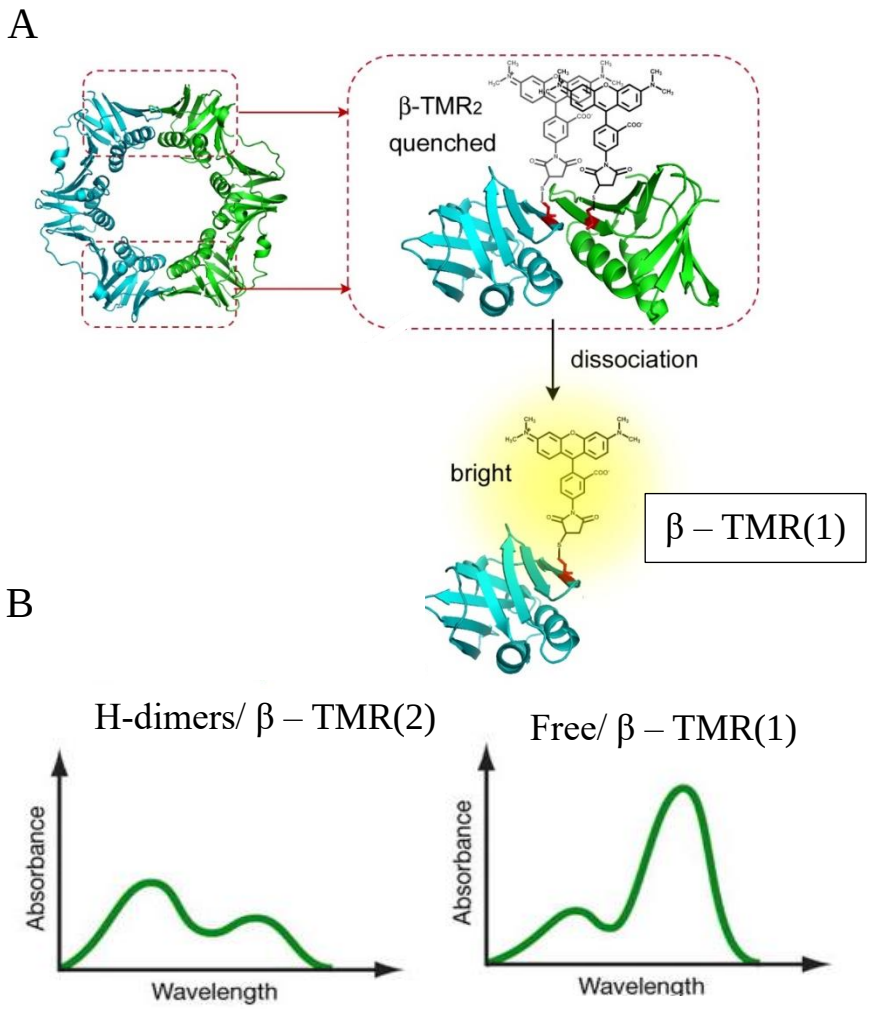

Figure 1.5 A. H-dimer formation with two TMR dye molecules (image made by Dr.Levitus) B. Excitation spectra for H-dimer/ β -TMR(2) and Single labeled β -TMR(1) (from **ref 70**)

1.7 Experimental strategy

We used time-resolved single-photon counting (TCSPC) to measure the kinetic rate of dissociation (k_d) of dimer into monomer in different NaCl concentrations and different pH as well. When the pH is higher than the isoelectric point, Arginine will be deprotonated, which would lead to disrupting the electrostatic interactions. However, in another study by Dr. Binder showed that mutation at positively charged Arg residue nor high NaCl concentrations neither facilitates the formation of an open clamp loader-clamp complex. In their research, they proposed a "bind-open-lock' model[25] in which the clamp loader binds a closed clamp and opens it up through an interface. After that, subsequent conformational rearrangements helps to stabilize the clamp loader-clamp complex. Their study supports a model in which the clamp loader actively opens up the clamp. We used fluorescence correlation spectroscopy to determine the diffusion rates of monomers and dimers present in the equilibrium in a wide range of NaCl concentrations. Initially, NaCl was chosen because it is neither a chaotropic nor a kosmotropic salt[27], and it lies in the middle of the Hofmeister series. Hence, it minimizes ion effects other than electrostatic screening. The Hofmeister series originates from the ranking of various ions toward their ability to salt in or salt out of proteins. Ions that have the greatest effect in exhibiting weaker interactions with water than water itself are known as structure-breakers or chaotropic, whereas ions having the opposite effect are known as structure-makers or kosmotropes (exhibiting strong interactions with water molecules). Strongly hydrated ions considerably increase the difference between the hydrogen bond donating and accepting capacity of the linked water molecules resulting in the breakdown of the tetrahedral network. Anions hydrate more strongly than cations for the same ionic radius as water hydrogen atoms can approach

(about 0.8 Å) more closely than the water oxygen atoms (but note that most anions are larger than most cations), giving rise to greater electrostatic potential. Also, anions are far more polarizable than cations due to their more diffuse extra electron(s). Anions are also thought more likely to promote the salting-out of amphiphiles. Although we put forward the surface charge density as being the important determinant of Hofmeister's effects, others state it is the polarizability that is important. The protein sample Dr. Binder used for her study was labeled at Cys, which was incorporated by knocking out Arg103. However, later, we thought instead of labeling at Arg103, we should choose another nearby amino residue for labeling. It would help us in monitoring the effect of Arg 103 mutation without labeling the protein at the same position. Hence, Ser109 and Gln299 were found at appropriate positions for labeling from the crystallography structure of the β clamp. These two amino acid residues juxtapose each other at the dimer interface. They were mutated out with Cys and covalently labeled with two TMR dye molecules that form an H dimer. We used two doubly labeled samples for the subunit exchange study. One is S109C/Q299C-$(TMR)_2$, and the other one is S109C/Q299C/R103S-$(TMR)_2$. Positions of these amino acids are shown in Figure 3.1. It is revealed from the subunit exchange study, the protein sample lacking Arg103 is less stable in low salt concentration (50mM NaCl) compared to other mutants, which contains Arg103. FCS measurements were done with a single labeled I305 mutant in a wide range of NaCl concentrations, and we observed a linear increase in the logarithm of the equilibrium dissociation constant with the square root of the NaCl concentration. We found similar results with KCl, as well. These results are consistent with the Debye-Hückel limiting law that describes the effect of ionic strength on electrostatic forces.

1.8 Hofmeister salt effect

The effect of Hofmeister salts on proteins arises from the net accumulation and exclusion of the ions of the salt from the solvent accessible surface area. Solutes that interact favorably with the protein surface are protein destabilizers. On the other hand, solutes which interact unfavorably with the surface of the protein surface is known as protein stabilizers. We were advised by one of the reviewers from our previous publication that beside NaCl, it would be interesting to study the effect of other salts such as potassium glutamate (KGlu) on clamp proteins. KGlu is the most abundant cytoplasmic metabolite. During osmotic upshift, KGlu concentration increases (up to 0.3 M) initially due to water efflux and later with K^+ transport and Glu^- synthesis[28]. Accumulation of KGlu, along with other solutes, allows water influx and resume cell growth[29,30]. In the presence of proline and glycine betaine rate of water uptake, increases even more, which reflects in rapid cell growth[31-33]. This is the reason these solutes are called osmoprotectants. In vitro, it is also reported that KGlu acts as a potent protein stabilizer because of its unfavorable interactions with hydrocarbons and amide oxygen groups[34]. It suggests that KGlu has some biological relevance in *E. coli*. In Hofmeister series, KGlu lies between KF and K_2SO_4 in driving protein folding and assembly. Hence, we decided to investigate the effect of KGlu on the clamp proteins.

However, when we did FCS experiments in KGlu with 1 nM labeled protein, we observed an increase in diffusion time (τ_D) at high KGlu concentrations, which suggests the formation of the clamp assembly. This effect of KGlu and glycine betaine on protein oligomerization has been explained in detail in chapter four.

Techniques

1.9 Time correlated single photon counting (TCSPC)

Fluorescence lifetimes of biomolecules are acquired using a multi-exponential single photon counting instrument (TCSPC). The definition of fluorescence lifetime is the average amount of time a fluorophore remains in the excited state following excitation. It uses a pulsed laser for excitation and detects less than or approximately 1% of emitted photons. The principle of this technique is to calculate the time from the point the laser pulse excites the molecule to the emitted photon detection. These emission time values stored as a histogram. The excited fluorophores emit photons, which resulted in an exponential decay of the excited population. Intensity decay *I*(t) can be expressed with Equation 1.1[35]

$$I(t) = I(0)\, e^{-\frac{t}{\tau}} \tag{1.1}$$

The lifetime (τ) can also be measured as the inverse of the deactivation rate. Histogram generated during the experiment can be fit with Equation 1.1 to measure lifetime. It has been observed that for free dye- molecule mono-exponential decay fit is required, whereas for dye molecules attached to DNA or protein mostly require multi-exponential fit. Thus, in multi-exponential fit can be described by Equation 1.1, where contributions of each lifetime (τ_i) component are weighted by their fractions (α_i)

$$I(t) = \sum_{i=1}^{n} \alpha_i\, e^{-\frac{t}{\tau_i}} \tag{1.2}$$

1.10 Signal processing in the TCSPC setup

The detector of the TCSPC setup cannot detect more than one photon at a time, so there is a time when the detector cannot count emitted photons, which causes pulse pile up. This

effect causes histograms of lifetimes skewed to shorter times. This phenomenon happens when the photon count rate is too high. To get rid of this effect, the photon count rate should be much lower (2% of the pulse rate), which reduces the chance of arriving two photons or more than that a time.

Initially, the electrical pulse travels to the CFD and TAC to trigger the START signal. CFD controls the arrival time of the pulse laser, and TAC initiates the measurement of time elapsed from the START signal. TAC is a capacitor which accumulates voltage with time. Once an emitted photon detected, the detector, a PMT, sends an electrical signal to CFD to trigger the STOP signal. As soon as TAC receives a STOP signal, it stops accumulating voltage and sends an electrical signal to ADC, which converts the voltage to time in the nanosecond scale. These voltage signals from many photons generate a histogram of the intensity decay[36] — lifetime values extracted by fitting this intensity decay.

The above described electronic setup has one limitation, which lies in the TAC efficiency. TAC is not able to accept a new START signal until reset to zero. TAC may operate at a lower frequency compared to the repetition rate of the laser so that it may miss a new START signal[37]. To resolve this problem, most of the TCSPC instruments use reverse mode. In this setup, an emitted photon triggers the START signal, and the STOP signal comes from the trigger. The reverse method generates a negative histogram where photons with short lifetimes arrived at longer times after the excitation pulse. This can be transformed into proper form by a data processing program.

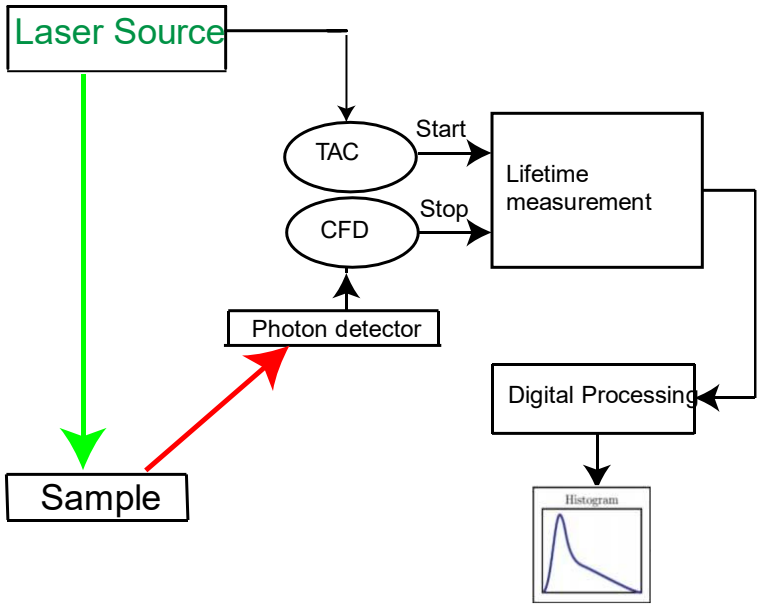

Figure 1.6 The signal processing in a TCSPC instrument. The electrical pulse travels to the CFD and TAC to trigger the START signal. Once an emitted photon detected, the detector, a PMT, sends an electrical signal to CFD to trigger the STOP signal. As soon as TAC receives a STOP signal, it stops accumulating voltage and sends an electrical signal to ADC.

1.11 Data analysis

IRF (Instrument response function) is another crucial parameter for lifetime measurement to deconvolute the intensity decay of the sample. The IRF can be measured using some scattered excitation light. The ASU fit software deconvolutes the decay from the IRF (ASUFIT, URL: www.public.asu.edu/~laserweb/asufit/asufit.html).

The fluorescence lifetime measurement is done by setting the emission polarizer at the magic angle (54.7°) to avoid the effects of depolarization.

It was discussed above; the intensity decay can be mono or multiexponential, depending on the system. A fluorophore dye molecule may display more than the one-lifetime value if it interacts with other molecules. For instance, when TMR (Tetramethyl Rhodamine) is free in water or buffer, it shows only one-lifetime value, but when attached with a protein

molecule, more than one lifetime values were measured[38]. The multiexponential decay for TMR in the protein environment can be expressed with Equation 1.3

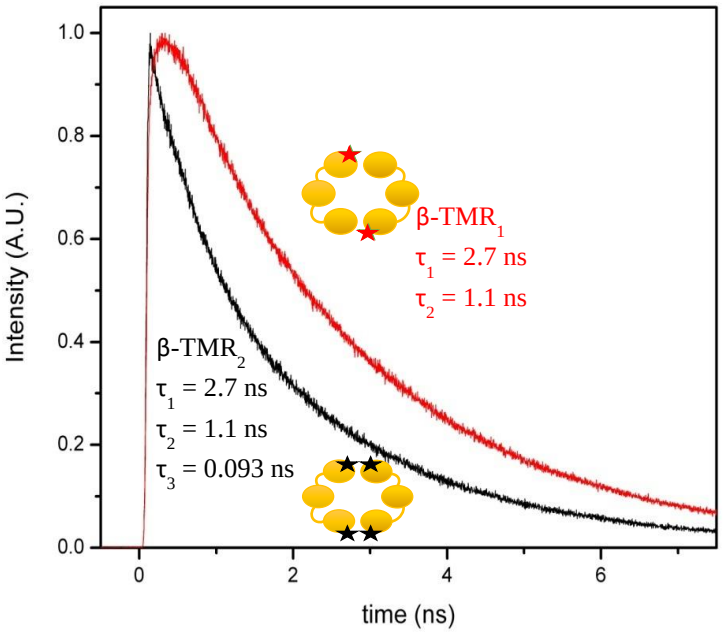

Figure 1.7 The singly labeled (one dye at each interface) protein shows two-lifetime values whereas, doubly labeled (two dyes at each interface) protein shows three-lifetime values. The shortest lifetime value (0.093 ns) indicates that two dye molecules at the interface are forming a dark state (H dimer).

$$I(t) = \alpha_1 e^{-t/\tau_1} + \alpha_2 e^{-t/\tau_2} + \alpha_3 e^{-t/\tau_3} \quad (1.3)$$

The goal of measuring intensity decay is to calculate decay times and amplitudes. Amplitudes are proportional to concentrations of each species present in the protein dissociation-association equilibrium.

1.12 Fluorescence Correlation Spectroscopy (FCS)

In the past few decades, fluorescence has become a profound technique for biological research. It is hard to imagine any biological research at the cellular level without using fluorophores. Fluorophore's ability to be detected easily has made fluorescence technique

one of the powerful tools in a biological assay. It possesses the unique ability to absorb and emit light at specific wavelengths. The following energy diagram by Jablonski can enlighten us to understand how fluorescence occurs.

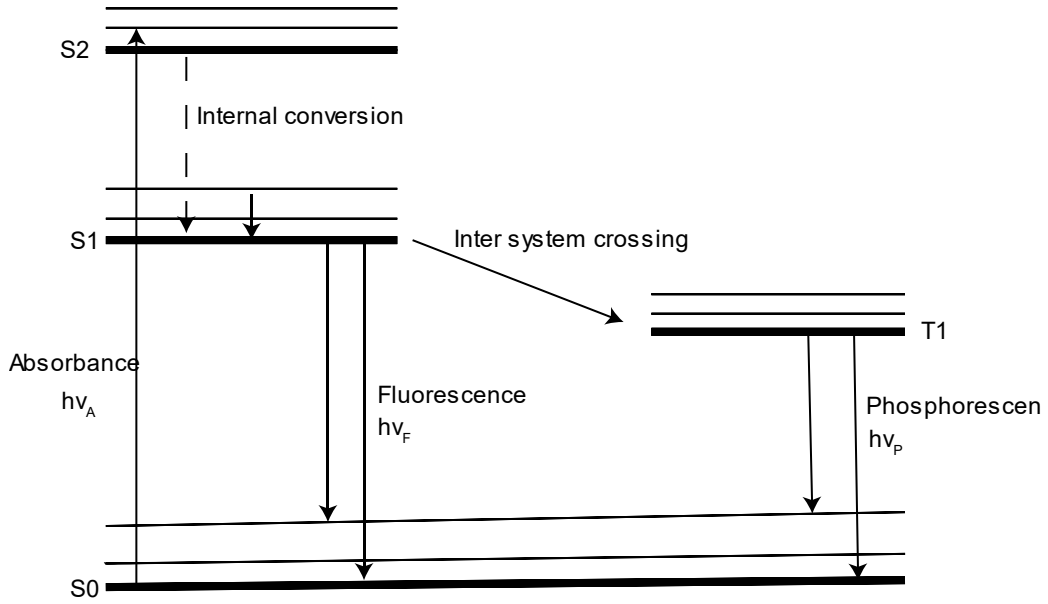

Figure 1.8 Jablonski Diagram illustrates the excited states of a molecule and the radiative and non-radiative transitions that can occur between them.

Robert Brown, in 1828, first observed diffusion. He observed erratic and irregular movements of pollen particles in water and named it as Brownian motion. However, a quantitative explanation of the Brownian motion was given by Einstein later in 1905.

This thesis is only concerned about the diffusion of particles in aqueous solution because FCS set up was used for studying biological samples. Adolf Fick formulated the equations which describe diffusion quantitatively in 1855[39]. Fick derived his first- and second law based on simple assumptions, which are the following differential equations

$$J_x = -D\frac{\delta C}{\delta x} \tag{1.4}$$

$$\frac{\delta C}{\delta t} = D\frac{\delta^2 C}{\delta x^2} \quad (1.5)$$

Fick's first law Equation 1.4 describes the steady-state flux J_x of the particles which are induced by the concentration gradient $\frac{\delta C}{\delta x}$. D is the diffusion coefficient and has the units m^2s^{-1} and relates to how far a particle can move due to its diffusive motion. C is the concentration of the particles, and x is the one-dimensional space coordinate.

Fick's second law, Equation 1.5, states how the concentration varies over time. The numerical solution to this equation describes the mean squared displacement (MSD) $<x^2>$ of the diffusive particle in one dimension. MSD represents the area that the particle covers at a specific time.

$$\langle x^2 \rangle = 2 \cdot D \cdot t \quad (1.6)$$

The above equation in two and three dimensions can be written in terms of $< r^2>$. In two dimensions, the square of the distance from the origin to the point (x,y), is $r^2 = x^2 + y^2$, therefore

$$\langle r^2 \rangle = 4 \cdot D \cdot t \quad (1.7)$$

In three dimension, $r^2 = x^2 + y^2 + z^2$ thus

$$\langle r^2 \rangle = 6 \cdot D \cdot t \quad (1.8)$$

This relation displays linearity between the mean square of the translation distance of a particle and time. This statement can be verified by following the trajectory of a single particle over time, or by averaging the diffusion paths of many particles. Later, Einstein derived the famous Stokes-Einstein[40,41] Equation 1.9 for macroscopic particles in liquids

$$D = \frac{k_B T}{6\pi n R} \quad (1.9)$$

where k_B is the Boltzmann constant, T is the absolute temperature, η is the viscosity of the solution, and R is the hydrodynamic radius of the particle.

1.13 Application of Fluorescence Correlation Spectroscopy

Fluorescence Correlation Spectroscopy (FCS) is a well-known experimental technique that deciphers the dynamics of molecular events using statistical analysis of the temporal fluctuations occurring in a small observed volume (in fl). This technique requires a fluorescently labeled sample or a sample that has intrinsic fluorophore. FCS has rapidly become a well-established technique that facilitates investigation of a wide range of biophysical phenomena such as diffusion, binding processes, oligomerization and conformational changes in proteins, etc.

FCS is a statistical method, which analyzes the fluctuations in fluorescence signals. These fluctuations typically originate from Brownian motions of the dye or dye-labeled molecules through a small confocal volume (~ 5 fl). A very sensitive detector, i.e., avalanche photodiode(s) (APD), records single photons emitted by the dye molecules in the confocal volume, which results is fluorescent fluctuation. The relevant information about the dynamics of the system, such as diffusion time, size, number of particles, and concentration, can be extracted by using correlation functions that convert fluorescent fluctuations into a correlation decay curve.

Since the size of the confocal volume created through the optical setup is very small (~ 5 fl), there will be considerable fluctuations in the fluorescent signal. Therefore, it is likely that at any given time, there might be one or several fluorescent molecules present at the small detection volume.

1.14 Autocorrelation Function

The fluorescence intensity as a function of time can be written as Equation 1.11

$\langle I(t)\rangle$ is the average fluorescence intensity over time *t* and $\delta I(t)$ is the fluctuation of the intensity at time t.

$$I(t) = \langle I(t)\rangle + \delta I(t) \tag{1.11}$$

The auto-correlation function facilitates the transformation of data from the measured time to the correlation time domain. In other words, the recorded intensity at time *t* is correlated with that recorded at time ($t + \tau$). If the intensity of the signal has not changed considerably in the specified time period, then the correlation is high. On the other hand, if the signal is entirely different, the correlation is low. The correlation function $G(\tau)$[35] is defined as Equation 1.12:

$$G(\tau) = \frac{\langle I(t)\cdot I(t+\tau)\rangle}{\langle I(t)\rangle^2} \tag{1.12}$$

Three essential parameters can be extracted from the autocorrelation function:

1. the average no. of fluorescent particles present <*N*> in the observable volume

2. the size of the confocal volume (*r*, *z*)

3. diffusion time which can be described as the average time required for a molecule to move through observable volume

Now, taking into account the parameters of the confocal volume, which can be approximated by a 3-dimensional Gaussian profile with an ellipsoidal shape, then the autocorrelation function can be written as Equation 1.13

$$G(\tau) = G(0)\left(1 + \frac{4D\tau}{r^2}\right)^{-1}\left(1 + \frac{4D\tau}{z^2}\right)^{-\frac{1}{2}} \tag{1.13}$$

where $G(0)$ is the amplitude of the decay, D is the diffusion coefficient, r is the shorter radial component of the ellipsoidal volume, and z is the longer axial component of the ellipsoidal volume. For our FCS set up, $z >> r$. Then we can rewrite the Equation 1.13 for a monodisperse sample freely diffusing in the solution as Equation 1.14:

$$G(\tau) = \frac{1}{\langle N \rangle} \frac{1}{1+\frac{\tau}{\tau_D}} \quad (1.14)$$

here, τ is the correlation lag time, τ_D is the characteristic diffusion time, and $< N^{-1} >$ is the mean number of fluorescent particles in the observation volume.

1.15 The Overview of the FCS setup

The primary goals of FCS measurements are:

A. To create a small detection volume to ensure a meager number of particles at the observable volume to achieve a correlation function with a high amplitude

B. high efficiency of photon detection that leads to a sound rejection of the background fluorescence

These requirements can be achieved by building a confocal FCS setup. The following components are required for the setup:

a. Optical table b. Excitation source (532 nm laser) c. Optical density filter d. Mirrors e. dichroic mirror f. the stage and reflective mirror g. Objective h. Bandpass filter i. the pinhole j. Pinhole lenses k. Lens before the detector l. detector

The optical table is considered as an essential part of the FCS set up because of its ability to absorb the shock gives the stability to the whole set up. The more stability the table provides, minor adjustments will be required for alignment. The optical table is supported by hydraulic stands. The choice of lasers as the excitation source for the FCS setup is based

on the excitation wavelength of fluorophores. In the clamp project, TMR dye was used to tag the protein dimer at the clamp interface. Hence, a green laser (532 nm) was used to excite the dye to monitor protein stability and interface dynamics. To control the power of the laser, an optical density filter is placed in front of the laser source. Optical density can be expressed as a function of the transmittance:

$$OD = log_{10}\frac{1}{T} \tag{1.15}$$

However, the calculated laser powers are not the same as actual laser powers due to the loss of intensity of the beam to the different optical components. The loss of laser power at the objective is partially due to the reflection by the surface of lenses and other parts, and some are lost because of its imperfect transmission through lenses. FCS requires a highly collimated beam of an appropriate diameter to obtain a small observable volume. The next step is to direct the laser light coming from the lens towards the reflective mirror, which in turn reflects the beam into the back of the objective. Here, the dichroic mirror plays an important role. It reflects the laser light < 540 nm coming from the lens and directs it towards the objective. The dichroic mirror also can transmit the fluorescence > 540 nm emitted by the fluorophore tagged at the protein interface towards the detector through the pinhole assembly.

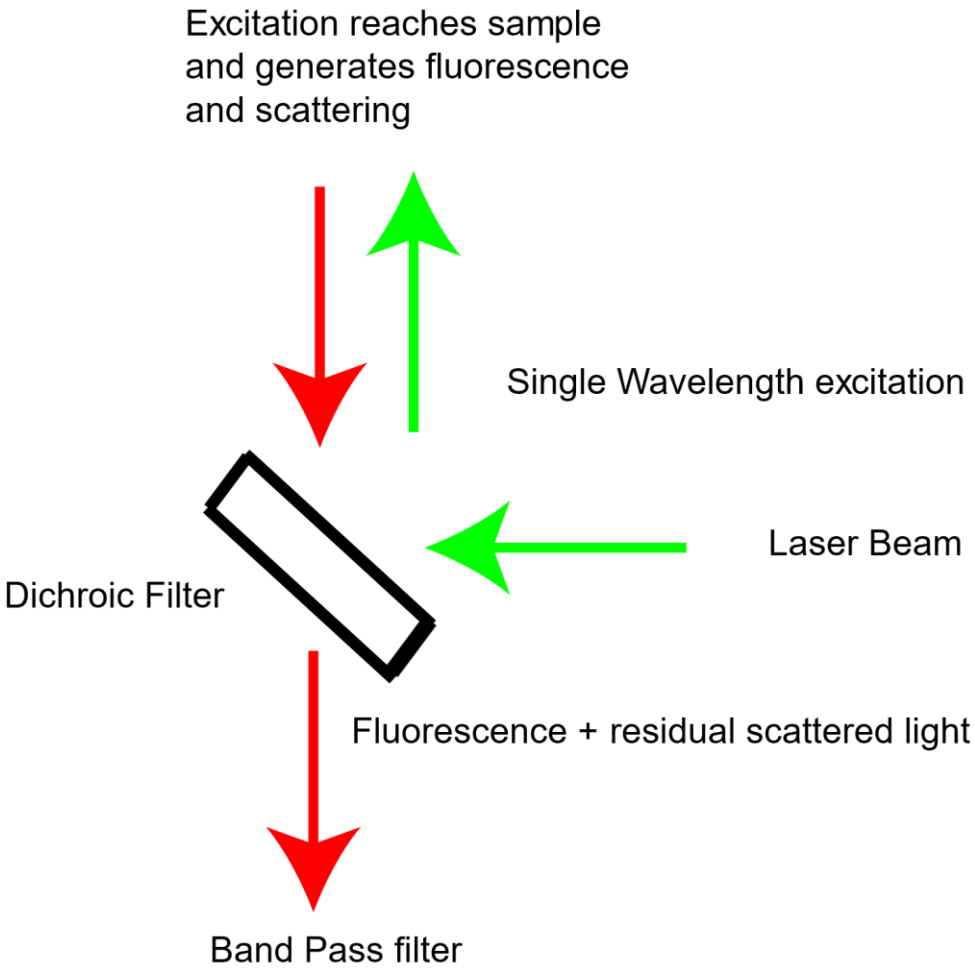

Figure 1.9 An illustration of the principle of a dichroic mirror. The excitation light is reflected towards the objective, and the fluorescence (and residual scattered excitation light) from the sample is transmitted towards the bandpass filter.

In the FCS set up, the objective is critical for the generation of small detection volumes as well as the collection of the fluorescence from the sample. Thus, it should be high-transmitting and efficient in the light collection. For this study, a commercially available NA objective was used. This setup, objective goes upwards, and the laser beam to and from the sample goes through a thin cover glass. This means that the medium between the objective and the coverglass is air. Due to the refraction at the air-glass interference, the

numerical aperture is limited to ~ 1.4. Since FCS requires efficient fluorescence collection and transmission, high power objectives ($NA > 1$) are ideal. This can be described with Snell's law:

$$NA = \eta \cdot \sin(\alpha_{object}) \quad (1.16)$$

where η is the refractive index of intervening media. For air $\eta = 1$, water $\eta = 1.33$ and for microscope immersion oil $\eta = 1.52$. The *NA* of an objective can have a significant effect on its light collection efficiency, and α_{object} is the half collection angle.

However, it must be noted that objectives perform to their best capability when it is being used under the right conditions (with immersion oil). The bandpass filter is another important part of the setup. The samples used for the FCS measurements are in the aqueous phase, which brings an unwanted contribution of the background noise from water molecules. In the sample, water molecules are in larger numbers than dye molecules.

There are mainly two sources of these unwanted contributions:

1. Raman scattering by the water-molecules: It contributes photons at both higher and lower wavelengths compared to the laser excitation light. This is the primary source of background noise.

2. Rayleigh scattering by the water-molecules: These scatterings contribute to the background signal at the excitation wavelengths.

To minimize these unwanted noises, a bandpass filter is placed between the dichroic mirror and the lens before the pinhole. This emission filter blocks scattered light due to Raman scattering and transmits wavelengths between 550 - 650 nm. Once the signal is filtered by the emission filter, it reaches the lens, which focuses the light on a spot, and a pinhole is placed right in the same position. The pinhole is, of course, an extremely important element

of this setup as it defines the confocal volume and prevents unwanted noise from reaching the detector.

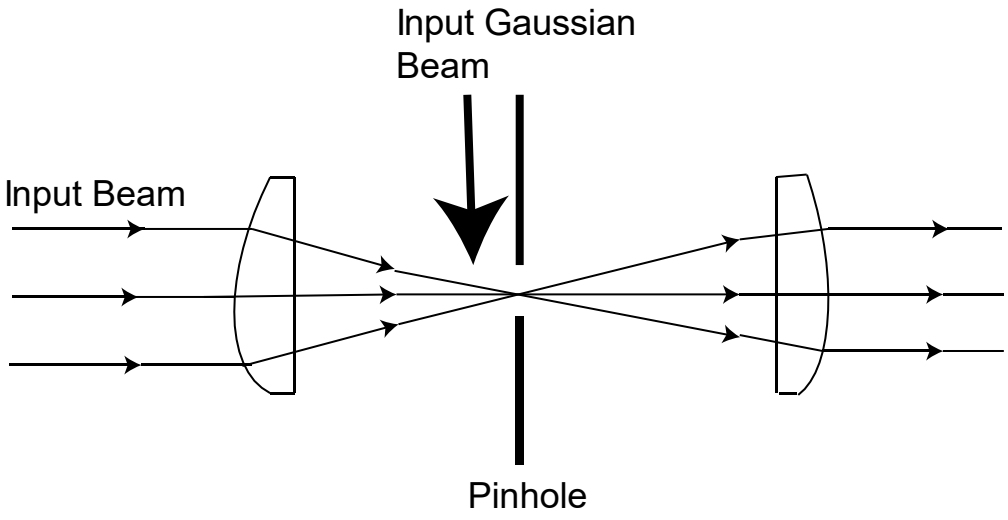

Figure 1.10 An illustration of a lens-pinhole-lens system. This system provides an as near-Gaussian beam profile as practically possible.

The fluorescence light propagating through the pinhole will have a near Gaussian intensity profile if the pinhole is placed perfectly at the focus.

The alignment of the pinhole, along with the construction of a Gaussian beam, is the most vital and challenging step of the FCS setup. At this point, the light from the laser to the lens after the pinhole must be well aligned and collimated. The detector is a critical component of FCS setups, and the single-photon detector used in this setup is APD (avalanche photodiode). A detector suitable for FCS measurements must fulfill some basic requirements necessary for conducting single molecule fluorescence experiments: 1) high quantum efficiency (QE) over the spectral range of the wavelengths of the light 2) high signal detection and 3) sufficiently fast response time.

1.16 FCS setup alignment check

A proper FCS measurement requires low-noise photon counting. The photon-counting efficiency of a detector significantly affects the signal to noise ratio (S/N). In the following figure, the red trace indicates the misalignment of the optical setup. The emission intensity is not focused through a pinhole, which results in very low S/N. In the other hand, the blue trace shows the perfect alignment. Hence, the S/N is very high, and the FCS decay fit also looks much better. We use 1 nM or 10 nM TMR dye to measure FCS decay and then fit the decay with the autocorrelation function (Equation 1.13) to determine the *r*-value. Ideally, *r* value should lie between 0.4 – 0.45 µm because that indicates we have a small observable volume (in fl). However, if we look at the fitting of the data in Figure 1.12, we can conclude that with proper optical alignment, fitting looks much better.

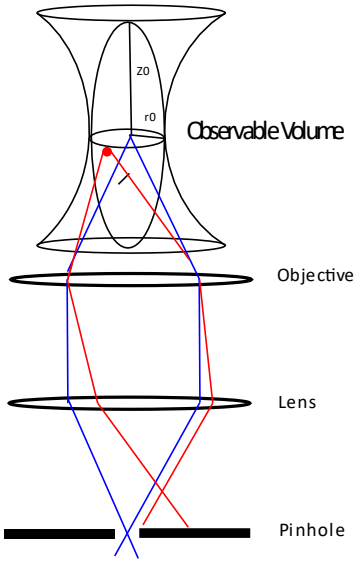

Figure 1.11 Illustration of the pinhole principle that creates a small detection volume ~ 5 fl and reduces noise in the signal.

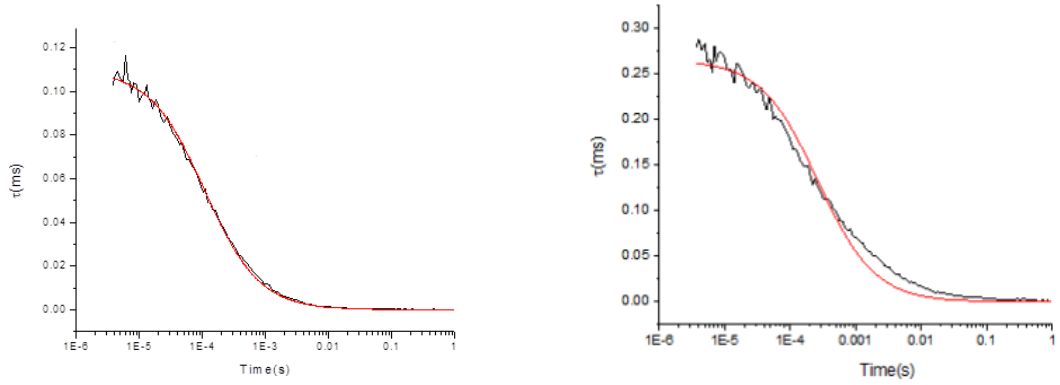

A B

Figure 1.12 A. It shows an FCS decay when the pinhole is placed right at the focus. B. An FCS decay when the alignment is poor.

1.17 Diffusion times and protein size

The diffusion time increases with protein size. The reason behind this is due to high molecular weight; large proteins diffuse slow compare to smaller proteins. We utilized this concept in our project to characterize protein dissociation and association kinetics. We observed protein dissociation with NaCl and protein association with KGlu. The mathematical relation between diffusion time and the protein size can be derived using the following Equations:

$$D = \frac{k_B T}{6\pi n R}$$

$$R = \sqrt{\frac{3m/N_A}{4\pi\rho}} \qquad (1.17)$$

Where R is the radius of the protein, N_A is Avogadro's number, m is the mass of the protein, and ρ is the density of the protein. For β clamp, When the monomers form a dimer, the mass of the protein becomes double. However, the radius remains the same. Hence, the ratio of diffusion times of dimer (τ_D) and monomer (τ_M) is 1.26 ($2^{1/3}$). If the protein forms

oligomers (*n*), in that case, we can use Equation 1.18 to determine the number of monomers present in the protein assembly.

$$\tau_2 = \tau_1 n^{1/3} \quad (1.18)$$

CHAPTER 2

Oligomerization of protein studied through FCS analysis

2.1 Introduction

A large portion of cellular proteins is oligomeric. These oligomers have biological relevance in regulating gene expression, enzyme activity, and cell recognition. Therefore, it is interesting to study the thermodynamic and kinetic parameters of the oligomerization process. Different experimental approaches help us to investigate oligomer formation. The essential parameter for this study is to determine the equilibrium dissociation constant(K_d). However, for stable oligomers, K_d value is minimal, which prevents us from experimenting with such low protein concentration. Here, the Fluorescence Correlation Spectroscopy (FCS) appears to be a savior. We can use from 10 pM to 100 nM protein concentration in the FCS study. Hence, it indicates that the FCS technique is very sensitive, and it can detect a significant amount of dissociation or association even in low protein concentration. However, analysis of the FCS data is the most crucial part. It requires a proper model to determine the concentrations of different oligomeric species present in the solution at any given time. In this section, I'll discuss how we analyzed FCS data to determine equilibrium dissociation constants using a monomer-dimer oligomerization kinetics model. This model was developed by Dr. Levitus and David Kanno in 2014. We used the same algorithm to analyze the FCS data for both chapter three and chapter three.

2.2 Monomer-Dimer equilibrium

Dr. Binder observed in her previous work that with low protein concentration (1 nM) at a high salt concentration (1 M), protein dimer dissociates into monomers. The dissociation equilibrium constant can be written as Equation :

$$K_d = \frac{k_d}{k_a} = \frac{[M]^2}{[D]} \tag{2.1}$$

The autocorrelation function of a solution containing single species can be expressed as Equation*:*

$$G(\tau) = G(0)(1 + \frac{4D\tau}{r^2})^{-1}(1 + \frac{4D\tau}{z^2})^{-\frac{1}{2}} \tag{2.2}$$

Where τ is the correlation lag time, r is the radial dimension, z is the axial dimension, $\langle N \rangle$ is the average number of particles present in an observable volume. The above equation can be further simplified if we assume that the axial dimension of the observable volume is much larger than the radial dimension of it. This criterion is fulfilled in most of the FCS experiments because the spatial resolution of the confocal microscope is less efficient along the axial dimension than in the radial dimension. Hence, we can rewrite the above equation as Equation 2.3:

$$G(\tau) = \frac{1}{\langle N \rangle} \frac{1}{1+\frac{\tau}{\tau_{app}}} \tag{2.3}$$

2.3 Autocorrelation of N number of species present in a solution

The partial dissociation of dimer into monomers or association of monomers form different higher-order structures in the solution. The autocorrelation function $G(\tau)$ for N number of species present in a solution can be shown as Equation 2.4:

$$G(\tau) = \frac{\sum_{i=1}^{n} B_i^2 N_i \left(1+{\tau}/{\tau_{D_i}}\right)^{-1}}{\left(\sum_{i=1}^{n} B_i N_i\right)^2} \tag{2.4}$$

Where N_i is the average number of molecule present in the observable volume for species *i*, B_i is the molecular brightness of species *i*, and $g_i(\tau)$ is the autocorrelation function of a homogeneous solution of species *i* normalized to an amplitude of unity. We assume that all oligomeric species present in the solution carries a single fluorophore at each subunit. Hence, the autocorrelation can be described as Equation 2.5 :

$$G(\tau) = \frac{1}{V_{eff} N_A C_0^2} \sum_{n=1}^{m} n^2 C_n g_n(\tau) \quad (2.5)$$

Where C_0 is the total protein concentration expressed in terms of monomers, C_n is the molar concentration of the oligomers containing *n* subunits, N_A is the Avogadro's number, *m* is the largest oligomer present in the solution. We assume that the brightness (B_i) is directly proportional to the number of fluorophores present in each subunit. The optimum FCS signal to noise ratio can be achieved between 10 pM - 100 nM labeled protein concentration. The experiments which require higher protein concentration, we use a mixture of labeled and unlabeled protein samples. This helps us to determine the degree of dissociation in terms of total protein concentration, and amplitude and noise of the FCS decay depend on the concentration of labeled protein. The mixture of labeled and unlabeled protein molecules leads to form an equilibrium where the random redistribution of subunits take place. Hence, we expect an arbitrary number of fluorescent labels per protein molecule. The number of the fluorescent molecule at each protein molecule is a binomial random variable. The oligomers having a different number of fluorescent labels have different brightnesses (B_i). Hence, they should be treated as distinct species. Therefore, for the oligomers containing *n* subunits and *b* labels, the autocorrelation function can be written as Equation 2.6 :

$$G(\tau) = \frac{\sum_{n=1}^{m}\sum_{b=1}^{n} N_{n,b} b^2 g_n(\tau)}{\left(\sum_{n=1}^{m}\sum_{b=1}^{n} N_{n,b} b\right)^2} \quad (2.6)$$

The total concentration of protein C_0 can be estimated by adding up the labeled(C_L) and unlabeled(C_U) protein concentrations. The parameter f denotes the labeling efficiency of the protein sample. The protein labeling procedure is always challenging, and the parameter f helps us to determine the exact labeled protein concentration(C_L f) in the solution, and the fraction of labeled protein present is C_L f / C_0. The labeling efficiencies of protein samples can be measured using other spectroscopic techniques. Both C_0 and C_L have known values. The only unknown value is C_n, which varies depending on the equilibrium and kinetic rate constants. We need to measure C_n experimentally. We can think that since C_n is the only unknown parameter in Equation 2.7, it can be determined easily.

$$G(\tau) = \sum_{n=1}^{m} A_n g_n(\tau) \qquad \text{where } A_n = \frac{nC_n[\,1+(n-1)(\frac{C_L f}{C_0})}{f V_{eff} N_A C_L C_0} \quad (2.7)$$

However, this idea would not work because the diffusion coefficients of different species in the solution lie in a very narrow range, and it is found that even one diffusion coefficient can be used to fit the autocorrelation function when multiple species are present in the solution. Therefore, our idea was to fit each experimental decay with a single diffusion coefficient first, and then we analyzed them to determine C_n values.

The diffusion coefficient we obtained from the single component fit of the FCS decay, is called the apparent diffusion coefficient. It is called apparent because even for the polydisperse solution (multiple species present in the solution), we use only one diffusion coefficient to fit the autocorrelation function. τ_{app} represents a mixture of monomers, dimers for β clamp and monomers, dimers, and trimers for PCNA.

2.4 Determination of Equilibrium Dissociation constants

Here, I'll discuss the monomer-dimer equilibrium for β clamp. The equilibrium dissociation constant (K_d) was calculated from the experimental values of diffusion times for different species present in the solution. The diffusion times for a monomer-dimer equilibrium can be expressed as Equation:

$$\tau_{app}^2 - (c(\tau_D - \tau_M)\tau_{app} - \tau_D\tau_M = 0 \quad (2.8)$$

The positive root of the above equation is:

$$\tau_{app} = \frac{1}{2}\left(c(\tau_D - \tau_M) + \sqrt{c^2(\tau_D - \tau_M)^2 + 4\tau_D\tau_M}\right. \quad (2.9)$$

The concentration of protein can be shown as Equation:

$$c = 1 - 2\frac{\alpha_1}{1+(1-\alpha_1)\left(\frac{C_L f}{C_0}\right)} \quad (2.10)$$

α_1 is the degree of dissociation of dimer into monomers. The relation between K_d value with the degree of dissociation is shown in Equation:

$$\alpha_1 = \frac{1}{4C_T}\left(-K_d + \sqrt{8C_0K_d + K_d^2}\right) \quad (2.11)$$

These equations were used to estimate the value of equilibrium dissociation constant. At low labeling efficiency ($f \rightarrow 0$) the apparent diffusion time (τ_{app}) is equal to $(\tau_D\tau_M)^{\frac{1}{2}}$ However, from the experimental point of view, the equilibrium dissociation constant can also be estimated from the concentration at which the apparent diffusion time is halfway between the diffusion times of dimer and monomer ($\tau_{app} = \tau_M + \frac{(\tau_D - \tau_M)}{2}$). This suggests that without the above mathematical treatment K_d value can easily be determined from the experiment. However, we need to obtain the information on τ_D and τ_M from the experiment. But, it may not be easy to get τ_D and τ_M values for specific proteins if they are

not soluble or form aggregates at higher concentrations. The limitation of the FCS technique is that it is challenging to do measurements below 100 pM. Hence, it is not easy to determine K_d value with precision if τ_D and τ_M values can not be measured from the experiment accurately. In that case, we need to use the mathematical approach to extract K_d value for a polydisperse solution.

2.5 Determination of dissociation and association rate constants

The dimer to monomer dissociation kinetics for β clamp can be written as the Equation 3.12:

$$\frac{d[D]}{dt} = -k_d\,[D] + \frac{k_d}{K_d}\,[M]^2 \qquad (2.12)$$

It is not possible to determine k_d (rate dissociation constant) through FCS experiments because in FCS experiments, we use the change in diffusion times to determine other parameters. However, in this system, the maximum change in diffusion time can be ~1.26 times from monomer to dimer which is not sufficient to calculate the rate dissociation constant(k_d). On the other hand, the association rate constants (k_a) for typical protein-protein interactions are in the range 10^5 - 10^6 $M^{-1}s^{-1,}$ which also indicates that the dissociation kinetics of the dimeric protein at 1 nM concentration is too fast to monitor through the FCS technique. FCS kinetic experiments are not possible to do when the protein dissociation is near to the equilibrium because of the measurement of k_d depends on the change in apparent diffusion time (τ_{app}), which is expected to be changed only by 1.26 times when the dissociation is complete. Therefore, to maximize the range of measured τ_{app} values, the protein should be diluted from a high protein concentration

where $C_0 >> K_d$ to a final concentration where the degree of dissociation will be much higher because of $C_0 < K_d$.

Therefore, David Kanno and Dr. Levitus modeled a hypothetical system to measure time-dependent τ_{app} changes with C_0 = 0.1 nM, k_a = 10^5 $M^{-1}S^{-1}$, f = 1 and K_d values in the 0.1 – 10 nM range, as shown in (Figure 2.1).

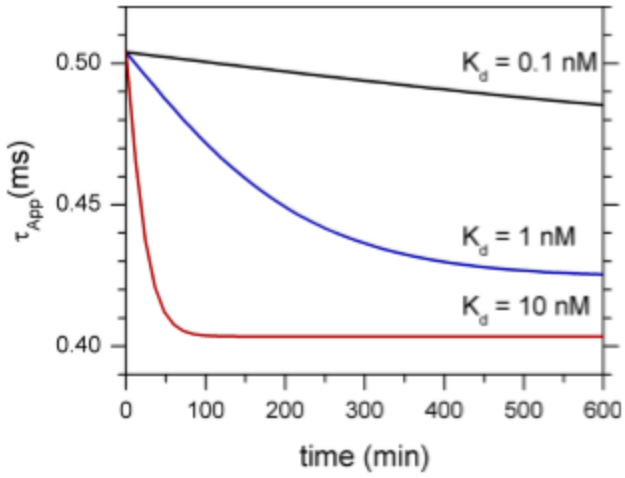

Figure 2. 1 Hypothetical system to measure time-dependent changes in apparent diffusion times (τ_{app}) for K_d values in the 0.1 – 10 nM range.

However, Dr. Binder measured the k_d value of the dimer-monomer equilibrium from the subunit exchange experiment using the time-resolved fluorescence (TCSPC) technique. After that, the lifetime of the closed ring was calculated by taking the reciprocal of k_d value. In this experiment, Dr. Binder used doubly-labeled clamps with H-dimers and mixed with a five times excess of unlabeled protein. In this way, over time, the quenched clamps will dissociate into the labeled monomers. Since excess unlabeled protein was in the solution, statistically, a labeled monomer is more likely to find an unlabeled monomer and will form a bright species. Over time, the intensity will increase as more of these complexes are created, and as you can see, in 40 hours, the intensity goes up. The data

from the lifetime experiment was analyzed using global analysis, and what that means is that we take all of these decays and fit them with the same two lifetimes. We plot the contributions from the amplitudes for each lifetime over time, and we see that the contribution from the longer lifetime increases over time, whereas the contribution from the shorter lifetime(due to H dimer) decreases over time. Dr. Binder measured a lifetime of the closed complex of 43 hours. The fractional amplitudes in this experiment are proportional to the mole fraction of each species present in the solution.

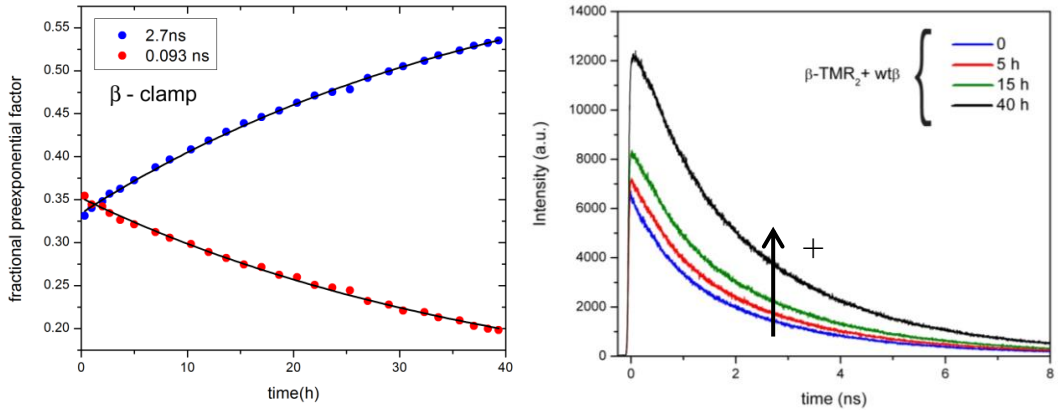

Figure 2.2 The fractional amplitude of the longest lifetime (shown in blue) increases, and the shortest lifetime (shown in red) decreases with subunit exchange. Fluorescence intensity increases from 0 to 40h.

CHAPTER 3

Electrostatic interactions stabilize the β-clamp interface

3.1 Introduction

In this work, we characterized the role of electrostatic interactions in stabilizing the β-clamp interface. We used time-resolved fluorescence spectroscopy to determine the kinetic rate of subunit dissociation and fluorescence correlation spectroscopy to determine the concentrations of monomers and dimers in equilibrated diluted solutions of β clamp in a wide range of NaCl concentrations. In previous work, Dr. Binder [25] showed that clamp dimer dissociates into monomers in the presence of high salt concentrations suggesting that one or more salt bridges play a key role in stabilizing the clamp interface.

NaCl was chosen because its ions are relatively nonchaotropic and nonkosmotropic, which minimizes ionic effects other than electrostatic screening. If the electrostatic interactions in the clamp interfaces are stabilizing, the screening of Coulombic interactions by ions will decrease the stability of the dimer and favor dissociation. We observed a linear increase of the logarithm of the equilibrium dissociation constant with the square root of the NaCl concentration, which is consistent with the Debye-Hückel limiting law that describes the effect of ionic strength on electrostatic forces. This indicates that one or more charged amino acids contribute to the remarkable stability of the interface at physiological salt concentrations. Consistent with this, mutation of a charged amino acid (Arg-103) results in higher concentrations of monomers in equilibrium and faster dissociation kinetics.

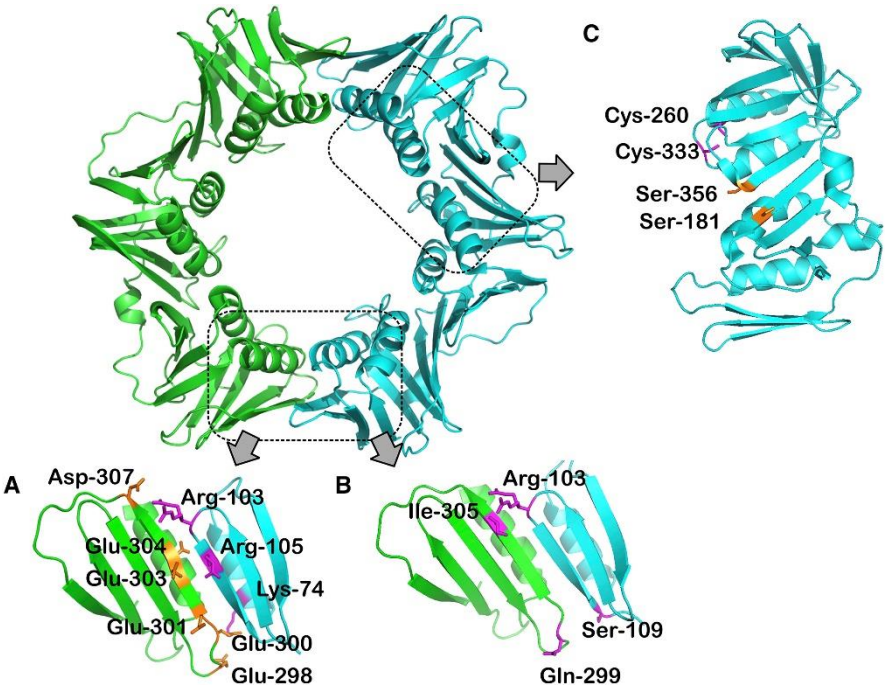

Figure 3.1 X-ray crystallographic structure of the β -sliding clamp (PDB:1MMI) with one monomer in green and one in cyan. (A) An enlarged view of a β-dimer interface rotated 90° relative to the main structure. Negatively charged amino acid residues (orange sticks) on one side of the interface (green monomer) are aligned with positively charged amino acid residues (magenta sticks) on the other side (cyan monomer). (B) An enlarged view of the same β-dimer interface. Residues that were mutated to Cys and labeled with TMR are depicted as sticks (magenta). TMR attached to residue 305 pairs with TMR attached to residue 103, and TMR attached to residue 299 pairs with TMR attached to residue 109. (C) An enlarged view of two globular domains within the same β-monomer. Each β-monomer is comprised of three domains that are similar in the fold. The topology of the interface between two domains within the same monomer is similar to the topology of two domains at a dimer interface. Ser-181 and Ser-356 (orange sticks) are located at a topological site that is similar to residues Ile-305 and Arg-103, respectively, at the dimer interface (see B). The native cysteine residues Cys-260 and Cys-333 are shown in magenta.

Deprotonation of basic residues at high pH also weakens interface interactions. I would like to acknowledge Dr. Binder, Dr. Bloom, and Dr. Levitus, for their significant contributions to the research work explained in this chapter. To be precise, Dr. Binder did FCS measurements with single labeled protein in various pH conditions in borate buffer and investigated the interface dynamics in μs scale. DSF measurements were done by Dr. Bloom's lab. I did all TCSPC measurements and a few FCS measurements in various NaCl

concentrations. Dr. Levitus analyzed all FCS data to determine K_d values in a monomer-dimer equilibrium.

This research work titled 'Electrostatic Interactions at the Dimer Interface Stabilize the *E. coli* β Sliding Clamp' was published in June 2017 in Biophysical Journal.

Materials and methods

3.2 Protein expression and purification

Site-directed mutagenesis of dnaN (β) was done using the QuikChange II kit (Agilent, Santa Clara, CA) as per the manufacturer's directions. For differential scanning fluorimetry (DSF) experiments, either Arg-103 or Arg- 105 was mutated to Ser. For fluorescence experiments, surface Cys residues (Cys-260 and Cys-333) were replaced with Ser in β proteins to prevent unwanted labeling of these sites. Four separate β constructs were made by replacing Ser-109, Ile-305, Arg-103, or Gln-299 with Cys to site-specifically label these sites with tetramethyl rhodamine (TMR) maleimide and create singly labeled clamps. Two doubly labeled clamps were made by mutating Gln-299 and Ser-109 or Ser-181 and Ser-356 to Cys residues in the C260S/C333S background and labeling the Cys residues with TMR. An additional doubly labeled clamp containing R103C and I305C mutations in the C260S/C333S background was made in previous work and labeled with TMR[42]. To assess the contribution of Arg-103 to dimer stability, another mutant was prepared in which Arg-103 was mutated to Ser in the clamp containing S109C and Q299C mutations to make a doubly labeled Arg-103 mutant. A complete list of β mutants and nomenclature is given in Table 1. The sliding clamps were overexpressed in *E. coli* and purified as described previously with minor modifications[43].

3.3 Fluorescent labeling of β

Purified β proteins were labeled with TMR maleimide (Thermo Fisher Scientific, Waltham, MA), as described previously[25]. Protein concentrations were determined by a Bradford-type assay (Bio-Rad, Hercules, CA) using native unlabeled wild-type β standards that were quantified by denatured absorbance measurements at 280 nm using a calculated extinction coefficient of 14,700 M^{-1} cm^{-1} [43]. The concentration of TMR was calculated from the absorbance measured at 555 nm using an extinction coefficient of 98,000 M^{-1} cm^{-1} for the free dye in methanol. Typical labeling yields were 70% of available Cys residues.

3.4 Dissociation of β dimers into monomers

The dissociation of β dimers into monomers was investigated using fluorescence correlation spectroscopy, as reported in the previous work[25]. The home- built instrument uses a 532 nm continuous-wave laser (Compass 215M-10, Coherent, Santa Clara, CA) attenuated to 100 mW, a 1.4 NA objective lens (PlanApo 100×/1.4 NA oil, Olympus, Center Valley, PA), and an avalanche photodiode detector (SPCM-AQR14; Perkin-Elmer Optoelectronics, Waltham, MA). A multiple-T digital correlator (ALV-5000/60X0; ALV, Langen, Germany) was used to acquire the autocorrelation decays ($G(T)$). Experiments were performed with 1 nM solutions of singly labeled clamps (i.e., one label per subunit) prepared in a buffer containing 20 mM Tris-HCl (pH 7.5), 0.1 mg/mL bovine serum albumin (BSA), and variable concentrations of NaCl (as indicated in the text). pH-dependent experiments were performed in 20 mM borate buffer containing 0.1 mg/mL BSA and 50 mM NaCl. The 1 nM protein solution was prepared in an Eppendorf tube, and 30 μL of this solution was used for fluorescence correlation spectroscopy (FCS)

experiments at t = 0 (i.e., right after the 1 nM solution was prepared from a concentrated stock) and again at t = 24 h. The solution was kept at room temperature between the two measurements.

The autocorrelation functions measured in the FCS experiments were fitted using Eq. 3.1:

$$G(\tau) = \frac{1}{\langle N \rangle} \frac{1}{1+\tau/\tau_D} \quad (3.1)$$

Where τ is the correlation lag time, τ_{app} is the characteristic apparent diffusion time (see text), and *G0* is the amplitude of the decay. Equation 4.1 assumes that the axial dimension of the observation volume is much larger than its radial dimension, which is the case in our instrument. In the case of a single diffusing species, the apparent diffusion time equals a characteristic diffusion time (τ_D) that is related to the particle's diffusion coefficient (D) by $\tau_D = 4r^2/D$, where r is the radial semiaxis of the confocal volume. The values of τ_{app} were obtained from nonlinear least-squares fitting of the experimental autocorrelation decays.

3.5 FCS of doubly β labeled proteins

The autocorrelation decays of 1 nM solutions of doubly labeled β proteins were acquired using the FCS setup described above at room temperature. All experiments were carried out in a buffer containing 20 mM Tris-HCl (pH 7.5), 0.1 mg/mL BSA, and 50 mM NaCl. All decays were normalized to match the diffusion contributions in the millisecond timescale so as to emphasize the differences at shorter timescales. Actual amplitudes were ~0.4–0.8.

TABLE 1 β Mutants and Nomenclature

β-Designation	Mutations
β-WT	None
β-R103S	R103S
β-R105S	R105S
β-S109C-TMR	C260S + C333S + S109C
β-R103C-TMR	C260S + C333S+R103C
β-I305C-TMR	C260S+C333S+I305C
β-S109C/Q299C-$(TMR)_2$	C260S+C333S+S109C+Q299C
β-S109C/Q299C/R103S-$(TMR)_2$	C260S+C333S+ S109C+Q299C+R103S
β-R103C/I305C-$(TMR)_2$	C260S+C333S+R103C+I305C
β-S181C/S356C-$(TMR)_2$	C260S+C333S+S181C+S356C

3.6 Kinetics of subunit exchange

The kinetics of subunit exchange between labeled and unlabeled dimers was investigated by measuring changes in the fluorescence lifetime of the doubly labeled proteins β -S109C/Q299C-(TMR)2 and β -S109C/ Q299C/R103S-(TMR)2. Doubly labeled proteins were mixed with the corresponding unlabeled protein (β -WT or β -R103S, respectively) in a 5:1 ratio to final concentrations of 2 mM (unlabeled) and 400 nM (doubly labeled). Solutions were prepared in a buffer containing 20 mM Tris-HCl (pH 7.5), 0.1 mg/mL BSA, and variable concentrations of NaCl (as indicated in the text). Fluorescence intensity

decays were measured at room temperature using the time-correlated single-photon counting technique at regular intervals over many hours (15h). The instrument is fully described elsewhere[44]. All individual fluorescence decays were collected for 15 min using 540 nm excitation (full width at half- maximum, ~50 ps) and 590 nm emission (collected at the magic angle). Data were analyzed with software written in-house (ASUFIT, www. public.asu.edu/~laserweb/asufit/asufit.html). All traces were deconvoluted from the instrumental response function and fitted globally with the sum of three exponentials:

3.7 DSF

β proteins were diluted to 0.2 mg/mL in buffer containing 0.1% SYPRO Orange dye (Invitrogen, Carlsbad, CA). Buffer contained 20 mM HEPES (pH 7.5) rather than Tris-HCl, because the pH of HEPES is not as sensitive to temperature. Buffer also included differing concentrations of NaCl, as indicated in the Results. Melting temperature (T_m) measurements were made using a RG-3000 quantitative polymerase chain reaction (PCR) instrument (Corbett Research, Sydney, Australia) to increase the temperature from 30 to 99°C in 0.5°C increments every 6s. Tm values were calculated from the maximum value of the first derivative (dF/dT, where F is fluorescence and T is temperature) of the melting curve. Experiments were repeated three times, and average Tm values and standard deviations are reported. These experiments were done at our collaborator's (Dr. Linda Bloom, University of Florida) laboratory.

Results

3.8 Mutations to amino acid residues at the β-dimer interfaces

Mutations were made to the β-dimer interfaces to assess the contributions of amino acids at the interface to the stability of the β dimer. A surface-exposed hydrophilic amino acid (Ser-109), a hydrophobic amino acid (Ile-305), or two charged amino acid residues (Arg-103 and Arg-105) were mutated to create four separate β mutants. For experiments that required a fluorescent probe, these residues were converted to Cys for labeling with TMR maleimide, and for experiments with Arg mutants that did not require a fluorescent probe, Arg was converted to Ser (see Table 1 for a complete list of mutants used in this study).

3.9 Effects of salt concentration and mutations to the β-dimer interface on the stability of β-dimers

FCS was used to assess the stability of three β-dimer mutants in solution where either a hydrophilic residue (Ser-109), hydrophobic residue (Ile-305), or charged residue (Arg-103) was mutated to Cys and labeled with TMR, resulting in incorporation of a single fluorophore in each β -monomer (see Fig. 3.1; Table 1). FCS experiments were performed on 1 nM solutions of each of these mutants in a wide range of salt concentrations. Briefly, FCS involves the measurement of fluctuations in fluorescence that occur when molecules diffuse freely into and out of a micro- meter-sized confocal volume[45]. In the case of a single fluorescent species, a nonlinear fit of the FCS decay gives the diffusion coefficient of the diffusing species. The FCS decay of a mixture of monomers and dimers is a linear combination of the individual decays for pure monomers and dimers weighted by their relative concentrations and molecular brightnesses. However, the diffusion coefficient of the dimer is predicted to be only $2^{1/3}$, 1.26 times smaller than the diffusion coefficient of

the monomer, resulting in an experimental FCS decay with a shape that cannot be experimentally distinguished from the decay expected for a single species. Therefore, these measurements yield a single apparent characteristic diffusion time (τ_{app}), which depends on the relative amounts of β -monomers and β -dimers present in equilibrium in the field of view[46]. The τ_{app} value is inversely proportional to the diffusion coefficient of the dimer when dissociation is negligible, and it decreases as the number of β molecules that exist in monomeric form increases due to dissociation. Concentrated stock solutions of β-mutants were diluted to a concentration of 1 nM and FCS measurements were made on these solutions immediately after dilution (Fig. 3.2A, solid symbols) and after equilibration for 24 h at room temperature (Fig.3.2A, open symbols). FCS decays were then analyzed as described in Materials and Methods to extract the apparent diffusion times of the protein solutions. Apparent diffusion times (τ_{app}) for the Ser-109 and Ile-305 mutants varied with salt concentration in the same manner. At low salt concentrations, 0 – 100 mM NaCl, the clamps are still predominantly dimeric after 24 h incubation, as reflected by high τ_{app}. As the concentration of salt increases beyond this range, the lower τ_{app} values reflect an increasing fraction of monomeric clamps. As shown in Fig. 3.2 B, the ratio of the diffusion times measured at t = 0 and t = 24 h for the Ser-109 mutant approaches the expected theoretical value of $2^{1/3}$ at 500 mM NaCl, indicating the complete dissociation of the dimeric ring. In contrast, the Arg-103 mutant is considerably less stable, and at low salt concentrations (0 – 100 mM NaCl), there is already a significant amount of monomer present in solution after 24 h incubation (Fig. 3.2A). Moreover, at salt concentrations > 400 mM NaCl, the τ_{app} measured immediately after dilution (t_0) decreases with increasing salt, indicating that the Arg-103 mutant dissociates rapidly such that some dissociation is

already apparent in the 20 min that it takes to make the first FCS measurement. Together, these experiments show that electrostatic interactions at the dimer interface contribute to the stability of the β-dimer. Mutation of a positively charged Arg residue at the dimer interface destabilizes the dimer in comparison to mutation of a Ser or Ile and increasing the salt concentration increases the population of β-monomers for both β-S109C- TMR and β-I305C-TMR.

FCS experiments as a function of pH show that deprotonation of one or more basic residues at high pH values also destabilizes the interface. Experiments were performed at pH values in the 7.5 – 10 range, using borate buffer containing 50 mM NaCl. Basic pH-induced dissociation of the β-dimer was more pronounced for the already weakened Arg-103 mutant and negligible for the Ile-305 mutant. Results with the Ser-109 mutant show significant dissociation after 24 h only at pH 10. In this case, the degree of dissociation of the clamp at high pH and low salt is similar to that observed at pH 7.5 and 1 M salt (Fig. S4). As shown in Fig. 3.2, C and D, the fraction of monomers present in solution after 4 h incubation of 1 nM solutions of β-R103C-TMR clamps increases with increasing pH. A shorter incubation time is shown in this case because, in contrast to the experiments performed at pH 7.5, solutions of β-R103C-TMR were not stable over a 24 h incubation time at higher pH values, possibly indicating that monomers are less stable than dimers and do not remain folded at the higher pH conditions. Furthermore, experiments at pH 10 with this mutant gave an initial diffusion time that indicates significant dissociation during the 20 min acquisition of the first data point (Fig. 3.2 C, solid square at pH 10), and unrealistically low diffusion times at $t > 2$ h that suggest protein denaturation (data not shown).

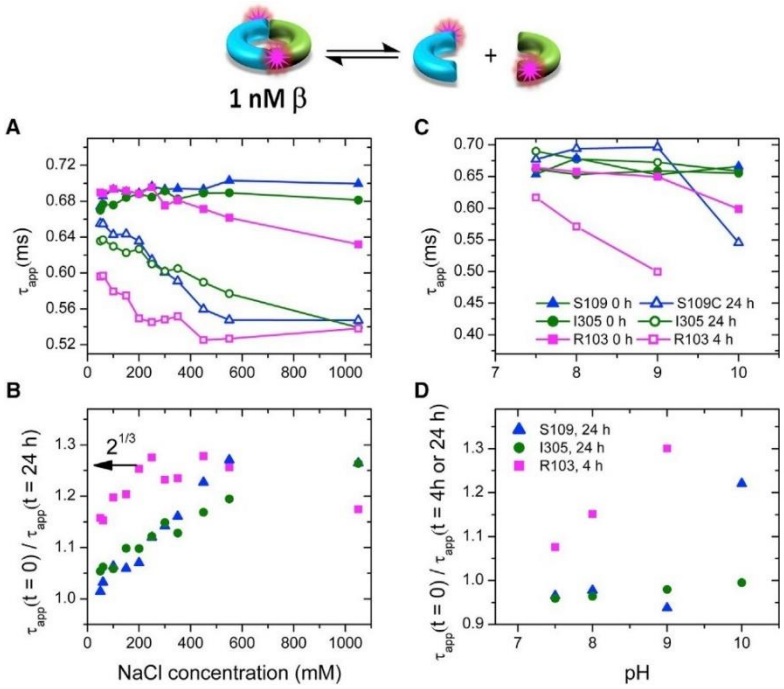

Figure 3.2 Stability of mutant β-clamps. (A) The stability of singly labeled β mutants β-S109C-TMR (blue triangles), β-I305C-TMR (green circles), and β-R103C-TMR (magenta squares) was determined by using FCS to measure the apparent diffusion coefficient (τ_{app}) of 1 nM protein in solutions of differing NaCl concentration. Solid symbols are τ_{app} values measured at t = 0 (i.e., right after diluting a concentrated protein stock to 1 nM), and open symbols are values measured after equilibrating the solutions for 24 h. Error bars are not shown, for clarity (see Appendix A Fig. S1 for the results of individual repeat trials and error analysis). The assay buffer contained 20 mM Tris-HCl (pH 7.5) and the indicated concentration of salt. (B) The ratio of τ_{app} immediately after dilution (t = 0) and after equilibration for 24 h (t = 24) from (A) is plotted. The arrow points to $2^{1/3} \sim 1.26$, the theoretical value expected for the complete dissociation of a dimer. (C and D) Same as (A) and (B), but with 1 nM protein solutions prepared in 20 mM borate buffer of varying pH values containing 50 mM NaCl. A 24 h incubation time is shown for S109 and I305 and a 4 h incubation time is shown for R103

To further characterize the role of electrostatic interactions in stabilizing the β-dimer interface, DSF was used to measure the thermal stability of wild-type (WT) β and two Arg mutants[47] [48] [49]. In these experiments, Arg-103 or Arg-105 was converted to Ser to confirm that mutations to positively charged residues, which potentially disrupt salt bridges, destabilize the β-clamp. Melting temperatures (T_m) were measured for solutions

containing 0.2 mg/mL (2.5 mM) β-dimer in assay buffer with 0.05 to 1 M NaCl (Fig. 3). For β-WT, the greatest decrease in T_m value, 7.7°C, occurred between 50 and 300 mM NaCl. At salt concentrations between 300 and 1000 mM NaCl, Tm values decreased steadily, but by a smaller amount, 2.6°C. In contrast, both Arg mutants were much less stable than β-WT at low salt concentrations, with T_m values that were at least 8°C lower at 50 mM NaCl. At salt concentrations >300 mM NaCl, melting temperatures were 2°C lower for the Arg mutants than for β-WT. Similar results were obtained for β constructs used in subunit exchange kinetics below. For these clamps, additional mutations (S109C/Q299C/C260S/C333S) were introduced for site-specific fluorophore labeling. These mutations reduced the overall stability of the clamp such that T_m values are 8–10°C lower; however, the effect of the R103S mutation on protein stability in this background is similar to that in the wild-type β background (Fig. S2). In 50 mM NaCl, mutation of Arg-103 to Ser reduces the T_m by 6–8°C.These results support a role for electrostatic interactions in stabilizing the β clamp, and they show that mutation of positively charged Arg-103 and Arg-105 destabilizes the clamp, with destabilization being greatest at salt concentrations < 300 mM NaCl

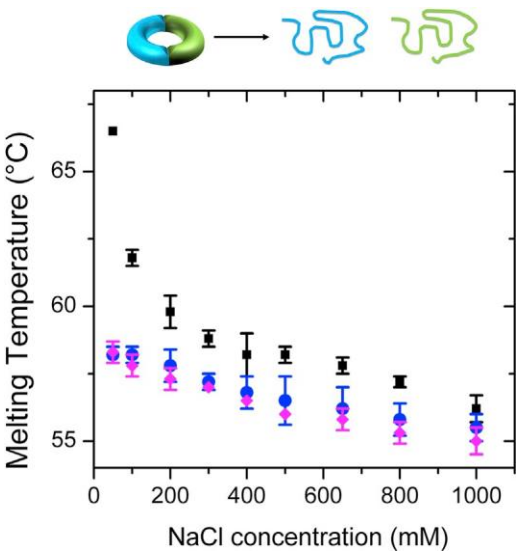

Figure 3.3 DSF was used to assess the relative stabilities of β-WT (black squares), and two Arg interface mutants, R103S (blue circles) and R105S (magenta diamonds). Melting curves and derivatives are provided in Fig. S3. Melting temperatures were measured by measuring the fluorescence of SYPRO Orange for samples containing 0.2 mg/mL protein at salt (NaCl) concentrations ranging from 0 to 1 M in 20 mM HEPES (pH 7.5)

3.10 β-subunit exchange kinetics

The experiments above show that electrostatic interactions contribute to β-dimer stability, and to quantify these effects, dimer dissociation rate constants were measured. The thermodynamic dissociation constant can be expressed as the ratio of the kinetic dissociation and association rate constants ($K_d = \frac{k_d}{k_a}$), where k_d^{-1} represents the lifetime of the dimer (τ_{dimer}) and is therefore a direct measure of the intrinsic stability of the clamp in the dimeric state. To measure k_d, a doubly labeled β-mutant was used in subunit exchange experiments, as described in previous work[25]. Two amino acid residues, Ser-109 and Gln-299 that are juxtaposed on opposite sides of the dimer interfaces (Fig. 3.1) were mutated to Cys and covalently labeled with TMR, a rhodamine dye that forms ground-state dimers with negligible fluorescence quantum yield and very short fluorescence lifetime. Therefore, significant fluorescence quenching is expected when the clamp interface is

closed. When the clamp dissociates into monomers, the fluorophores are separated, and fluorescence increases. We note that the crystal structure of the β-dimer doubly labeled with Alexa 488 (another rhodamine dye structurally similar to TMR) shows that the overall structure of the dimer interface is the same as in the WT protein.

The rate constant of dissociation of the dimeric clamp was obtained from the kinetics of subunit exchange between solutions of unlabeled (2 μM) and doubly labeled (400 nM) β-dimers. The doubly labeled proteins (β-S109C/Q299C-$(TMR)_2$ and β-S109C/Q299C/R103S-$(TMR)_2$) were mixed with the corresponding unlabeled proteins (β-WT or β-R103S, respectively) so that the residue Arg-103 was either present or absent in the interfaces of both the labeled and unlabeled proteins in the same solution. The labeled monomers formed upon spontaneous dissociation of a quenched, doubly labeled β-dimer are more likely to reassociate with the more concentrated unlabeled monomers, thus creating mixed dimers with bright TMR dyes. Dimer dissociation into monomers is much slower than monomer association to form dimers at protein concentrations much higher than the K_d, and therefore, under the conditions of this experiment, dimer dissociation is the rate-limiting step and the kinetic rate constant of the exchange reaction is therefore a direct measurement of k_d.

Subunit exchange results in an increase in both fluorescence intensity and lifetime, but lifetime measurements were favored in this work because they are less prone to artifacts over the many hours of the measurement (e.g., laser power fluctuations). Fluorescence decays were acquired at regular intervals for a period of ∼20 h, and then fitted globally with three lifetimes with time-dependent fractional contributions (see Materials and Methods). The longest lifetime ($\tau_1 \sim 2.7$ ns) is due to the bright TMR monomers, and

therefore, its fractional amplitude (α_1) is a direct measure of the concentration of mixed dimers containing one labeled and one unlabeled subunit. The shortest lifetime ($\tau_3 \sim 0.09$ ns) is due to the ground-state rhodamine dimers that form around each interface in the doubly labeled clamps, so its fractional amplitude (α_3) is proportional to the concentration of the doubly labeled dimers that remain in solution. As observed previously[25], the fractional contribution of the intermediate lifetime ($\tau_2 \sim 1$ ns) changes minimally during the exchange reaction and is also present in a singly labeled control sample, indicating that it likely reflects the effect of the protein environment on the photophysical properties of the dye. For this reason, the time-dependent changes of only α_1 and α_3 were considered in the kinetic analysis of the subunit exchange reaction.

The stabilities of two doubly labeled clamps—one with only the mutations required for fluorophore labeling, β-S109C/Q299-$(TMR)_2$ (see Table 1), and a second that also contained an Arg-103 to Ser mutation, β-S109C/ Q299/R103S-$(TMR)_2$—were compared. Arg-103 was mutated because this residue likely forms a salt bridge with Glu-304, and because Glu-304 is not accessible to water, this salt bridge is likely to be stronger than those that are solvent exposed[50]. Experiments with β-S109C/ Q299-$(TMR)_2$ in a buffer containing 50 mM NaCl show only small changes in the fluorescence decays over 15 h. The fractional amplitudes α_1 and α_3 obtained from fitting these data are shown in Fig. 3.4 (green symbols), and the small changes indicate that protein dimers do not spontaneously dissociate in these timescales at low salt concentrations. An exponential fit to the data gives $\tau_{dimer} = 34 \pm 18$ h, which represents an estimate due to the fact that the fitted lifetime is

twice as long as the duration of the experiment. This outcome is consistent with the results of the FCS experiments, which show negligible changes in

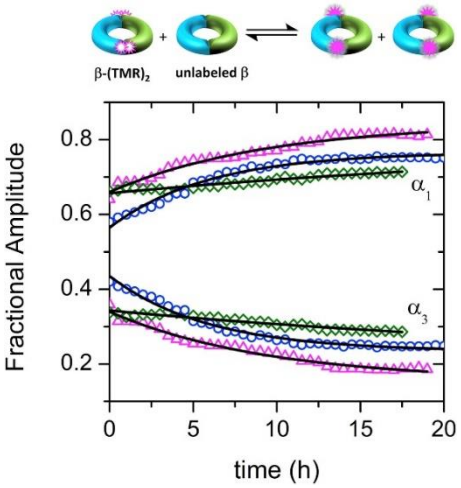

Figure 3.4 Results of the subunit exchange kinetic experiments between doubly TMR-labeled clamps (0.4 μM dimer) and unlabeled clamps (2 μM dimer). Fluorescence decays were measured at room temperature at regular intervals and fitted as described in Materials and Methods to obtain the fractional amplitudes of the unquenched (α_1) and the quenched (α_3) lifetimes. Fractional amplitudes are shown as a function of incubation time for β-S109C/Q299C-$(TMR)_2$ (green diamonds, 50 mM NaCl; magenta triangles, 500 mM NaCl), and β-S109C/Q299C/R103S-$(TMR)_2$ (blue circles, 50 mM NaCl). Assay buffer was 20 mM Tris-HCl (pH 7.5).

diffusion coefficient when a 1 nM solution of β-TMR equilibrated for 24 h. It also suggests that the presence of the second TMR label around the interface does not have a negative impact on the stability of the β-clamp interface. The same experiment in a buffer containing 500 mM NaCl shows a significant reduction of the lifetime of the dimer (τ_{dimer} = 9 ± 1 h; Fig. 3.4, magenta symbols), consistent with the nearly total dissociation observed in the FCS experiments with 1 nM samples and 500 mM NaCl over 24 h (Fig. 4.2 B). Because ions screen Coulombic interactions between charged amino acids, this result provides direct evidence that electrostatic interactions play an important role in stabilizing the β-clamp dimer interface (see Discussion). A similar reduction in the lifetime of the dimer

was observed in experiments with β-S109C/Q299/R103S- $(TMR)_2$ in low salt buffer (50 mM NaCl). In contrast to the experiments with β-S109C/Q299$(TMR)_2$, the protein lacking Arg 103 shows marked changes in α_1 and α_3, consistent with the formation of labeled-unlabeled mixed dimers over several hours (Fig. 3.4, blue symbols). An exponential fit to the data gives τ_{dimer} = 5.8 ± 0.3 h, indicating that the removal of Arg-103 reduces the intrinsic lifetime of the β-clamp dimer by about an order of magnitude.

3.11 β dimer interface conformational dynamics

It has been suggested that clamps open and close spontaneously in solution[51,2], and to test this hypothesis, a new set of FCS experiments were designed to measure potential conformational fluctuations around the clamp interface. In contrast to the experiments described in previous sections, which were designed to measure the diffusion coefficient of singly labeled clamps, the samples used in these new experiments were doubly labeled clamps similar to the ones used in the exchange kinetics experiments[described above. As discussed previously, the autocorrelation function acquired in FCS experiments with singly labeled clamps can be adequately fitted with Eq. 3.1, which describes the decay expected when fluorescence fluctuations are solely due to Brownian motion of the labeled proteins within the observation volume. The plateau up to ~ 40 μs observed in measurements with β-I305C-TMR (Fig. 3.5, magenta line) indicates that in these timescales, diffusion does not lead to significant changes in the positions of the protein particles in the observation volume, and therefore, it does not result in changes in the measured fluorescence intensity. Measurements with doubly labeled clamps, in contrast, cannot be adequately fitted with Eq. 3.1. This is evident from the different shape of these decays when compared to the decay measured with the singly labeled clamp. In particular, the decays measured with the

doubly labeled clamps show features in the microsecond timescale (up to ~ 40 μs) that are absent in measurements with the singly labeled clamps (Fig. 3.5). These features of the FCS decay indicate microsecond-time- scale fluorescence fluctuations that are not due to diffusion and are only present in the clamps containing two rhodamine chromophores in close proximity. Similar results were reported by McCann et al. in FCS studies aimed to characterize conformational fluctuations in tandem PDZ domains. In that article, the authors reported differences in the autocorrelation decays of TMR singly labeled and doubly labeled PDZ tandems, which were interpreted as arising from intramolecular protein dynamics in the micro- second timescale. However, the interpretation of the FCS autocorrelation curves obtained with doubly labeled proteins is not straightforward. The differences between the autocorrelation decays obtained with singly and doubly labeled proteins indicate that the microsecond-timescale fluctuations are due to the presence of two rhodamine chromophores in close proximity, but this does not necessarily indicate that the fluctuations in the fluorescence signal are due to dynamics in the protein. In the best case scenario, fluorescence fluctuations that do not exist in the singly labeled proteins are indicative of dynamic opening-closing motions of the rhodamine dyes, which are being brought into close proximity, or separated, by motions in the protein to which they are attached. This would indeed lead to fluorescence fluctuations that report on protein conformational dynamics. However, it is also possible that fluctuations are related to dynamics within the rhodamine dimers that do not involve protein motions. For example, it is possible that dyes are dynamic around their linkers, leading to different degrees of excitonic interactions depending on whether chromophore stacking is optimal or not. Single-moleculee work by Hernando et al[52] demonstrated that optimally stacked

chromophores are not fluorescent due to strong coupling, but more extended arrangements lead to weak coupling and less quenching. In the case of β, it is also possible that the microsecond-timescale fluctuations are indeed indicative of conformational motions in the protein, but these motions do not necessarily involve the opening of the clamp interface.

Three different doubly labeled clamps were investigated by FCS to further investigate the origin of the micro- second-timescale features observed in the autocorrelation decays: 1) β-R103C/I305C-$(TMR)_2$, 2) β-S181C/S356C-$(TMR)_2$, and 3) labeled β-WT (see below). The first contains TMR fluorophores on two amino acid residues (R103 and I305) that are juxtaposed on opposite sides of the protein dimer interface (Fig. 3.1). This construct was used in our previous work on clamp stability using lifetime measurements and FCS[25]. The second doubly labeled clamp contains the rhodamine dimers attached to amino residues 181 and 356, which are topologically equivalent to 103 and 305 except that they are part of the same chain and therefore, their relative distance is not affected by clamp opening (Fig. 3.1). The FCS decays of β-R103C/I305C- $(TMR)_2$ and β-S181C/S356C-$(TMR)_2$ are virtually identical (Fig. 3.5), indicating that the fluctuations observed in these FCS decays are not due to conformational fluctuations that involve a significant opening of the clamp interface. In addition, fluctuations in a similar timescale were observed in experiments with labeled β-WT. This construct was prepared by labeling the wild-type protein at native Cys residues. Wild-type β was previously reported to be site- specifically labeled at Cys-333[53], and it was intended to be a singly labeled control. However, labeled β-WT displays clear signatures of rhodamine dimers in the UV-Vis spectrum and fluorescence lifetime decay (Fig. S5). This suggests efficient labeling of the two solvent-exposed native cysteine residues C260 and C333, which are in close proximity in the

crystallographic structure (Fig. 3.1). Although the amplitude of the fast fluctuations was smaller for this sample, the fact that they were still observed supports the conclusion that the fluctuations observed in this set of experiments do not originate from conformational dynamics around the interface. Although it is certainly possible that the observed fluorescence fluctuations in all three doubly labeled samples are due to motions in the protein that affect the stacking of the two rhodamine molecules, we cannot rule out alternative models that involve photophysical effects that do not correlate with protein dynamics. A thorough photophysical characterization of the properties of rhodamine dimers in protein environments would be necessary to address this possibility, but that is beyond the scope of this work.

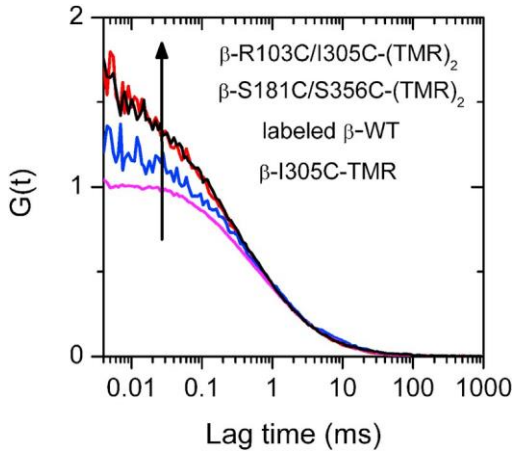

Figure 3.5 Autocorrelation decays obtained in FCS experiments with a singly labeled sample, β-I305C-TMR (magenta) and three doubly labeled clamps, β-R103C/I305C-$(TMR)_2$ (red), β-S181C/S356C-$(TMR)_2$ (black) and labeled β-WT (blue). The amplitudes were arbitrarily multiplied by a constant to match the curves in the millisecond timescale to emphasize the differences at shorter timescales.

3.12 Discussion

The overarching objective of this research is to determine how the clamp stability contributes to the clamp-opening stage of the clamp-loading reaction. The rationale for this work is that if clamp-loader-catalyzed clamp opening depends on the ease with which the

clamp opens, then conditions that destabilize the clamp would promote clamp-loader-catalyzed clamp opening. In this work, we report the results of experiments aimed to characterize the factors that contribute to stability of the dimer interfaces in the closed conformation and whether clamp dynamics contribute to the formation of the open conformation. The question of how clamp stability and dynamics correlate with clamp-loader-catalyzed ring opening is addressed in ongoing research and will be published elsewhere.

Previous work along with the structure of the β sliding clamp suggested that electrostatic interactions may contribute to the stability of the dimeric form of the clamp[50,25,54]. Charged amino acid residues at the β dimer interface are arranged such that positively charged amino acid residues are on one side and negatively charged residues are on the other side (Fig. 3.1). At least three salt bridges may form: Lys-74 is in position to interact with Glu-300 or Glu-298, Arg-105 with Glu-301 or Glu-303, and Arg-103 with Glu-304 or Asp-307. When the clamp is opened by the clamp loader, the clamp adopts an out-of-plane conformation where the domains twist relative to one another[55]. Perhaps, alignment of one positively charged amino acid residue with two negatively charged amino acid residues allows positively charged residues to swap interaction partners at the closed clamp interface when the clamp loader opens the opposite interface[56].

Intuitively, it can be expected that salt bridges always contribute favorably to the stability of proteins and protein-protein interfaces, but computational and experimental evidence shows that salt bridges can be stabilizing or destabilizing[57,58]. The favorable Coulombic interactions between amino acids of opposite charge can be overcome by the unfavorable desolvation energy associated with the burial of the charges[58-60]. Here, we showed that

either mutation of Arg residues or high NaCl concentrations destabilizes the clamp to increase the population of monomers in equilibrium and to decrease the Tm value for the protein. The measured apparent diffusion times of 1 nM solutions of β-clamps in low salt buffers show that dimers are stable over 24 h when a surface-exposed hydrophilic (Ser-109) or hydrophobic (Ile-305) amino acid at the interface is mutated to Cys. Increasing the ionic strength of the solution by the addition of NaCl results in increasingly large fractions of monomers present when equilibrated solutions of these mutants are measured at 24 h. Deprotonation of one or more residues at basic pH values further destabilize the clamps. The subunit exchange experiments with β-S109C/Q299-$(TMR)_2$ further indicate that the dissociation rate constant of dimer (k_d) is also greatly affected by salt concentration. The reciprocal of k_d, which is a direct measure of the lifetime of the dimeric clamp, decreases from 34 ± 18 h at 50 mM NaCl to 9 ± 1 h at 500 mM NaCl. This results in a concurrent increase in the dissociation equilibrium constant of the clamp, which leads to significant dissociation, as observed in the FCS experiments. We note that we previously reported a lifetime of 43 ± 3 h obtained from similar exchange experiments performed with β-R103C/I305C-$(TMR)_2$ and β-WT in a 1:5 ratio in 50 mM NaCl. As in the case of β-S109C/Q299$(TMR)_2$, this value is longer than the duration of the experiment and should therefore be taken as an estimate. The β-R103C/I305C-$(TMR)_2$ construct contains an R103C mutation for labeling, which in light of our new studies likely weakens the dimer interface and can be therefore expected to accelerate subunit exchange kinetics. However, because the majority of the protein in this experiment was unlabeled β-WT (fivefold excess), the kinetics of subunit exchange measured in this experiment was limited by dissociation of protein dimers not containing mutations or labels. This explains why the

results of our previous work are consistent with the new experiments with β-S109C/Q299C-$(TMR)_2$, which contains the native Arg-103 residue at the interface, and different from the results obtained with β-S109C/Q299C/R103S-$(TMR)_2$, which was mixed with unlabeled protein also containing the R103S mutation.

The results discussed above support the hypothesis that one or more salt bridges at the interface contribute to the remarkable stability of the dimeric ring at 50 mM salt. High concentrations of salt decrease the effective electrostatic interactions between amino acids of opposite charge due to screening effects, resulting in faster dissociation rates and higher dissociation equilibrium constants. To a first approximation, screening effects can be modeled using Debye-Hückel's limiting law, which predicts a linear relationship between the logarithm of the dissociation constant and the square root of the ionic strength of the solution[61]. On the other hand, the stabilizing and destabilizing effects of chaotropic and kosmotropic salts lead to a linear dependence of $\log(K_d)$ with salt concentration[62,63]. To test these models, the data obtained with β-I305C-TMR and reported in Fig. 3.2 A were further analyzed to obtain dissociation constants. The fraction of monomers and dimers present in equilibrium at each salt concentration was calculated from the measured values of the apparent diffusion times as described in previous work and summarized in the Supporting Material[46]. Briefly, the apparent diffusion time of an equilibrated sample (plotted in Fig. 3.2 A) of a dimeric protein depends on the degree of dissociation of the protein and the diffusion times of the pure dimers and monomers. The relative contribution of each species to the apparent diffusion time takes into account the fact that dimers are twice as bright. The diffusion time of the pure dimer (τ_2) was taken as the value measured immediately after dilution (t = 0), and the diffusion time of the pure monomer was calculated as $\tau_2 = 2^{1/3}$

τ_1, which is very close to the value measured at the highest salt concentration. Equilibrium dissociation constants were then calculated from the fractions of monomers and dimers in equilibrium. The observed increase of K_d with NaCl concentration is consistent with the presence of stabilizing electrostatic interactions in the clamp surface. Furthermore, Fig. 3.6 shows that our data are in excellent agreement with Debye- Hückel's model, suggesting that the effect of salt on the measured K_d values can be interpreted in terms of electrostatic screening of interactions between amino acids of opposite charge in the protein interface. The fact that a linear relationship is observed even at relatively high NaCl concentrations is somewhat surprising, but we note that similar observations were reported by de los Rios and Plaxco [62] in a study of electrostatic effects in the folding of a simple two-state protein. As the authors discuss in this work, published data on salt-dependent equilibrium folding of many other proteins suggests that the observed linearity at high NaCl concentrations may be a general phenomenon. Here, we deliberately chose NaCl because its ions lie in the middle of the Hofmeister series and are therefore relatively nonchaotropic and nonkosmotropic [64]. This minimizes specific interactions between ions and amino acids that would confound the effects of ionic strength. A rigorous test of the Debye-Hückel model would require proof that the increase of K_d with salt concentration correlates exclusively with ionic strength independent of the nature of the ion. In support of that theory, experiments with KCl and β-I305C-TMR show that the degree of dissociation does not change when Na^+ is substituted by K^+ (Fig. S6). Unfortunately, experiments with multivalent cations (e.g., Mg^{2+}) or ions (e.g., PO_4^{3-}) are not viable in this case, because ions

with high charge density are kosmotropes [64], so their effect on protein stability is expected to be significantly more complex than that predicted by the Debye-Hückel model.

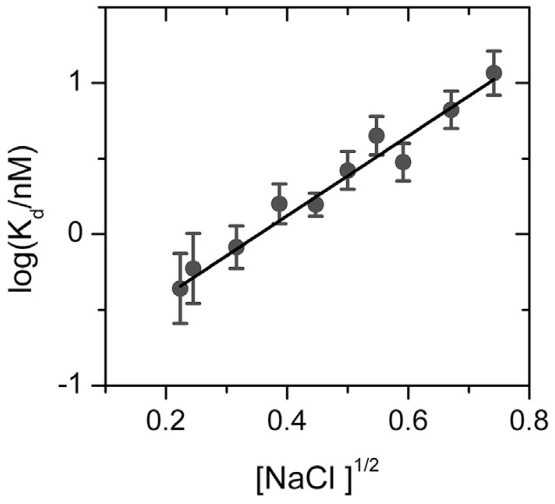

Figure 3.6 Equilibrium dissociation constants of the Ile-305 mutant plotted in logarithmic scale as a function of the square root of the molar concentration of NaCl present in the buffer. Equilibrium constants were calculated from the data of Fig. 3.2, A and B, for β-I305C-TMR as described in the text and in the Supporting Material.

Our measurements with NaCl and KCl are in excellent quantitative agreement with Debye-Hückel's model and therefore, with the interpretation that the observed salt effects are due to simple screening of charge-charge interactions at the interface. The experiments with the β-mutant that converted the charged amino acid residue Arg-103 to Cys further validate this analysis. This mutant dissociates with a relaxation time of 5.8 h at low salt (50 mM), which results in complete dissociation of the dimer when 1 nM solutions of clamps are incubated for 24 h at room temperature. Any remaining ionic interactions are further weakened by the addition of NaCl, and at 500 mM NaCl, the clamp dissociates within minutes, so that the acquisition of an FCS decay of pure dimers is not possible. Therefore, experiments with this mutant indicate that Arg-103 is involved in stabilizing electrostatic

interactions that are weakened when the ionic strength of the solution increases, resulting in a salt-concentration-dependent dissociation equilibrium constant that follows Debye-Hückel's limiting law.

The FCS experiments with doubly labeled clamps were designed to investigate potential conformational fluctuations around the clamp interface. The α-carbon atoms of residues 103 and 305 are located at a distance of 5.5 Å around the dimer interface (Fig. 3.1), and rhodamine self-quenching requires efficient stacking that occurs at distances < 1 nm. Therefore, significant conformational fluctuations in the protein around the interface would result in fluorescence fluctuations only when the dyes are placed around the interface, as in β-R103C/I305C-$(TMR)_2$ but not β-S181C/S356C-$(TMR)_2$. Because all three investigated doubly labeled clamps displayed similar behavior in the FCS experiments, we conclude that clamps are not significantly dynamic around the interface in the timescales of these experiments (microseconds to milliseconds). These experiments do not allow us to rule out conformational fluctuations in timescales shorter than microseconds, short-scale conformational fluctuations that do not disrupt rhodamine-rhodamine stacking or very rare events that result in negligible fractions of open states. The remarkably low dissociation rates of the dimeric clamps suggest, in fact, that conformational changes that open the interface should be rare. Beuning and colleagues[2] reported hydrogen- exchange studies that revealed local unfolding of portions of all three domains of the ring. In that study, the authors reported EX1 kinetics consistent with cooperative unfolding events that allow multiple amide hydrogens to exchange simultaneously. EX1 kinetics was observed in all three domains, but preferentially in domain 1, which contains the positively charged amino acids located in the interface (Fig. 3.1 A). The half-life for deuterium uptake in these

peptides was 3.5 h, which suggests that the conformational changes that expose the amino acids that are involved in hydrogen exchange are indeed rare.

The fluorescence fluctuations detected in FCS may reflect global conformational fluctuations that result in transient quenching and unquenching of the rhodamine dimers in all positions, but we cannot rule out bright-dark transitions in the rhodamine dimers that do not involve changes in the conformation of the protein. These could involve local motions of the fluorophores around their linkers, or transitions to non-fluorescent states in the rhodamine dimers that do not necessarily involve the unstacking of the ground-state dimer. More experiments, beyond the scope of this work, would be needed to discriminate between these possibilities. In summary, our data are not enough to discriminate among the different scenarios that can potentially lead to the fluorescence fluctuations observed at time- scales faster than diffusion, but results are inconsistent with the hypothesis that the interface is significantly dynamic in the microsecond-millisecond timescales.

CHAPTER 4

Potassium Glutamate and Glycine Betaine induce the self-assembly of sliding clamps into higher-order oligomers

4.1 Introduction

In our previous work, we characterized the stability of the clamp protein in low (50 mM) and high (1 M) NaCl concentrations. We observed that in NaCl concentration > 150 mM, 1 nM clamp dimer dissociates into monomers. The effect of salts on protein stabilization or destabilization has been studied extensively for decades. Salt effects on proteins and other biopolymers arise from the net accumulation or exclusion of the ions from the protein surface. In the previous work[27], Cheng et al. showed that the favorable or unfavorable interactions between solute and the six functional groups present in the protein surface decide the stability of the protein structure. At salt concentrations below 100 mM, protein-ion interactions are typically governed by nonspecific electrostatic effects[65], and their sensitivity to salt concentrations can be described in terms of charge screening models[66]. In this research, we studied the impact of KGlu and glycine betaine on the stability of β clamp and PCNA in solution. It is widely studied that KGlu is the most abundant ion present in the *E. coli* cytoplasm[67] (100 mM-300 mM).

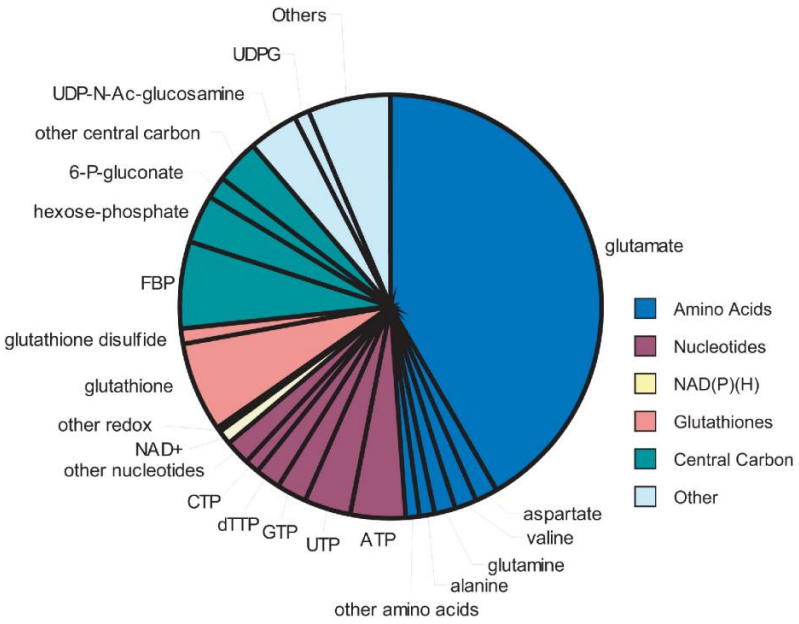

Figure 4.1 KGlu is the most abundant metabolite present in the *E. coli* cytoplasm.

KGlu accumulates at high concentrations in response to the osmotic stress in *E. coli*. Hence, we decided to investigate the stability of both clamp proteins in KGlu. We observed that KGlu not only prevents clamp dissociation; instead, it promotes the clamp association to form a larger assembly. We quantified the effect of KGlu on protein stability and also proposed a thermodynamic model to explain the molecular mechanism of KGlu interaction with the protein surface.

Materials and Methods

4.2 Purification of β and PCNA

Both the proteins β and PCNA contain wild type cysteine residues in their structures. Therefore, to create samples for FCS measurements that contain a single cysteine residue, surface cysteine residues (Cys-333, Cys-260 in β and Cys-22, Cys-62 Cys-81 in PCNA) were converted to serine. To label the clamps site specifically, Ser109 or Ile-305 were mutated to Cys in β, and Ile-181 was mutated to Cys in PCNA by using site-directed

mutagenesis (Quickchange mutagenesis kit) of the coding sequences of these two proteins. Clamp proteins were overexpressed in *E. coli* DE3 cells. These cells were l at 37 ºC until O.D reaches 0.6 at excitation wavelength 600 nm. After that, the temperature was reduced to 15 ºC, and protein expression was initiated by adding isopropyl β-D-1-thiogalactopyranoside (IPTG). The final concentration of IPTG was around 1 mM. Proteins were purified at 4 ºC. Cells were lysed using the French press technique, which disrupts the plasma membrane by passing them through a high-pressure valve. The cell lysate was clarified by centrifugation. Ammonium sulfate (0.2 g/ml) was added to the lysate, and the precipitate was discarded. Additional ammonium sulfate (0.15 g/ml) was added to the supernatant, and the precipitate was recovered by centrifugation. The pellet was resuspended and dialyzed in Buffer B, containing 10% glycerol. The dialyzed protein was loaded onto two 5 ml HiTrap Q-Sepharose columns in tandem (GE Healthcare) and eluted with a linear gradient of 50–700 mM NaCl. Purified proteins were then dialyzed against Buffer A and stored at -80 ºC.

4.3 Fluorescent labeling of β and PCNA

Both β and PCNA were labeled with TMR (Molecular Probes, Invitrogen)[68]. Two β mutants S109C and I305C were labeled with Alexa dye separately. Maleimides are electrophilic compounds that show high selectivity for the thiol group. Cysteine residues in the protein structure contain a thiol group in it. Thiols are prone to oxidative dimerization with the formation of disulfide bonds. Cysteine residues thus form disulfide bridges, which stabilize tertiary protein structures. Disulfides do not react with maleimides. Therefore, it is necessary to reduce disulfides prior to the conjugation and to exclude oxygen from the reaction. Sliding clamps (2 mg) were incubated in the dark with 20 equivalents of

fluorophore per cysteine residue for 2 h at room temperature followed by 4 °C overnight in a buffered solution containing 1 mM TCEP and 8% dimethyl sulfoxide. Buffer solutions contained 20 mM Tris–HCl (pH 7.5) and 0.5 mM ethylenediaminetetraacetic acid (EDTA) for β or 30 mM 4-(2-Hydroxyethyl)-1-piperazineethanesulfonic acid (HEPES, pH 7.5), 0.5 mM EDTA and 150 mM NaCl for PCNA. Labeled protein was separated from excess fluorophore by gel filtration chromatography using Bio-Gel P-6DG (Bio-Rad) desalting resin. Proteins were further purified by anion exchange chromatography on a 1ml HiTrap Q-Sepharose column (GE Healthcare). β was eluted with a linear gradient of 0.1–1 M NaCl in buffer containing 20 mM Tris–HCl (pH 7.5) and 0.5 mM EDTA. PCNA was eluted with a linear gradient of 0.15–1 M NaCl in buffer containing 30 mM HEPES (pH 7.5) and 0.5 mM EDTA. Proteins were dialyzed overnight against 20 mM Tris–HCl (pH 7.5), 0.5 mM EDTA and 10% glycerol for β and 30 mM HEPES (pH 7.5), 0.5 mM EDTA, 150 mM NaCl, 2 mM DTT (dithiothreitol), and 10% glycerol for PCNA. Proteins were aliquoted and stored at −80 °C. The protein concentrations were determined by a Bradford-type Assay (Bio-Rad) using native β or PCNA standards quantified by denatured A280. The concentration of TMR was calculated from the absorbance measured at 555 nm using an extinction coefficient of 98,000 M^{-1} cm^{-1}. The concentration of Alexa was calculated from the absorbance measured at 556 nm using an extinction coefficient of 104,000 M^{-1} cm^{-1}. Both PCNA and β were labeled at one site per subunit at positions I181C and I305C, respectively. Labeling efficiencies for different mutants are as follows: β I305C TMR (116%), β S109C TMR (50%), β I305C Alexa (106%) and PCNA I181C (80%).

4.4 FCS measurements

Fluorescence Correlation Spectroscopy (FCS) provides information about both kinetic and thermodynamic properties of fluorescent molecules in solution. In this study, we used the FCS technique to investigate the oligomerization process of protein molecules labeled with dye. A 532 nm CW laser (Coherent Compass 215M-10, Santa Clara, CA, USA) was focused on the protein sample using a 1.4 NA objective lens(Olympus PlanApo 100X/1.4 NA oil). The laser power used for this study was 110 μW. The set up has a very sensitive APD detector (Perkin-Elmer-Optoelectronics, SPCM-AQR14) that records the fluorescence coming from the dye-labeled protein sample through a pinhole (50 μm) assembly that creates a confocal volume of ~ 5 fl. The fluorescent fluctuations originate from the Brownian motion of the dye-labeled protein molecules in the observable volume. The autocorrelation function facilitates to transform this fluctuation data into time-correlated decay. The clean coverslips and sample chamber are required for the FCS measurements. We put coverslips on a tray and place it in the ozone gas apparatus for 10 minutes. Then flip the coverslips over and place the tray back in the machine for another 10 minutes. After both sides of the coverslips have been cleaned, we turn off the instrument and the ozone gas flow. Then we place the coverslips in a container and then fill it with a 3% Hellmanex solution. We sonicate the container for 40-45 minutes. After that, we pour Hellmanex out of the container and rinse the container multiple times with nanopore water to get rid of any residual Hellmanex. In the end, we dry the coverslips with nitrogen gas. Once the coverslips are ready, we keep them in a box for future use. We place the coverslip on the top of the objective. A sample chamber is placed on the surface of the coverslip. We put ~50 μl sample solution in the chamber.

We used 1nM labeled protein sample prepared in a buffer solution containing 20 mM Tris-HCl and pH 7.2. The protein sample we used for FCS measurements is singly labeled, which means each monomer is labeled with one dye molecule at its interface. To study the salt effect on protein oligomerization, various concentrations of potassium glutamate and glycine betaine were used. We added 50 µl of 1 nM protein sample to the sample chamber and acquired data. The stock protein sample was first diluted to 200 nM with Tris buffer. Then it was further diluted to 1 nM (final concentration) in 200 µl total sample volume in an Eppendorf. We mixed the sample thoroughly with a pipette before we added it to the sample chamber. For the experiments to check the effect of salt in higher protein concentration, we mixed variable concentrations of unlabeled protein to achieve total concentrations in the 1 nM-1 µM range without varying salt concentration.

4.5 Analysis of FCS data

The theory behind the FCS technique is based on Poisson statistics. The Poisson distribution states that the probability P(*n*) of finding n molecules in an observable volume depends on *n* and the average number of molecules *N* in the observable volume as shown in Equation:

$$P(n) = \frac{N^n}{n!} e^{-N} \tag{4.1}$$

For a 1 nM sample solution, if the observable volume is 1 fl, the average number of molecules is 0.6. The probability of finding molecules are P(0) = 0.55, P(1) = 0.33, P(2) = 0.1. Hence, with the higher the value of n, the probability of finding molecules becomes less. The more molecules are in the observable volume smaller the change in the fluctuations in the fluorescence intensity. The standard deviation of the Poisson distribution

is $\sqrt{n}$, suggests when the concentration is too high, the fluctuations will be no longer detectable in FCS measurement. Thus, for FCS measurements, we use 10 pM to about 50 nM.

The correlation between two fluorescence intensity peaks, at time *t* and $t + \tau$, is compared depending on how quickly a fluorescent-labeled molecule diffuses within the observable volume. Mathematically, the autocorrelation function is calculated from the product of the average values of two intensities and then normalized by the average intensity squared as shown in Equation:

$$G(\tau) = \frac{\langle I(t) \cdot I(t+\tau) \rangle}{\langle I(t) \rangle^2} \tag{4.2}$$

The brightness (*B*) of the fluorophore is also an essential parameter in determining the correlation of fluorescence fluctuations. The brightness (*B*) is the number of photons per second for a single fluorophore observed. It is not a molecular property like quantum yield, but it depends on the photon collection efficiency of the instrument and the counting efficiency of the APD detector. The autocorrelation function for monodisperse sample diffusing freely in the solution can be expressed as Equation:

$$G(\tau) = \frac{1}{\langle N \rangle} \frac{1}{1+\frac{\tau}{\tau_{app}}} \tag{4.3}$$

Where $\langle N \rangle^{-1}$ is the mean number of fluorophores present in the observable volume, τ is the correlation lag time, and τ_D is the characteristic diffusion time. The above equation is valid when the axial dimension of the observable volume is much larger than its radial dimension.

In the case of a polydisperse solution, the total autocorrelation function can be written as the sum of individual components weighted by the square of the brightness of each particle:

$$G(\tau) = \frac{\sum_{i=1}^{n} B_i^2 N_i \left(1+{}^{\tau}/_{\tau_{D_i}}\right)^{-1}}{\left(\sum_{i=1}^{n} B_i N_i\right)^2} \quad (4.4)$$

We used the FCS technique to determine the diffusion times of protein molecules to investigate their oligomerization kinetics. The diffusion times indicate the size of a fluorescent-labeled protein molecule and how fast it diffuses through the observable volume. The diffusion time increases if the proteins oligomerize and build higher-order structures from monomers.

4.6 UV-VIS measurements

We also performed UV-Vis measurements to investigate the effect of potassium glutamate on protein oligomerization. For UV-Vis measurements, we used 1 μM of labeled proteins (β I305C and PCNAI181C) in the cuvette and kept adding potassium glutamate salt to achieve the final concentrations from 50 mM to 1 M. The protein stock was diluted to 1 μM with a buffer containing 20 mM Tris-HCl pH 7.2. We kept protein concentration fixed at 1 μM in the cuvette for various potassium glutamate concentrations from 50 mM -1 M.

Results and discussion

4.7 KGlu promotes clamp association

Our previous research showed that in low NaCl concentration(50 mM), 1 nM β clamp dimer is highly stable, but at high NaCl concentration (1 M) β clamp dimer dissociates into monomers. This indicates that the equilibrium dissociation constant (K_d) of clamp protein also increases in higher NaCl concentration. We also recorded a similar result with KCl. We observed that the logarithm of K_d value increases linearly with the square root of the molar concentration. This is consistent with Debye-Hückel's law of simple charge-charge interactions. However, with KGlu salt, we observed clamp association for β-I305C-TMR

instead of clamp dissociation. Potassium glutamate (KGlu) is the most abundant and low molecular weight metabolite present in the cytoplasm of *E. coli*. In a previous study, it was also reported that when they replaced KCl by KGlu, later stabilized protein-nucleic acid complexes[69]. We thought it would be interesting to investigate the effect of KGlu on the stability of the clamp protein. We used Fluorescence Correlation Spectroscopy (FCS) to determine the change in the apparent diffusion time (τ_{app})[70] with increasing KGlu concentration (50 mM-1 M). We observed that unlike NaCl, KGlu salt not only prevents the dissociation of the clamp protein; instead, it promotes the clamp association. Hence, the apparent diffusion time (τ_{app}) increases with KGlu concentrations (50 mM – 1 M), as shown in (**Figure 4.2**).

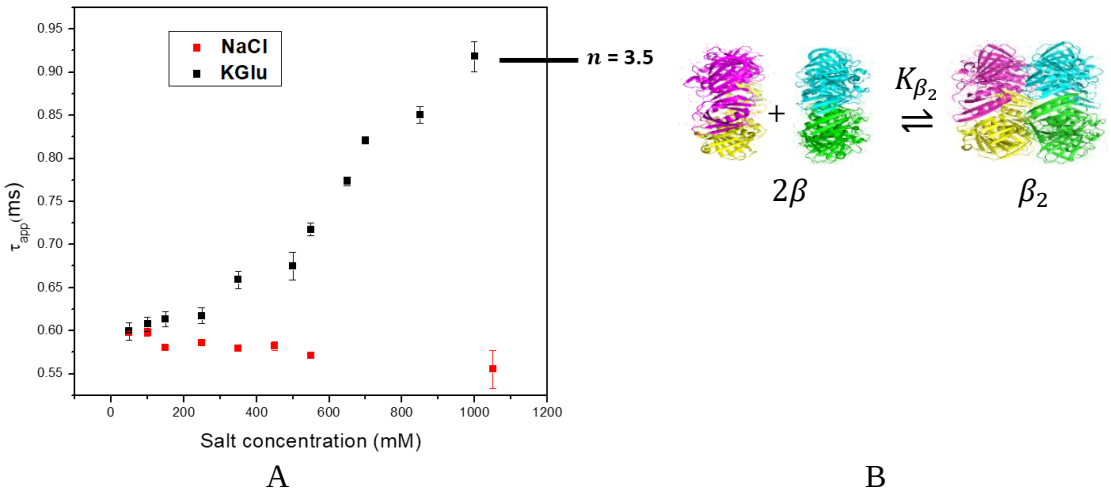

Figure 4.2 (A) Apparent diffusion times (τ_{app}) obtained from the FCS decays measured with 1 nM solutions of β -I305C-TMR in an assay buffer containing 20 mM Tris-HCl pH 7.2 and NaCl or KGlu varies from 50 mM-1 M. The n value denotes the number of protein dimer present in the assembly (B) The equilibrium kinetics of β clamp assembly formation, where K_{β_2} is the equilibrium association constant. The images of crystal structures were made using PyMol.

The strategy of measuring apparent diffusion time to investigate the effect of salt on protein stability has already been discussed in chapter 2 in detail. Here, we will discuss how the diffusion times are related to the size of the protein. In the protein solution, there are different sizes of protein species present, and they all contribute to the FCS decay. However, FCS decay was fitted with a single diffusion time, which we all apparent diffusion time (τ_{app}). The apparent diffusion time depends on the fractional concentrations of labeled oligomers, their diffusion coefficients, and relative brightness. We used 20 mM Tris-HCl in the solution made sure it doesn't change the viscosity of the medium. The apparent diffusion times (τ_{app}) were determined using a mathematical treatment[46] by David Kanno and Dr. Marcia Levitus (published in 2014). The mathematical calculations of apparent diffusion times (τ_{app}) are already explained in detail in chapter 2. The increase in

τ_{app} indicates that KGlu is inducing to form homo-oligomers of β clamp. We also used a protein sample (I305C) labeled with Alexa 546 beside TMR labeled sample. Alexa 546 is bulkier in size, and it has a long aliphatic chain along with sulphonic groups which prevent this dye to aggregate in the solution. However, we observed a similar increase in τ_{app} for both labeled proteins indicating that Alexa 546 did not interfere in clamp assembly.

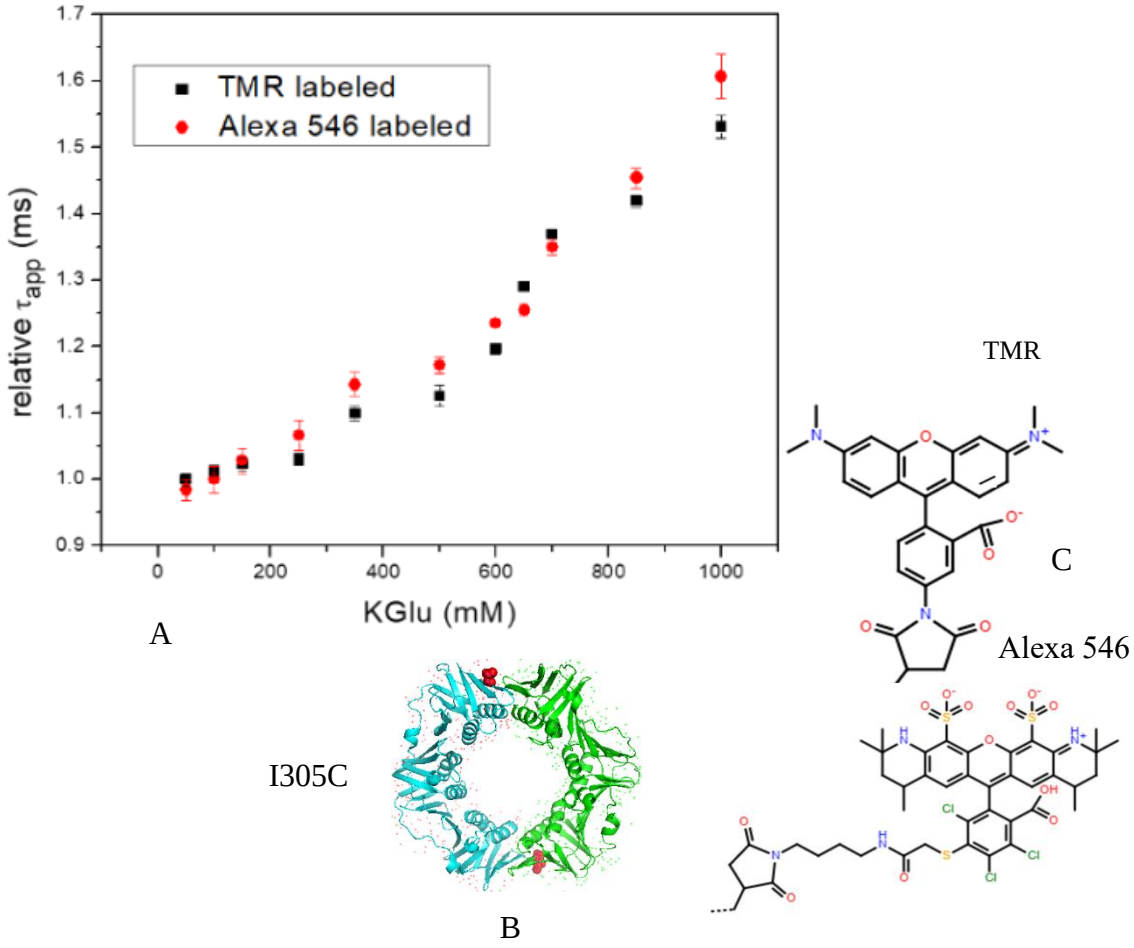

Figure 4.3 (A) Apparent diffusion times (τ_{app}) were normalized to the initial value measured with 1 nM β-I305C-TMR and β-I305C-Alexa (B) Crystallographic structure of the protein sample (β-I305C-TMR/Alexa) used for this study. The image was created using PyMol. The dye position is the same for both samples. (C) The structures of TMR-maleimide and Alexa 546 dye.

We also investigated the clamp association in KGlu, among other mutants. Two different protein mutants labeled at C333 and S109C.

I305C S109C R103C

Figure 4.4 The crystal structures of the β clamp with different mutations. TMR dye is labeled at I305, S109, and C333 positions, respectively.

The locations of these mutations are different in the protein structure. However, we still recorded a similar increase in diffusion times for each of these mutants, which indicates that the clamp association solely depends on KGlu concentration.

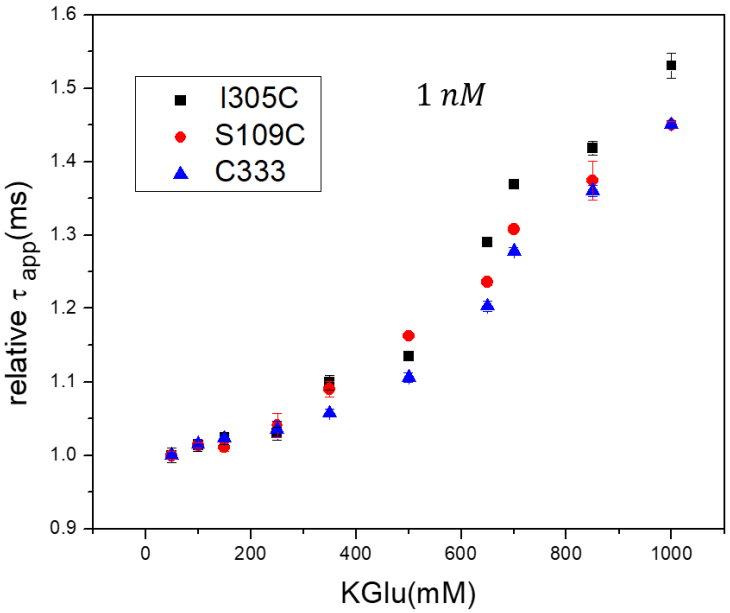

Figure 4.5 Apparent diffusion times (τ_{app}) are normalized to the initial value for measurements with 1nM β-I305C-TMR, β- S109C-TMR, and β-C333-TMR.

We performed control experiments to make sure the effect of KGlu is real. We investigated the impact on clamp association in NaGlu. The idea behind this was to replace the K^+ by Na^+ and confirm that the clamp association is solely an effect due to Glu^-. Figure 4.6 shows that both KGlu and NaGlu are showing a similar impact on clamp oligomerization.

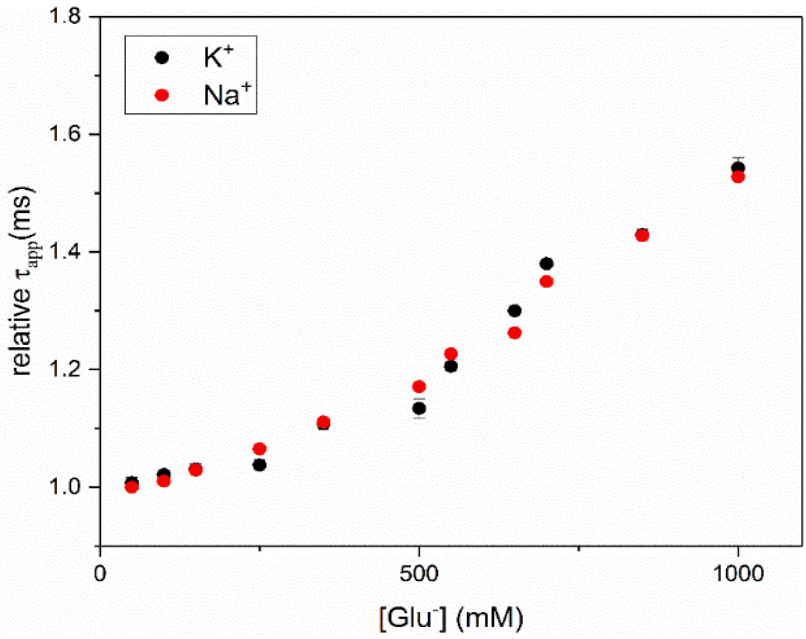

Figure 4.6 Apparent diffusion times (τ_{app}) (normalized to the initial value measured in KGlu reported in Figure 4.2A) and in NaGlu.

4.8 β clamp oligomerization is a reversible process

We noticed that from 50 mM- 1M KGlu, the clamp is associating. Hence, we wanted to check if the oligomerization process is reversible. We started with 200 nM β-I305C-TMR in 1 M KGlu and then did 200-fold dilutions to reach 1 nM labeled protein in different KGlu concentrations (1 M -10 mM). We found that in both directions from low to high (50 mM – 1 M) and high to low (1 M -10 mM) KGlu concentrations, the values of apparent diffusion times are similar. Hence, we can infer that the oligomerization process is solely dependent on KGlu concentration.

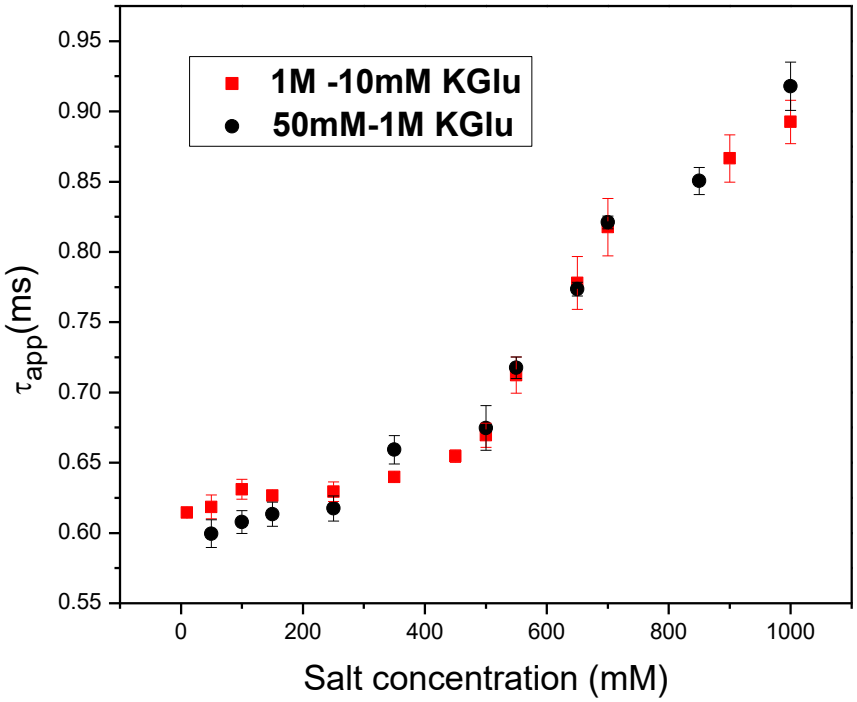

Figure 4.7 Apparent diffusion times (τ_{app}) were measured for β-I305C-TMR by removing KGlu from the sample solution (red). The β clamp sample was made in high KGlu (1 M) and then diluted to 10 mM KGlu, keeping the labeled protein concentration fixed at 1 nM. For the experiment in black (reported in Figure 4.2A), the protein was diluted from the stock containing no KGlu into a buffer containing a calculated amount of KGlu in it.

4.9 Clamp association increases with clamp concentration

In the last experiment, we saw that clamp association occurs even at 1nM concentration at high KGlu, which made us think that if we fix the KGlu concentration and increase the protein concentration, that would give us even bigger clamp assembly. We saw exactly similar results during our measurements. However, we increased the protein concentration by adding the unlabeled WT protein with 1 nM labeled protein to achieve final concentrations (1 nM – 1 μM) because the FCS measurements require labeled protein concentration between 1 nM – 100 nM. The idea of adding unlabeled protein to the labeled protein concentration helped us to keep the labeled protein concentration fixed, and the

average number of labeled rings in the clamp assembly remains low, which avoids the formation of very bright oligomers. The number of dimer rings comes together to form an oligomer was calculated using this Equation ($\tau_{app} = 0.6\, n^{1/3}$) where n denotes the number of the rings in the clamp assembly, the diffusion time for a single dimer ring is 0.6 ms and the τ_{app} is the measured diffusion time at a given KGlu concentration. As we can observe in Figure 4.8, *n* value increases with both the KGlu concentration and total protein concentration (except for 10 mM KGlu).

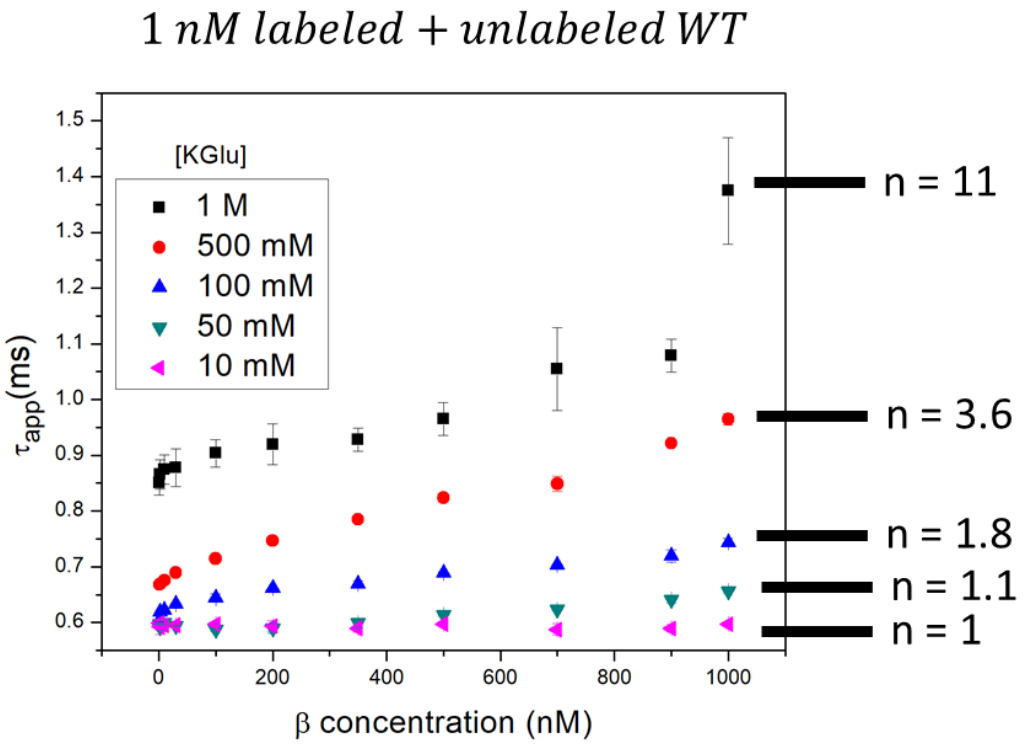

Figure 4.8 Apparent diffusion times were measured with 1 nM - 1 μM total protein concentration, keeping labeled β-I305C-TMR concentration at 1 nM. Unlabeled WT protein was added to achieve the final concentrations. The buffer condition is 20 mM Tris-HCl pH 7.2.

4.10 Dimer rings interact face to face to form a bigger clamp assembly

It was confirmed from the FCS study that dimer rings are coming together to form a bigger assembly. However, the mechanism was still unknown how dimers are interacting with each other to create that big complex. Hence, we decided to do UV-Vis measurements with 1 µM of labeled protein in different KGlu concentrations (50 mM – 1 M) to check if we are getting any change in the UV-vis spectra. We observed that the intensity of the peak at 520 nm of the TMR dye increases with KGlu concentration starting from 350 mM to 1 M. This can only happen when two TMR dye molecules come close to each other in such a way that their transitional dipole moments are parallel to each other and perpendicular to the vector connecting two dyes. It is known as H dimer[71]. The dimer rings can interact with each other in different ways, but the only way the dye molecules can form an H dimer is when dimer rings stack up on top of each other in the face to face fashion, as shown in (Figure 4.9)

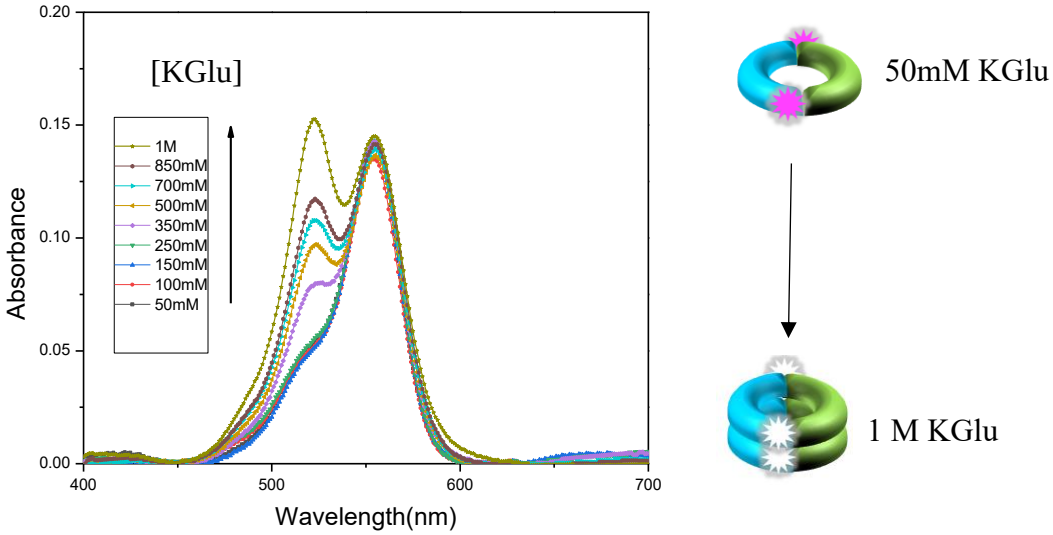

Figure 4.9 A. UV-Vis measurements of 1 µM β-I305C-TMR in Tris-HCl buffer with 50 mM-1 M KGlu in the cuvette B. TMR H dimer is forming at higher KGlu concentrations.

However, in UV-Vis experiments, we did not see any change in 520 nm peak between 50 mM to 250 mM KGlu concentration. This can be explained with the fact that up to 250mM KGlu, there's not enough amount of clamp stacked up to show the change in the UV-Vis spectra. We also performed a control experiment with 1 μM free TMR dye in 50 mM and 1 M KGlu to make sure that it is not the property of the TMR dye to form an H dimer at high KGlu concentration. We observed no change in the 520 nm peak intensity between 50 mM and 1 M KGlu.

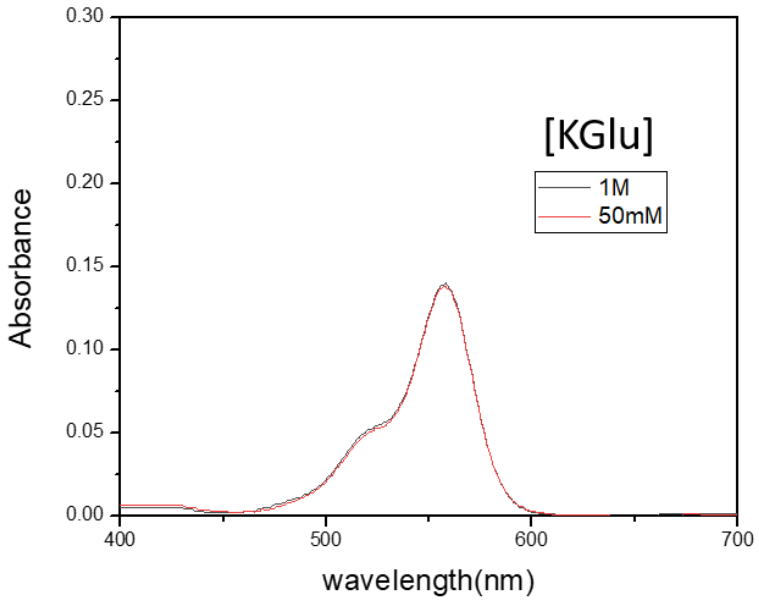

Figure 4.10 A control experiment was performed to measure the absorbance spectra of 1 μM free TMR dye with 50 mM and 1 M KGlu.

4.11 Thermodynamic interpretation of the formation of the clamp assembly

The FCS measurements and UV-Vis study both showed that the clamp rings are stacking up each other to form oligomers. However, a possible thermodynamic interpretation was required to support this phenomenon. A study by Sengupta et al. showed that replacing KCl with KGlu in *E. coli* cytoplasm stabilizes the protein folding and protein-nucleic acid complexes[34]. In their study, they quantified the protein stabilizing effect of KGlu on the

ribosomal protein domain NTL9 and compared its influence with other K^+ salts from the Hofmeister series. The stabilizing or destabilizing effect depends on the net accumulation or exclusion of the ions of the salt from the protein surface which is exposed or buried (for $2\beta \rightarrow \beta_2$) in the process. The accumulation or exclusion of solute ions depends on the binding affinity of the protein surface for water molecules and the solute molecules. If the binding affinity of the protein surface for the water molecules is larger than the solute molecules, then due to preferential interaction[72,73], solute molecules will be excluded from the surface. The exclusion of the solutes results in stabilizing the protein structure. We can interpret this effect using a three-component thermodynamic system[74], which consists of water, protein, and solute. After we added a certain amount of the solute to the protein in the water medium, it will either stabilize or destabilize the protein structure depending on the change in the free energy during this process. In our research, $2\beta \rightarrow \beta_2$ is not a favorable process in the water medium (standard free energy change $\Delta G_W^0 > 0$)However, when we added a certain amount of KGlu, FCS measurements showed that dimer rings stack upon each other and form a larger clamp assembly. This indicates that in KGlu the change in the standard free energy should be ($\Delta G_{Glu^-}^0 < 0$). Dr. Levitus constructed a thermodynamic cycle to explain this protein stabilization effect by interpreting the data we measured using the FCS technique. We can imagine that when protein goes from water to KGlu, the change in the free energy is determined by the relative affinity of these water-binding sites for water and Glu^-. Here, we explain the thermodynamic cycle of the hypothetical process to interpret our measured data. The clamp dimers do not form any assembly in water which indicates the change in the standard free energy $\Delta G_W^0 > 0$. Now, we may write an Equation from the thermodynamic cycle $\Delta G_{Glu^-}^0 = \Delta G_W^0 + \Delta G_2^0 -$

ΔG_1^0 where, ΔG_2^0 is the standard free energy change when clamp assembly goes from the water medium to Glu$^-$ and ΔG_1^0 is the standard free energy change when a single clamp dimer goes from the water medium to the Glu$^-$. Both ΔG_1^0 and ΔG_2^0 are positive. The oligomerization process can only be spontaneous when the standard free energy change $\Delta G_{Glu^-}^0 < 0$. This is possible only when $\Delta G_W^0 < \Delta G_1^0 - \Delta G_2^0$ as $\Delta G_W^0 > 0$.

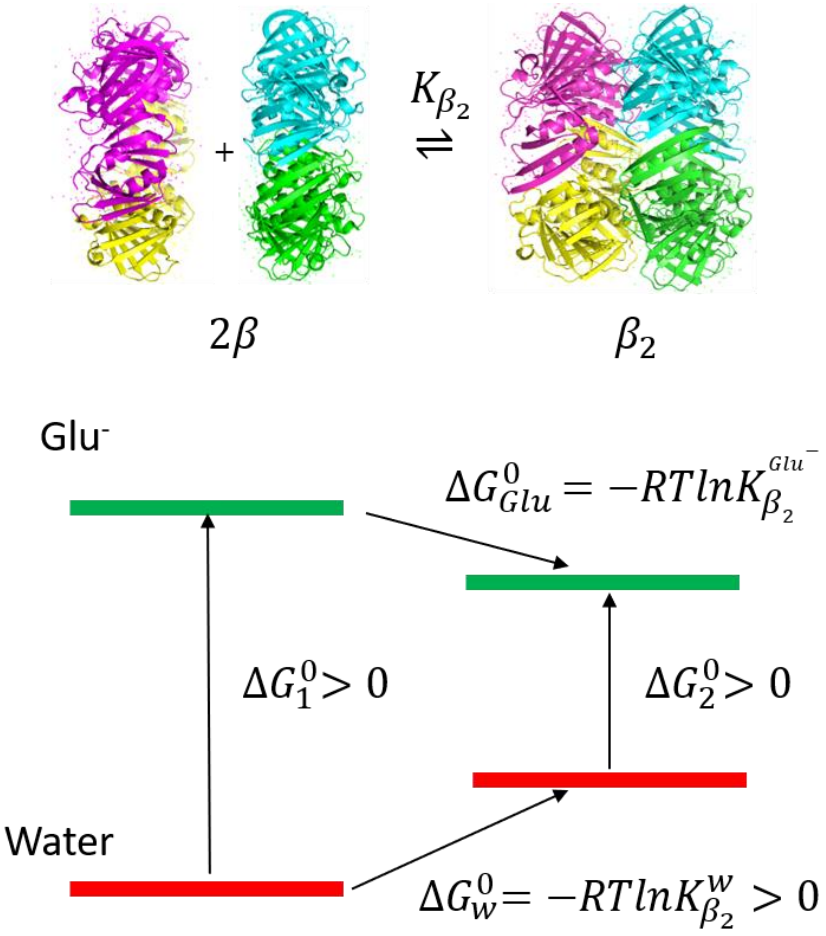

Figure 4.11 Thermodynamic cycle for KGlu induced clamp assembly formation. The vertical lines represent standard free energy changes when two β dimers (ΔG_1^0) and the β_2 dimer (ΔG_2^0) are hypothetically transferred from the water medium to the glutamate solution. ΔG_w^0 and $\Delta G_{Glu^-}^0$ are the standard free energy change for the association of two clamps in water and the presence of Glu$^-$, respectively. $K_{\beta_2}^w$ and $K_{\beta_2}^{Glu^-}$ are the thermodynamic equilibrium constants for the formation of the dimer: $2\beta \rightleftharpoons \beta_2$

However, Cheng *et al.* studied that the exclusion of the solute from the protein surface depends on the interaction with six functional groups[74], which are Sp^3, Sp^2, amide O, carboxylate O, amide N, and cationic N. It is also reported that aliphatic Sp^3 C and aromatic Sp^2C consist ~80% and amide O and N consist ~20% of the total protein surface[27]. It has been found that KGlu interacts unfavorably with the first four functional groups and interacts favorably with the last two groups, as shown in the (Figure 4.12).

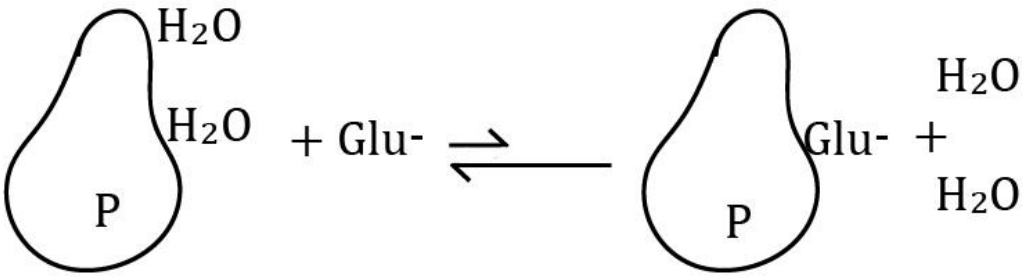

A

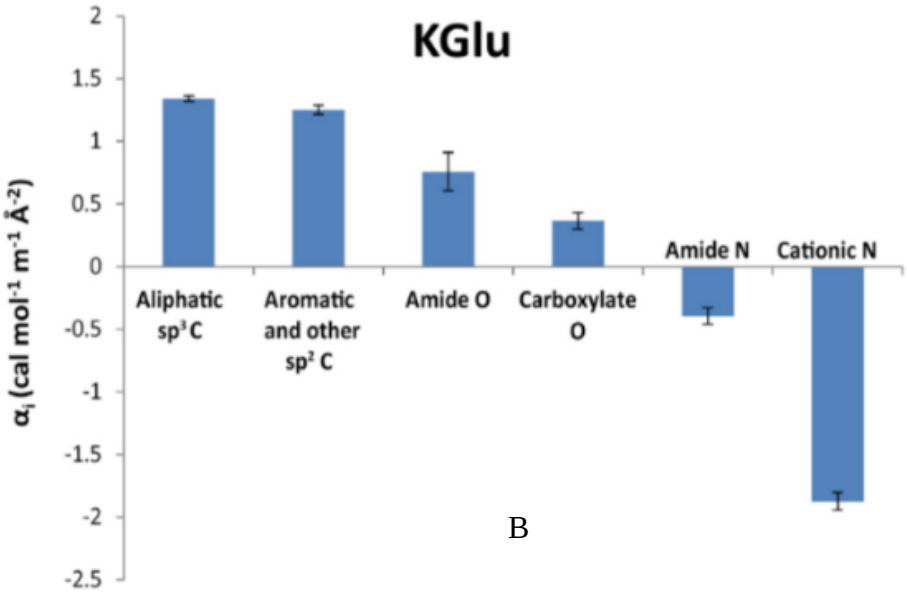

B

Figure 4.12 (A) The preferential interaction is a competition between water and solute ions, which decides the exclusion or accumulation of solute ions on the protein surface. (B) Interactions potentials (α) quantify the KGlu effect on the unit area of each functional group present on the surface of a protein. The positive value of α indicates unfavorable interactions (from **ref 64**)

But the overall interaction is unfavorable, and that's why KGlu is excluded from the protein surface[75]. In their study, they determined the interaction potentials per *ASA* (α_i) for each functional group and ΔASA_i (the change in accessible surface area of each functional group during clamp oligomerization). During the formation of clamp assembly, a fraction of water accessible surface area gets buried or obstructed between two clamp dimers, which also helps in the unfavorable interaction of KGlu. The net change in the standard free energy for this clamp assembly becomes negative. The equilibrium association constant (K_{β_2}) is determined quantitatively using the amount of ΔASA buried during the clamp association. The exclusion effect has been observed in other chemical agents as well, such as Proline and glycine Betaine. This suggests that besides KGlu, there are other salts that might have a similar effect on clamp protein. On the other hand, we thought we should investigate the KGlu effect on another protein called PCNA, a homotrimer found in eukaryotic cells. We were interested in this protein because we already had this in our lab received from Dr. Bloom's lab (our collaborator) at the University of Florida.

4.12 Calculation of equilibrium association constant (K_{β_2})

The thermodynamic interpretation of the process of the clamp assembly formation gives us an idea about the molecular mechanism of how KGlu interacts unfavorably with the clamp protein surface. However, the calculations of K_{β_2} were essential to get an idea of how the K_{β_2} values increase with KGlu concentrations (50 mM – 1 M). We used an algorithm[46] developed in our lab by David Kanno and Dr. Levitus in 2014 to calculate the K_{β_2} Values that we already explained in detail in chapter 2. The change in the standard free energy $\Delta G^0_{Glu^-}$ is calculated from the Equation $\Delta G^0_{Glu^-} = -RT\ lnK_{\beta_2}$ and plotted against

the KGlu concentrations in the molal unit. In the previous study by Sengupta *et al.,* they calculated *m* value for different Hofmeister salts. The *m* value determines how the unfolding equilibrium constant changes with salt concentration. The slope of the plot $-RT\ lnK_{\beta_2}$ vs. [KGlu] gives the value of *m* (Fig.). The experimental value we measured for *m* is – 5.1 ± 0.7 kcal mol^{-1} m^{-1}.

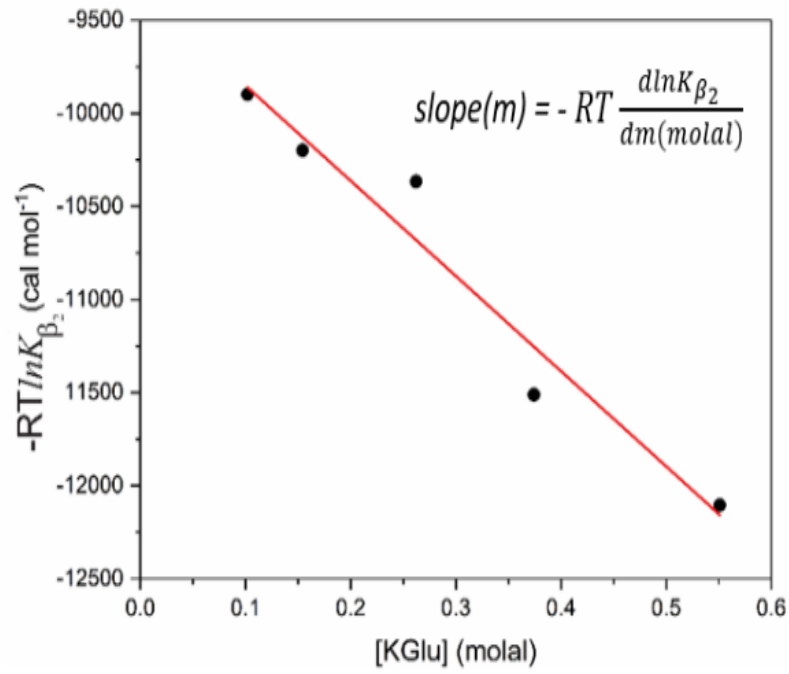

Figure 4.13 Determination of the *m*-value from the slope of the plot $-RTlnK_{\beta_2}$ vs. [KGlu] for clamp association. The standard free energy change for the association of two clamps, determined as $-RTlnK_{\beta_2}$, where T = 293 K and K_{β_2} is the equilibrium constant determined using the mathematical treatment developed by Dr.Levitus(2014)

4.12 Computational data supports the thermodynamic interpretation

As we discussed earlier that the unfavorable interaction of KGlu with the protein surface results in the exclusion of the Glu^- ions from water binding sites. The clamp dimers come close to each other and form a clamp assembly. The surface area buried during this process contributes to the *m* value we measured experimentally. The mathematical relation between

the m value and ΔASA is $m = \sum_i \alpha_i \Delta ASA_i \sim \alpha_{avg}\, \Delta ASA$ where α_i is the interaction potential for each functional group per unit of ΔASA and ΔASA is the total surface area buried during the oligomerization process[76]. In a previous study by Cheng *et al.* they calculated α_i for six functional groups for KGlu. The fact is that approximately 80% of the surface of native proteins have aliphatic carbon (α_i = 1.34 cal mol^{-1} m^{-1}Å^{-2}) and aromatics carbon (α_i = 1.25 cal mol^{-1} m^{-1}Å^{-2}) and about 20% is amide oxygen (α_i = 0.76 cal mol^{-1} m^{-1}Å^{-2}) and nitrogen (α_i = -0.39 cal mol^{-1} m^{-1}Å^{-2}) with an O:N *ASA* ratio of approximately 2.4:12. However here for our calculation, we used the average value of all α_i values (α_{avg}), which is 1.2 cal mol^{-1} m^{-1}Å^{-2}. We chose to use α_{avg} for our calculations because it is not possible to calculate α_i atom by atom as we do not know the crystallographic structure of the clamp assembly. We decided to use a surface racer program to calculate the surface area buried during assembly formation. The *m* value we determined experimentally is – 5.1 ± 0.7 kcal mol^{-1} m^{-1}. Now, when we plugged in this value to the above Equation, we found the ΔASA value -4,250 ± 600 Å^2 (required to achieve the experimental *m* value). We used PyMol to create β_2 structures and calculated *ASA*s computationally, The β_2 structures were created from two β dimer rings (pdb id : 1MMI) overlapping with each other by displacing one of the dimers given distance (d) along the axis normal to the plane of the ring and then rotating one of the clamps 180°. We made sure that these structures are compatible with rhodamine dimerization. The UV-Vis measurements showed that the TMR dye is forming an H dimer. The condition for forming an H dimer is dye molecules need to come close to each other within a few Å distances[71,77], and the transition dipole moments should be parallel to each other. The ΔASA values were calculated in surface racer program as

$\Delta ASA = ASA_{\beta_2} - 2ASA_{\beta}$. For displacements of d=34 Å, d=33 Å, and d=32 Å, the ΔASA values are -3230 Å^2, -4052 Å^2, and -4850 Å^2. These values are consistent with the experimentally measured ΔASA, which is -4,250 ± 600 Å^2. This indicates that the net unfavorable interaction of KGlu with functional groups on the protein surface is the driving force for the clamp oligomerization.

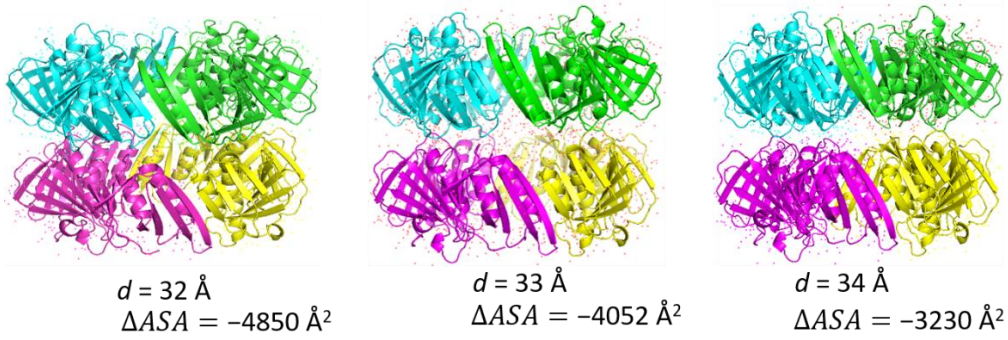

Figure 4.14 The structures of β_2 made in PyMol and change in accessible surface area were calculated using surface racer program.

4.13 KGlu effect on PCNA oligomerization

We observed the unfavorable interactions of KGlu with β clamp protein, which promotes the clamp oligomerization. We also investigated the effect of KGlu on PCNA, a homotrimeric clamp from yeast cell. The FCS measurements were performed with 1 nM PCNA I181C-TMR in different KGlu concentrations (50 mM – 1 M). We observed that just like β clamp, KGlu also promotes the formation of PCNA assemblies with increasing protein concentrations. The equilibrium association constant increases with increasing KGlu concentrations. However, we did not see any change in the 520 nm peak in UV-Vis measurements for 1 μM labeled PCNA in 50 mM – 1 M KGlu. This observation makes sense because PCNA is a homotrimer, so it is even more complex to form an H dimer. The condition for creating an H dimer needs specific geometrical requirements.

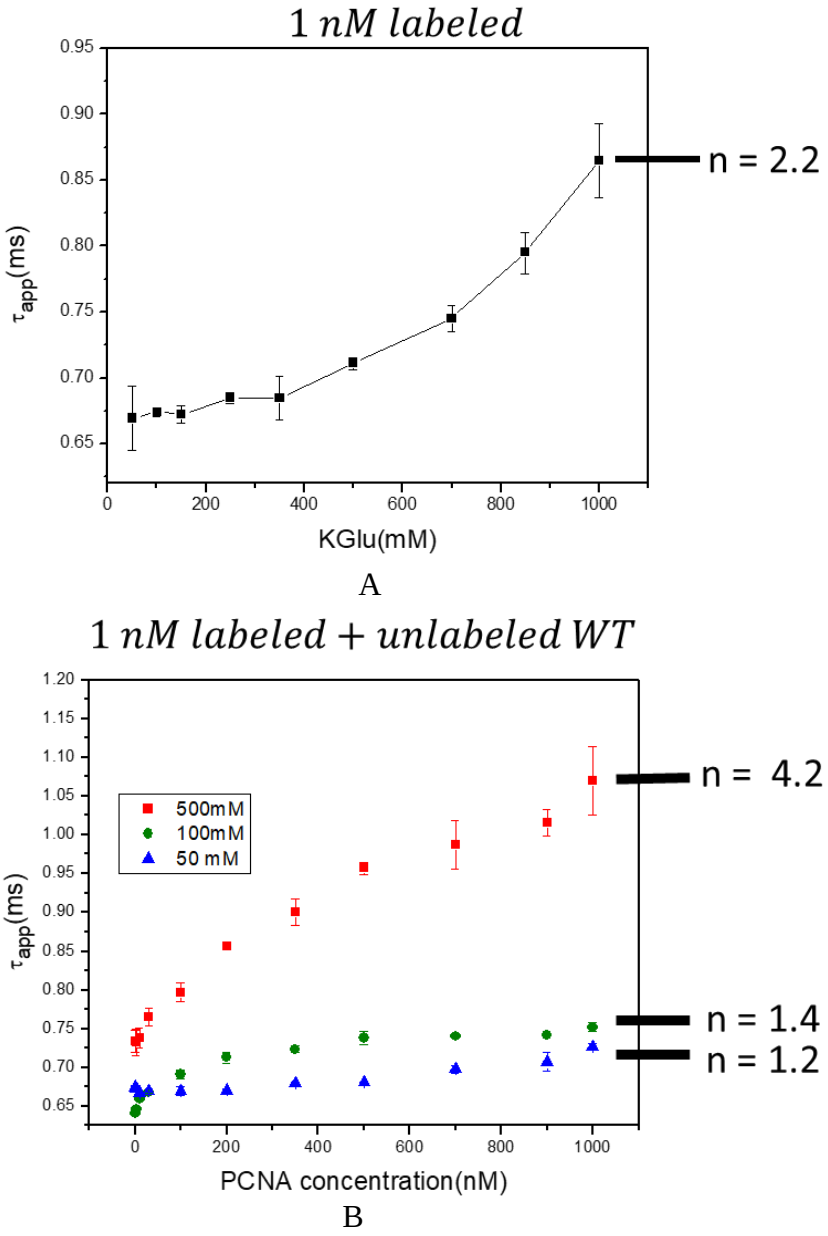

Figure 4.15 (A) Apparent diffusion times (τ_{app}) obtained from the FCS decays measured with 1 nM solutions of PCNA -I181C-TMR in an assay buffer containing 20 mM Tris-HCl pH 7.2 and [KGlu] varies from 50 mM-1 M. The n value denotes the number of protein trimers present in the assembly (B)Apparent diffusion times were measured with 1 nM -1 μM total protein concentration keeping labeled PCNA-I181C-TMR concentration at 1 nM. Unlabeled WT protein was added to achieve the final concentrations. The buffer condition is 20 mM Tris-HCl pH 7.2.

4.14 UV-Vis measurements with PCNA I181C

After we observed that, the apparent diffusion time (τ_{app}) for the PCNA sample increases with KGlu concentrations (50 mM – 1 M), we thought to investigate the KGlu effect using the UV-Vis instrument. We fixed the PCNA labeled protein concentration in the cuvette at 1 µM and kept adding KGlu from 50 mM – 1 M. As we explained earlier, with β clamp, we noticed that 520 nm peak intensity increases with KGlu concentration (> 250 mM). However, with the PCNA sample, we did not see any change in the 520 nm peak intensity with increasing KGlu concentration. In the FCS study it was clear that PCNA is forming larger assembly with higher KGlu concentrations as apparent diffusion time (τ_{app}) increases. Hence, it could be possible that the geometric requirements for forming an H dimer did not fulfill in case of PCNA oligomerization. This is also supported by the fact that PCNA is a homotrimeric clamp, so it might be more complicated for two TMR dyes to come close to each other to form an H dimer comparing to the β clamp assembly. However, it can also be possible that the mode of interactions might be different for PCNA.

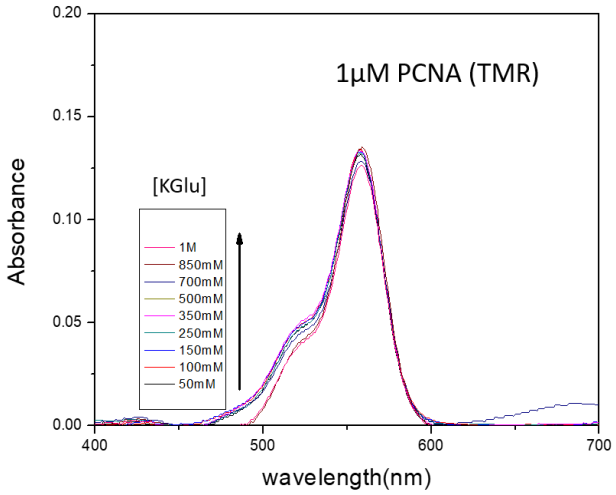

Figure 4.16 UV-Vis measurements of 1 µM PCNA-I181C-TMR in Tris-HCl buffer with 50 mM-1 M KGlu in the cuvette.

4.15 Clamp association is not specific to Glu^{-}

We discussed earlier that cheng et al. studied that besides KGlu, there are other metabolites (proline, glycine betaine) present in the *E. coli,* which shows unfavorable interactions with the protein as well. We calculated the average interaction potential per unit area of *ASA* for GB (glycine betaine), which is 0.5 cal mol^{-1} m^{-1}Å^{-2}. The differences between KGlu and GB interactions are GB interacts with aromatic hydrocarbons favorably, and it interacts with aliphatics carbon less unfavorably. As we explained earlier, that protein surface has ~80% aliphatic and aromatic carbon, GB shows overall less unfavorable interactions comparing to KGlu. We performed FCS experiments with 1 nM β-I305C-TMR in different GB concentrations (50 mM – 1 M). We observed an increase in the apparent diffusion time from low to high GB. However, if we take a look at *n* values mentioned in the plots, it is to be noticed that *n* values measured for GB are less than what we measured with KGlu. This supports the fact since GB interacts less unfavorably with the protein surface, its ability to induce clamp assembly formation is less than that of KGlu.

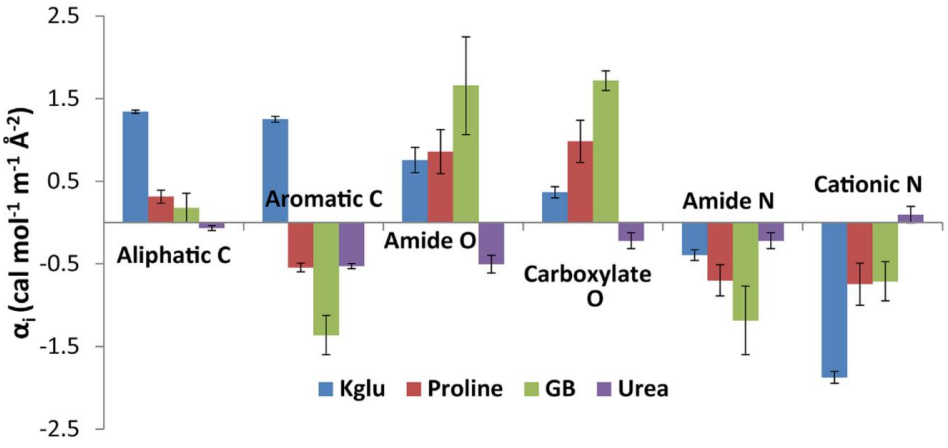

Figure 4.17 Interactions potentials(α) of different salts quantify the salt specific effect on unit area of each functional group present on the surface of a protein. The positive value of α indicates unfavorable interactions.

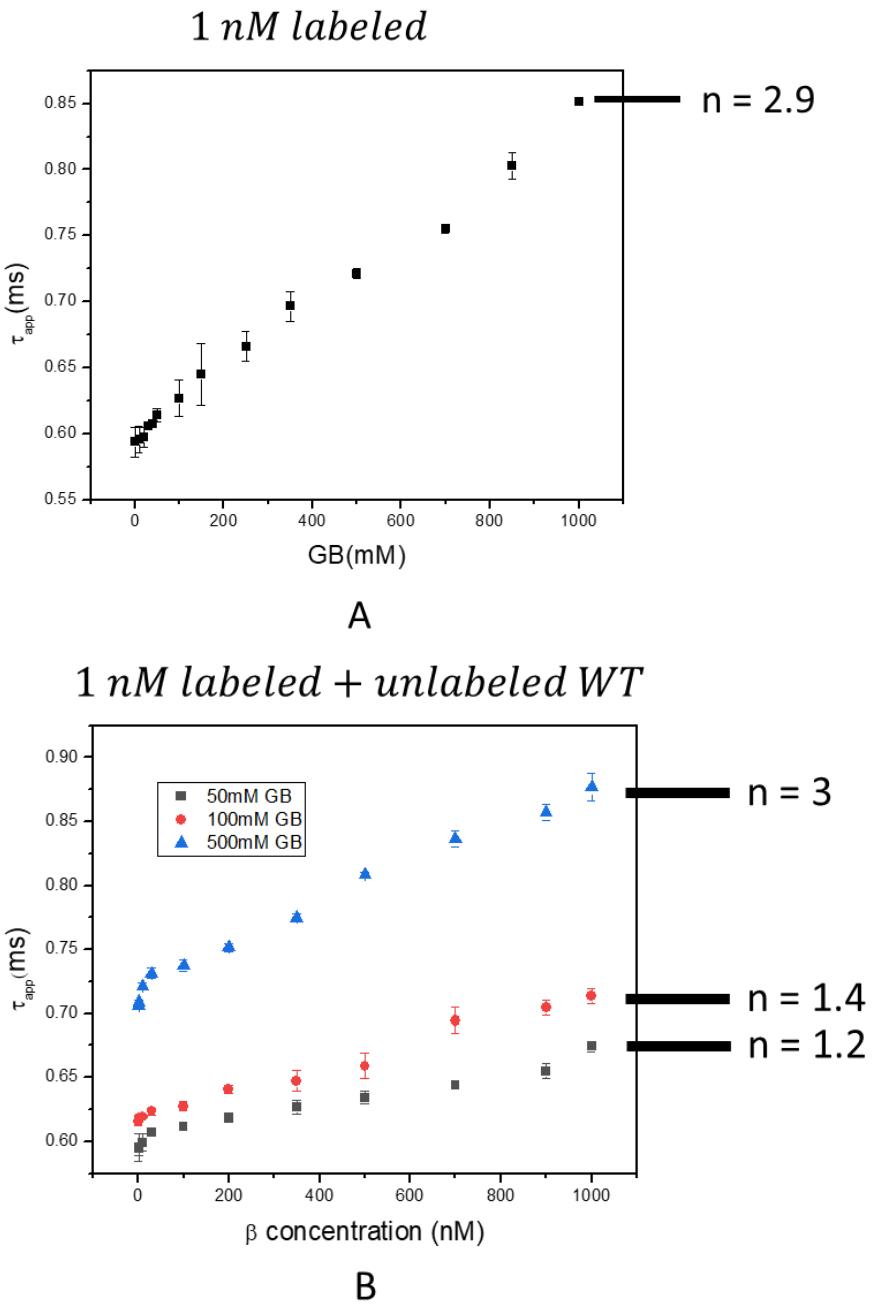

Figure 4.18 (A) Apparent diffusion times (τ_{app}) obtained from the FCS decays measured with 1 nM solutions of β-I305C-TMR in an assay buffer containing 20 mM Tris-HCl pH 7.2 and [GB] varies from 50mM-1M. The *n* value denotes the number of protein dimers present in the assembly (B)Apparent diffusion times were measured with 1 nM -1 μM total protein concentration keeping labeled β-I305C-TMR concentration at 1 nM. Unlabeled WT protein was added to achieve the final concentrations. The buffer condition is 20 mM Tris-HCl pH 7.2.

4.16 UV-Vis measurements with β-I305C-TMR in Glycine Betaine

After we observed that, the apparent diffusion time (τ_{app}) for the β-I305C-TMR sample increases with GB concentrations (50 mM – 1 M), we also used UV-Vis measurements to investigate GB effect on clamp assembly formation. We fixed the β-I305C-TMR labeled protein concentration in the cuvette at 0.5 µM and kept adding GB from 50 mM – 1 M. We noticed that 520 nm peak intensity increases with GB concentration (> 500 mM). However, with KGlu, we noticed an increase in 520 nm peak from 250 mM. The calculated *n* values for FCS experiments also indicate that KGlu induces the formation of clamp assembly more than GB.

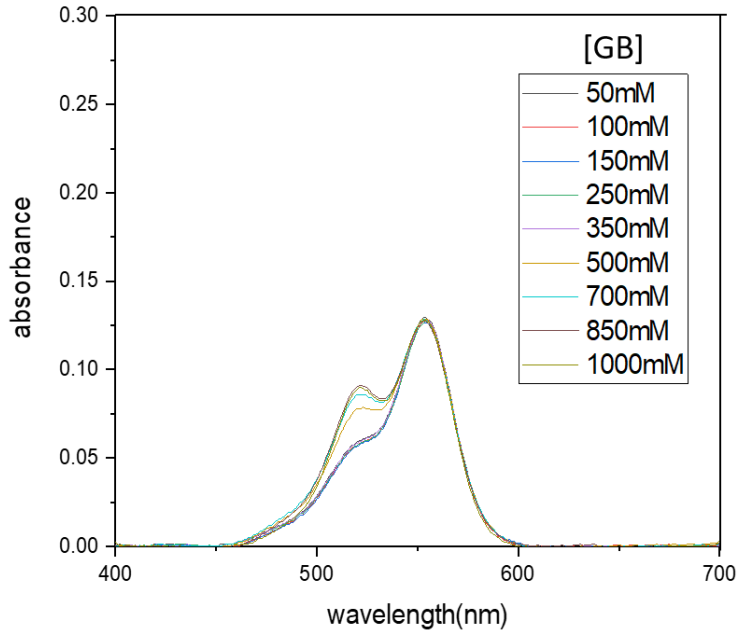

Figure 4.19 UV-Vis measurements of 0.5 µM β-I305C-TMR in Tris-HCl buffer with 50 mM-1 M GB in the cuvette

4.17 The biological significance of the clamp assembly formation

In this research, we characterized the effect of KGlu and glycine betaine on clamp stability and association. However, we had no idea about its biological significance. Dr. Linda

Bloom (our collaborator), at the University of Florida, helped us with figuring out the possible biological relevance of our observations with KGlu and glycine Betaine. It is previously reported that the concentration of β clamp in the *E. coli* cytoplasm[78] is between 500-600 nM, assuming the average cell volume[79] 1 fl. At a normal condition (without stress) KGlu concentration inside the cell is 100 mM. Our data indicate that in 100 mM KGlu clamp would exist as a mixture of single dimers or as an assembly of two dimers. During stress, *E. coli* cell increases KGlu concentration up to 300 mM[80], and our observations indicate that high KGlu promotes to form a bigger clamp assembly. There is no previous study reported on clamp assembly formation in the *E. coli* cell. Dr. Bloom proposed the idea that it could be possible that the formation of clamp protein assembly reduces the concentration of available clamp for DNA metabolism. As a result, DNA replication slows down. If clamp assembly is made of two dimers stacking up on the top of each other in head to tail fashion, then the effective concentration gets reduced by a factor of two. The functional sites of the clamp are being obstructed due to this type of assembly formation as both clamp loader and DNA polymerase bind with the clamp protein at the same site of one of the faces[81,82]. However, if dimers come together in the tail to tail fashion, the functional sites in the head side will still be available for other proteins to bind. This clamp stacking does not affect the clamp function, but it still might be physically blocking the binding interactions. Hence, we can argue that both head to tail and tail to tail interactions would reduce the DNA metabolism during stress. Clamp oligomerization can also help to balance dimer dissociation-association in the cell. As we know that clamp dimer binds with DNA polymerase to increase the processivity of the DNA replication[83]. It might be possible that there are dissociation factors present in the cell which promote

dimer dissociation. In that case, the clamp oligomerization process will help monomers to come together again to form a dimer and initiate the DNA replication.

Chapter Five

Future Outlook

5.1 Introduction

In chapter four, we have demonstrated that high concentrations of KGlu and GB induce clamp assembly formation for both β clamp and PCNA. We also proposed a thermodynamic model to explain this phenomenon. We verified that the experimentally calculated buried surface area is consistent with the buried surface area calculated computationally. Hence, our thermodynamic model is reasonable. We explained the effect of KGlu and GB on protein stabilization in terms of the relative binding affinities of the protein surface for water and solute molecules. For clamp proteins, the net exclusion of both KGlu and GB from the protein surface is the driving force for protein oligomerization. These observations motivate us to explore this clamp assembly formation in the future in the presence of different salts and proteins.

5.2 Study with proteins which exclude surface area during the association

We can continue our research with GB to investigate its effect on PCNA clamp oligomerization. In future research, we can think of studying other proteins, which exclude a significant amount of the surface area during their oligomerization like β clamp and PCNA. It'll also be interesting to investigate if we can explain other protein systems using our proposed thermodynamic model. However, the mode of interactions might be different from β clamp and PCNA, and that will depend on protein structures and surface amino acid compositions.

5.3 Study with salts or small molecule preferentially excluded from the protein surface

In the future study, we can investigate the effect of KGlu and GB on the oligomerization of other proteins. However, there are different salts and small molecules placed in the Hofmeister series according to their ability to stabilize, fold, or assemble protein structures. We can also design various experiments to study the effect of those salts and small molecules that show a net stabilization on the protein structure. We came to know about a compound called tetra ethylene glycol from the literature[84] and planning to investigate its effect on clamp stability in future research.

5.4 Clamp loader activity in the presence of clamp assembly and ATP

The biochemical pathway of DNA replication shows that in the presence of ATP clamp loader undergoes certain structural changes which increase its affinity for the clamp protein. After that, the clamp loader binds with the clamp protein to open it up through one interface[4]. The binding site for the clamp loader on the surface of the clamp protein is accessible when the clamp is in dimeric form. We know from previous FCS experiments that multiple clamp dimers can form bigger clamp assembly at high KGlu concentration. Therefore, an important question raised here is a binding site for the clamp loader on the surface of the clamp protein still accessible when the clamp dimers form a clamp assembly? We can answer this question by monitoring the clamp opening in the presence of a clamp loader and ATP. If we observe that even at high KGlu concentrations, a clamp loader still manages to open a clamp protein in the presence of ATP, then we can conclude that the binding site of the clamp loader is always accessible even the clamps form assemblies.

REFERENCES

1 Jeruzalmi, D., O'Donnell, M. & Kuriyan, J. Clamp loaders and sliding clamps. *Current opinion in structural biology* **12**, 217-224 (2002).

2 Fang, J., Engen, J. R. & Beuning, P. J. Escherichia coli processivity clamp β from DNA polymerase III is dynamic in solution. *Biochemistry* **50**, 5958-5968 (2011).

3 Leu, F. P. & O'Donnell, M. J. J. o. b. c. Interplay of clamp loader subunits in opening the β sliding clamp of Escherichia coli DNA polymerase III holoenzyme. **276**, 47185-47194 (2001).

4 Kelch, B. A., Makino, D. L., O'Donnell, M. & Kuriyan, J. How a DNA polymerase clamp loader opens a sliding clamp. *Science* **334**, 1675-1680 (2011).

5 Kelch, B. A., Makino, D. L., O'Donnell, M. & Kuriyan, J. Clamp loader ATPases and the evolution of DNA replication machinery. *BMC biology* **10**, 34 (2012).

6 Bell, S. P. & Labib, K. Chromosome duplication in Saccharomyces cerevisiae. *Genetics* **203**, 1027-1067 (2016).

7 Kang, S., Kang, M.-S., Ryu, E. & Myung, K. Eukaryotic DNA replication: Orchestrated action of multi-subunit protein complexes. *Mutation Research/Fundamental and Molecular Mechanisms of Mutagenesis* **809**, 58-69 (2018).

8 Krishna, T. S., Kong, X.-P., Gary, S., Burgers, P. M. & Kuriyan, J. Crystal structure of the eukaryotic DNA polymerase processivity factor PCNA. *Cell* **79**, 1233-1243 (1994).

9 Yao, N. *et al.* Clamp loading, unloading and intrinsic stability of the PCNA, β and gp45 sliding clamps of human, *E. coli* and T4 replicases. **1**, 101-113 (1996).

10 Lee, K.-y., Fu, H., Aladjem, M. I. & Myung, K. ATAD5 regulates the lifespan of DNA replication factories by modulating PCNA level on the chromatin. *Journal of Cell Biology* **200**, 31-44 (2012).

11 Georgescu, R. *et al.* Structure of eukaryotic CMG helicase at a replication fork and implications to replisome architecture and origin initiation. *Proceedings of the National Academy of Sciences* **114**, E697-E706 (2017).

12 Shibahara, K.-i. & Stillman, B. Replication-dependent marking of DNA by PCNA facilitates CAF-1-coupled inheritance of chromatin. *Cell* **96**, 575-585 (1999).

13 Hayashi, A., Suenaga, N., Shiomi, Y. & Nishitani, H. in *Cell Cycle Control* 367-382 (Springer, 2014).

14 Yao, N. Y. & O'Donnell, M. in *The Eukaryotic Replisome: A Guide to Protein Structure and Function* 259-279 (Springer, 2012).

15 Bowman, G. D., O'Donnell, M. & Kuriyan, J. Structural analysis of a eukaryotic sliding DNA clamp–clamp loader complex. *Nature* **429**, 724 (2004).

16 Miyata, T. *et al.* Open clamp structure in the clamp-loading complex visualized by electron microscopic image analysis. *Proceedings of the National Academy of Sciences* **102**, 13795-13800 (2005).

17 Zhuang, Z., Yoder, B. L., Burgers, P. M. & Benkovic, S. J. The structure of a ring-opened proliferating cell nuclear antigen–replication factor C complex revealed by fluorescence energy transfer. *Proceedings of the National Academy of Sciences* **103**, 2546-2551 (2006).

18 Sakato, M., Zhou, Y. & Hingorani, M. M. ATP binding and hydrolysis-driven rate-determining events in the RFC-catalyzed PCNA clamp loading reaction. *Journal of molecular biology* **416**, 176-191 (2012).

19 Bellaoui, M. *et al.* Elg1 forms an alternative RFC complex important for DNA replication and genome integrity. *The EMBO journal* **22**, 4304-4313 (2003).

20 Bell, D. W. *et al.* Predisposition to cancer caused by genetic and functional defects of mammalian Atad5. *PLoS genetics* **7**, e1002245 (2011).

21 Kubota, T., Nishimura, K., Kanemaki, M. T. & Donaldson, A. D. The Elg1 replication factor C-like complex functions in PCNA unloading during DNA replication. *Molecular cell* **50**, 273-280 (2013).

22 Kubota, T., Katou, Y., Nakato, R., Shirahige, K. & Donaldson, A. D. Replication-coupled PCNA unloading by the Elg1 complex occurs genome-wide and requires Okazaki fragment ligation. *Cell reports* **12**, 774-787 (2015).

23 Lee, K.-y. *et al.* Human ELG1 regulates the level of ubiquitinated proliferating cell nuclear antigen (PCNA) through Its interactions with PCNA and USP1. *Journal of Biological Chemistry* **285**, 10362-10369 (2010).

24 Unk, I. *et al.* Human HLTF functions as a ubiquitin ligase for proliferating cell nuclear antigen polyubiquitination. *Proceedings of the National Academy of Sciences* **105**, 3768-3773 (2008).

25 Binder, J. K. *et al.* Intrinsic stability and oligomerization dynamics of DNA processivity clamps. *Nucleic acids research* **42**, 6476-6486 (2014).

26 Tyagarajan, K., Pretzer, E. & Wiktorowicz, J. E. J. E. Thiol-reactive dyes for fluorescence labeling of proteomic samples. **24**, 2348-2358 (2003).

27 Cheng, X. *et al.* Basis of protein stabilization by K glutamate: unfavorable interactions with carbon, oxygen groups. *Biophysical journal* **111**, 1854-1865 (2016).

28 Csonka, L. N. Physiological and genetic responses of bacteria to osmotic stress. *Microbiology and Molecular Biology Reviews* **53**, 121-147 (1989).

29 Wood, J. M. Osmosensing by bacteria: signals and membrane-based sensors. *Microbiol. Mol. Biol. Rev.* **63**, 230-262 (1999).

30 Wood, J. M. *et al.* Osmosensing and osmoregulatory compatible solute accumulation by bacteria. *Comparative Biochemistry and Physiology Part A: Molecular & Integrative Physiology* **130**, 437-460 (2001).

31 Cayley, S., Lewis, B. & Record, M. Origins of the osmoprotective properties of betaine and proline in Escherichia coli K-12. *Journal of bacteriology* **174**, 1586-1595 (1992).

32 Cayley, S. & Record, M. T. Roles of cytoplasmic osmolytes, water, and crowding in the response of Escherichia coli to osmotic stress: biophysical basis of osmoprotection by glycine betaine. *Biochemistry* **42**, 12596-12609 (2003).

33 Record Jr, M. T., Courtenay, E. S., Cayley, D. S. & Guttman, H. J. Responses of *E. coli* to osmotic stress: large changes in amounts of cytoplasmic solutes and water. *Trends in biochemical sciences* **23**, 143-148 (1998).

34 Sengupta, R. *et al.* Positioning the intracellular salt potassium glutamate in the Hofmeister series by chemical unfolding studies of NTL9. *Biochemistry* **55**, 2251-2259 (2016).

35 Lakowicz, J. R. *Principles of fluorescence spectroscopy*. (Second edition. New York : Kluwer Academic/Plenum, [1999] ©1999, 1999).

36 Becker, W., Bergmann, A., Wabnitz, H., Grosenick, D. & Liebert, A. in *Biomedical Topical Meeting.* PD9 (Optical Society of America).

37 Patting, M., Wahl, M., Kapusta, P. & Erdmann, R. in *Photon Counting Applications, Quantum Optics, and Quantum Cryptography*. 658307 (International Society for Optics and Photonics).

38 Brismar, H., Trepte, O. & Ulfhake, B. Spectra and fluorescence lifetimes of lissamine rhodamine, tetramethylrhodamine isothiocyanate, texas red, and cyanine

3.18 fluorophores: influences of some environmental factors recorded with a confocal laser scanning microscope. *Journal of Histochemistry & Cytochemistry* **43**, 699-707 (1995).

39 Fick, A. V. On liquid diffusion. *The London, Edinburgh, and Dublin Philosophical Magazine and Journal of Science* **10**, 30-39 (1855).

40 Miller, C. C. The Stokes-Einstein law for diffusion in solution. *Proceedings of the Royal Society of London. Series A, Containing Papers of a Mathematical and Physical Character* **106**, 724-749 (1924).

41 Pratt, S. M. & Scientific, T. Einstein's landmark paper–100 years on. (2006).

42 Paschall, C. O. *et al.* The Escherichia coli clamp loader can actively pry open the β-sliding clamp. *Journal of Biological Chemistry* **286**, 42704-42714 (2011).

43 Johanson, K., Haynes, T. & McHenry, C. Chemical characterization and purification of the beta subunit of the DNA polymerase III holoenzyme from an overproducing strain. *Journal of Biological Chemistry* **261**, 11460-11465 (1986).

44 Stennett, E. M., Ma, N., Van Der Vaart, A. & Levitus, M. Photophysical and dynamical properties of doubly linked Cy3–DNA constructs. *The Journal of Physical Chemistry B* **118**, 152-163 (2013).

45 Thompson, T. *et al.* in *Molecular and Cellular Biology of Prostate Cancer* 337-344 (Springer, 1991).

46 Kanno, D. M. & Levitus, M. Protein oligomerization equilibria and kinetics investigated by fluorescence correlation spectroscopy: a mathematical treatment. *The Journal of Physical Chemistry B* **118**, 12404-12415 (2014).

47 Niesen, F. H., Berglund, H. & Vedadi, M. The use of differential scanning fluorimetry to detect ligand interactions that promote protein stability. *Nature protocols* **2**, 2212 (2007).

48 Ericsson, U. B., Hallberg, B. M., DeTitta, G. T., Dekker, N. & Nordlund, P. Thermofluor-based high-throughput stability optimization of proteins for structural studies. *Analytical biochemistry* **357**, 289-298 (2006).

49 Kopec, J. & Schneider, G. Comparison of fluorescence and light scattering based methods to assess formation and stability of protein–protein complexes. *Journal of structural biology* **175**, 216-223 (2011).

50 Kong, X.-P., Onrust, R., O'Donnell, M. & Kuriyan, J. Three-dimensional structure of the β subunit of *E. coli* DNA polymerase III holoenzyme: a sliding DNA clamp. *Cell* **69**, 425-437 (1992).

51 Tainer, J. A., McCammon, J. A. & Ivanov, I. Recognition of the ring-opened state of proliferating cell nuclear antigen by replication factor C promotes eukaryotic clamp-loading. *Journal of the American Chemical Society* **132**, 7372-7378 (2010).

52 Hernando, J. *et al.* Excitonic behavior of rhodamine dimers: a single-molecule study. *The Journal of Physical Chemistry A* **107**, 43-52 (2003).

53 Griep, M. A. & McHenry, C. S. Dissociation of the DNA polymerase III holoenzyme beta 2 subunits is accompanied by conformational change at distal cysteines 333. *Journal of Biological Chemistry* **265**, 20356-20363 (1990).

54 Jergic, S. *et al.* A direct proofreader–clamp interaction stabilizes the Pol III replicase in the polymerization mode. *The EMBO journal* **32**, 1322-1333 (2013).

55 Kelch, B. A. The lord of the rings: Structure and mechanism of the sliding clamp loader. *Biopolymers* **105**, 532-546 (2016).

56 Tondnevis, F., Weiss, T. M., Matsui, T., Bloom, L. B. & McKenna, R. Solution structure of an "open" *E. coli* Pol III clamp loader sliding clamp complex. *Journal of structural biology* **194**, 272-281 (2016).

57 Kumar, S. & Nussinov, R. Close-range electrostatic interactions in proteins. *ChemBioChem* **3**, 604-617 (2002).

58 Sheinerman, F. B., Norel, R. & Honig, B. Electrostatic aspects of protein–protein interactions. *Current opinion in structural biology* **10**, 153-159 (2000).

59 Bosshard, H. R., Marti, D. N. & Jelesarov, I. Protein stabilization by salt bridges: concepts, experimental approaches and clarification of some misunderstandings. *Journal of Molecular Recognition* **17**, 1-16 (2004).

60 Hendsch, Z. S. & Tidor, B. Do salt bridges stabilize proteins? A continuum electrostatic analysis. *Protein Science* **3**, 211-226 (1994).

61 Debeye, P. & Hückel, E. The Theory of Electrolytes I. The Lowering of The Freezing Point and Related Occurrences. *Phys. Zeitschrift* **24**, 185-206 (1923).

62 de los Rios, M. A. & Plaxco, K. W. Apparent Debye− Huckel electrostatic effects in the folding of a simple, single domain protein. *Biochemistry* **44**, 1243-1250 (2005).

63 Pegram, L. M. *et al.* Why Hofmeister effects of many salts favor protein folding but not DNA helix formation. *Proceedings of the National Academy of Sciences* **107**, 7716-7721 (2010).

64 Cacace, M., Landau, E. & Ramsden, J. The Hofmeister series: salt and solvent effects on interfacial phenomena. *Quarterly reviews of biophysics* **30**, 241-277 (1997).

65 Lo Nostro, P. & Ninham, B. W. Hofmeister phenomena: an update on ion specificity in biology. *Chemical reviews* **112**, 2286-2322 (2012).

66 Zhang, Y. & Cremer, P. S. Interactions between macromolecules and ions: the Hofmeister series. *Current opinion in chemical biology* **10**, 658-663 (2006).

67 Bennett, B. D. *et al.* Absolute metabolite concentrations and implied enzyme active site occupancy in Escherichia coli. *Nature chemical biology* **5**, 593 (2009).

68 Purohit, A. *et al.* Electrostatic interactions at the dimer interface stabilize the *E. coli* β sliding clamp. *Biophysical journal* **113**, 794-804 (2017).

69 Leirmo, S., Harrison, C., Cayley, D. S., Burgess, R. R. & Record Jr, M. T. Replacement of potassium chloride by potassium glutamate dramatically enhances protein-DNA interactions in vitro. *Biochemistry* **26**, 2095-2101 (1987).

70 Serban, A. J., Breen, I. L., Bui, H. Q., Levitus, M. & Wachter, R. M. Assembly–disassembly is coupled to the ATPase cycle of tobacco Rubisco activase. *Journal of Biological Chemistry* **293**, 19451-19465 (2018).

71 Arbeloa, I. L. & Ojeda, P. R. Dimeric states of rhodamine B. *Chemical Physics Letters* **87**, 556-560 (1982).

72 Timasheff, S. N. The control of protein stability and association by weak interactions with water: how do solvents affect these processes? *Annual review of biophysics and biomolecular structure* **22**, 67-97 (1993).

73 Timasheff, S. N. Control of protein stability and reactions by weakly interacting cosolvents: the simplicity of the complicated. *Adv. Protein Chem* **51**, 355-432 (1998).

74 Record, M. T., Guinn, E., Pegram, L. & Capp, M. Introductory lecture: interpreting and predicting Hofmeister salt ion and solute effects on biopolymer and model processes using the solute partitioning model. *Faraday discussions* **160**, 9-44 (2013).

75 Knowles, D., LaCroix, A. S., Deines, N. F., Shkel, I. & Record, M. T. Separation of preferential interaction and excluded volume effects on DNA duplex and hairpin stability. *Proceedings of the National Academy of Sciences* **108**, 12699-12704 (2011).

76 Myers, J. K., Nick Pace, C. & Martin Scholtz, J. Denaturant m values and heat capacity changes: relation to changes in accessible surface areas of protein unfolding. *Protein Science* **4**, 2138-2148 (1995).

77 Donaphon, B., Bloom, L. B. & Levitus, M. Photophysical characterization of interchromophoric interactions between rhodamine dyes conjugated to proteins. *Methods and applications in fluorescence* **6**, 045004 (2018).

78 Kubitschek, H. & Friske, J. Determination of bacterial cell volume with the Coulter Counter. *Journal of bacteriology* **168**, 1466-1467 (1986).

79 Levin, P. A. & Angert, E. R. Small but mighty: cell size and bacteria. *Cold Spring Harbor perspectives in biology* **7**, a019216 (2015).

80 Roussel, G., Lindner, E. & White, S. H. ACCELERATED COMMUNICATION. *PROTEIN SCIENCE* **28**, 984-989 (2019).

81 Jeruzalmi, D. *et al.* Mechanism of processivity clamp opening by the delta subunit wrench of the clamp loader complex of *E. coli* DNA polymerase III. *Cell* **106**, 417-428 (2001).

82 Burgers, P., Kornberg, A. & Sakakibara, Y. The dnaN gene codes for the beta subunit of DNA polymerase III holoenzyme of Escherichia coli. *Proceedings of the National Academy of Sciences* **78**, 5391-5395 (1981).

83 Bruck, I. & O'Donnell, M. The ring-type polymerase sliding clamp family. *Genome biology* **2**, reviews3001. 3001 (2001).

84 Knowles, D., LaCroix, A. S., Deines, N. F., Shkel, I. & Record, M. T. J. P. o. t. N. A. o. S. Separation of preferential interaction and excluded volume effects on DNA duplex and hairpin stability. **108**, 12699-12704 (2011).

85 Schreiber, G. Kinetic studies of protein–protein interactions. *Current opinion in structural biology* **12**, 41-47 (2002).

86 Northrup, S. H. & Erickson, H. P. Kinetics of protein-protein association explained by Brownian dynamics computer simulation. *Proceedings of the National Academy of Sciences* **89**, 3338-3342 (1992).

APPENDIX A

SUPPLEMENTARY INFORMATION

Reproducibility of FCS data

Error bars in figure 3.2 of the manuscript were omitted for clarity. Here, we show the results of five individual experiments with β-I305C-TMR that were used to calculate the average shown in figure 3.2A. There are six data points for three salt conditions (50 mM, 200 mM and 550 mM).

Error bars represent the standard deviation of the mean τ_{app} values, calculated as $\frac{\sigma}{\sqrt{N}}$ where σ is the standard deviation of all repeats performed at a given salt concentration and N = 5 (or 6). The average standard deviation in the measured τ_{app} values (σ) was 0.012 ms.

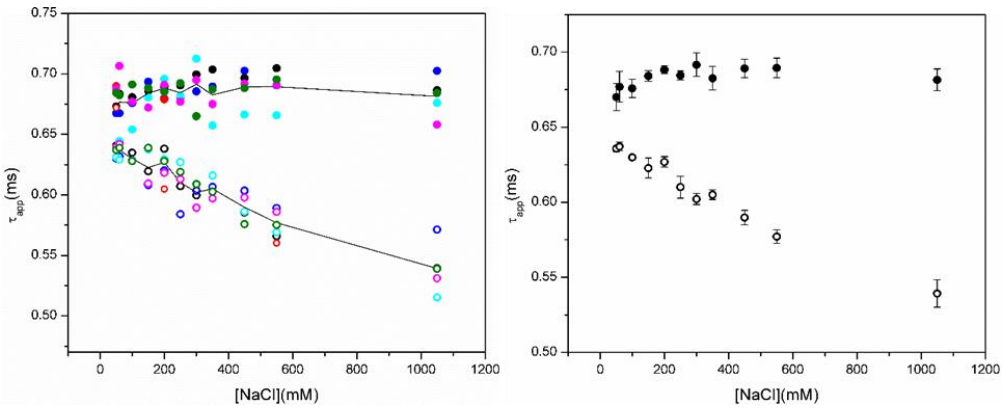

Figure S1 Apparent diffusion coefficients (τ_{app}) of 1 nM solutions of β-I305C-TMR in buffers of differing NaCl concentrations. Filled symbols are τ_{app} values measured at t = 0 (i.e. right after diluting a concentrated protein stock to 1 nM), and empty symbols are values measured after equilibrating the solutions for 24 hours. The left panel shows data for five independent trials with equal colors representing the same trial. The right panel shows the average of the five trials and error bars represent the error of the mean ($\sigma/\sqrt{N}$). Solid lines are the averages shown in Figure 3.2A in the manuscript. Assay buffer contained 20 mM Tris-HCl pH 7.5 and the indicated concentration of salt.

Stabilities of the β mutants used for kinetics of subunit exchange

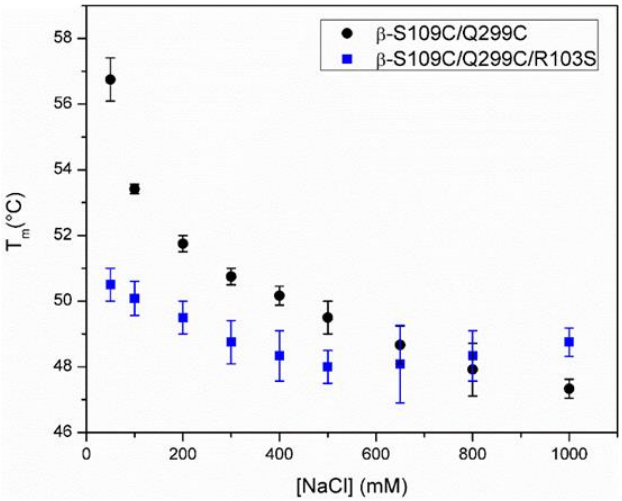

Figure S2 Stabilities of the β mutants used for kinetics of subunit exchange were measured by differential scanning fluorimetry using SYPRO orange as in Figure 3.3 in the main text. Protein concentrations were 0.2 mg/ml (2.5 μM) in 20 mM HEPES pH 7.5 with NaCl concentrations ranging from 50 to 1000 mM. Data points represent the average value of three independent experiments with standard deviation (error bars). The raw data used to obtain these T_m values is presented in Figure S3.

DSF data

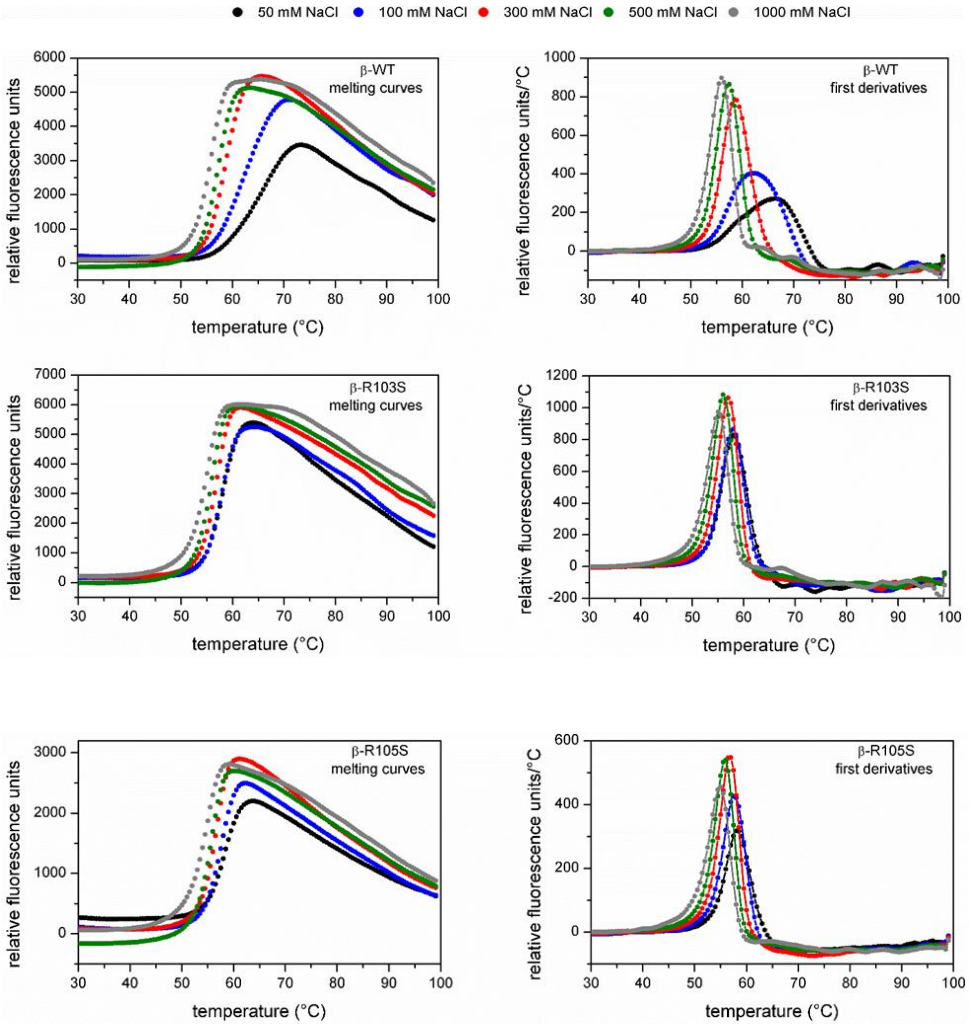
50 mM NaCl
100 mM NaCl
300 mM NaCl
500 mM NaCl
1000 mM NaCl
β-WT
melting curves
relative fluorescence units
temperature (°C)
β-WT
first derivatives
relative fluorescence units/°C
temperature (°C)
β-R103S
melting curves
relative fluorescence units
temperature (°C)
β-R103S
first derivatives
relative fluorescence units/°C
temperature (°C)
β-R105S
melting curves
relative fluorescence units
temperature (°C)
β-R105S
first derivatives
relative fluorescence units/°C
temperature (°C)

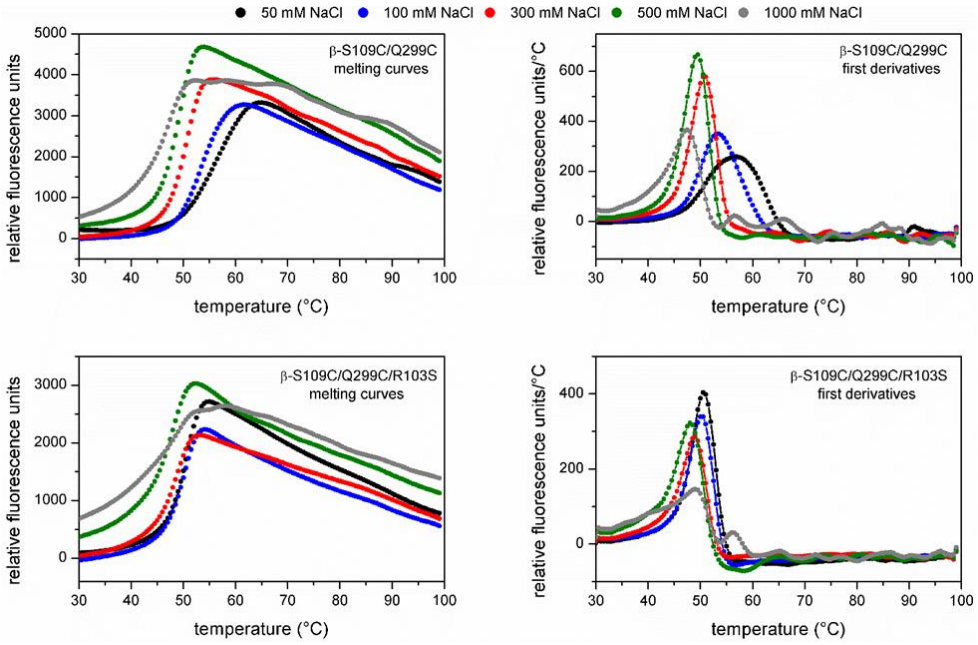

Figure S3 Melting curves (left panel) and first derivatives of these melting curves (right panel) are shown for DSF experiments corresponding to Figure 3.3 in the main text and Figure S2. For clarity, data are shown for five representative salt concentrations 50 mM (black), 100 mM (blue), 300 mM (red), 500 mM (green), and 1000 mM (grey) NaCl. Melting transitions for β proteins containing native Arg residues (β-WT and β - S109C/Q299C) at NaCl concentrations below 300 mM are not as sharp (broad first derivatives) as at high NaCl concentrations. In contrast, melting transitions for β proteins with Arg mutations are sharp at all NaCl concentrations.

Time-dependent dissociation of β-S109C-TMR at high salt and high pH

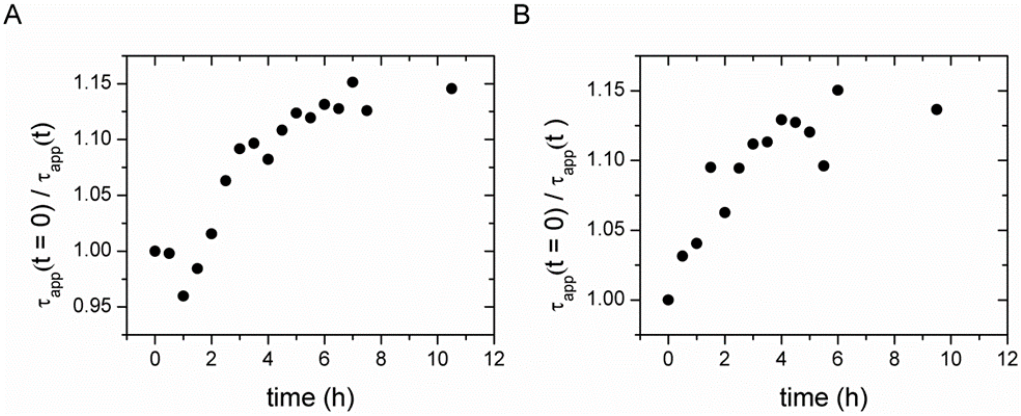

Figure S4 Comparison of the results of FCS experiments performed with β-S109C-TMR in (A) 20 mM Tris buffer pH = 7.5, 1 M NaCl and (B) 20 mM borate buffer buffer pH = 10, 0.05 M NaCl.

Solutions were prepared by diluting concentrated β-S109C-TMR stocks to a final concentration of 1 nM (t = 0), and FCS decays were measured at regular intervals over a *ca* 10 h period. Apparent diffusion times (τ_{app}) were obtained from the analysis of the autocorrelation functions as described in Materials and Methods. These plots show the ratio of the β_{app} values measured immediately after dilution and at an incubation time t .

Results show that the extent of dissociation (given by the τ_{app} (t = 0)/ (τ_{app} (t)) ratio at long times) and the kinetics of dissociation are similar in the two conditions shown above.

Spectroscopic properties of labeled β-WT

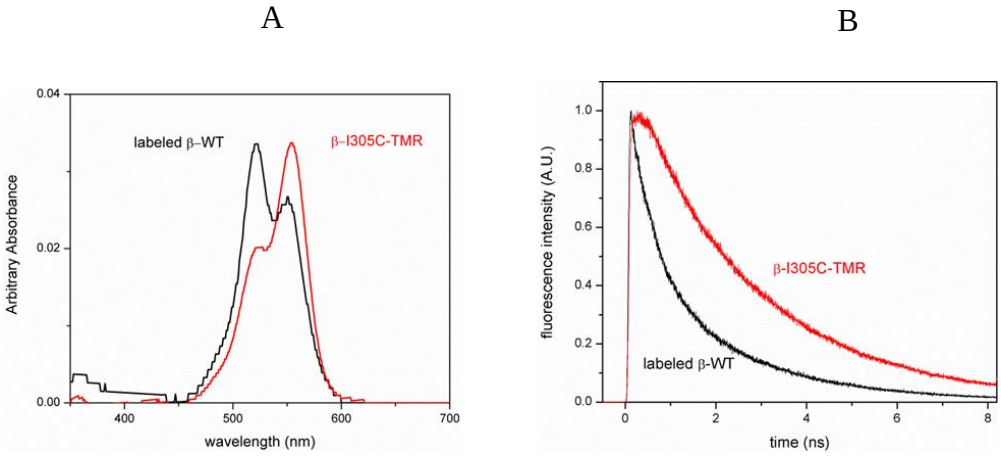

Figure S5 Spectroscopic properties of labeled β-WT (no mutations) showing clear characteristics of rhodamine dimers. Inspection of the crystallographic structure (Figure 3.1) and mutational analysis led us to conclude that cysteines C260 and C333, which are in close proximity in the folded protein, are efficiently labeled in this sample. The UV-VIS spectrum and fluorescence decay of β-I305C-TMR (which contains the background mutations C260S and C333S, see Table 1) is included for comparison.

(A) UV-Vis spectra were arbitrarily normalized to fit the same scale. The labeled β-WT samples shows an increase in the 520 nm band that is characteristic of rhodamine ground-state dimers. The spectrum of β- I305C-TMR is characteristic of monomeric rhodamine.

(B) Time-resolved fluorescence decays arbitrarily normalized to an amplitude of 1. The decay measured with β-I305C-TMR was published in our previous work.[1] The decay measured with labeled β-WT shows that fluorescence is greatly quenched. A fit to three exponentials gave τ_1 = 2.39 ns (30%), τ_2 = 0.56 ns (35%) and τ_3 = 0.098 ns (35%).

NaCl vs KCl

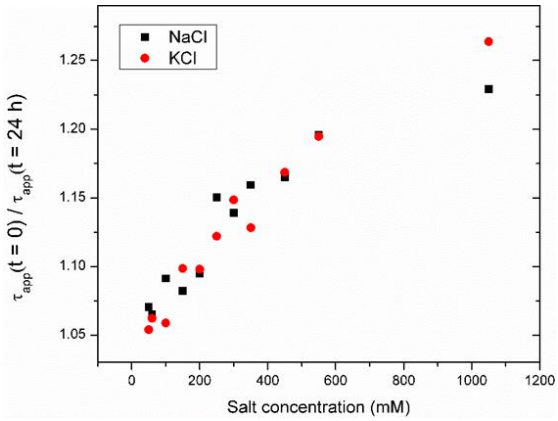

Figure S6 Comparison of the results of FCS experiments performed with β-I305C-TMR in 20 mM Tris buffer pH =7.5 with varying concentrations of NaCl (average of 5 repeats) or KCl (average of 3 repeats). The ratio of τ_{app} immediately after dilution (t = 0) and after equilibration for 24 hours (t = 24) is shown. The data for NaCl is the same as the data shown in Figure 3.2B in the manuscript. Results show that the extent of dissociation (given by the τ_{app} (t = 0)/ (τ_{app} (t = 24 h)) ratio) is the same for the two salts.

Theory of the Kinetics of Subunit Exchange:

In this section, we present a rigorous kinetic treatment to support our conclusion that the subunit exchange experiments presented in this manuscript are a direct measure of the dissociation rate constant of the β-dimer (k_d).

Let L_0 and U_0 be the initial concentrations of doubly-labeled and unlabeled protein dimers, respectively. Concentrations are expressed in terms of protein dimers, and L_0 and U_0 are both assumed to be much greater than the equilibrium dissociation constant (K_d) so that the concentration of monomers in equilibrium can be considered negligible. The equilibrium concentrations of doubly-labeled, singly-labeled, and unlabeled dimers are:

$$D_{LL}^{eq} = (L_0 + U_0) f_L^2 \quad \text{(S1)}$$

$$D_{LU}^{eq} = 2(L_0 + U_0)f_L(1 - f_L) \quad \text{(S2)}$$

$$D_{UU}^{eq} = (L_0 + U_0)(1 - f_L)^2 \quad \text{(S3)}$$

where f_L represents the fraction of labeled monomers and is given by $f_L = L_0 / (L_0 + U_0)$. The kinetic equations used to model the system are:

$$D_{LL} \rightleftarrows 2M_L$$

$$D_{LU} \rightleftarrows M_L + M_U$$

$$D_{UU} \rightleftarrows 2M_U$$

Where M_L and M_U represent the concentrations of labeled and unlabeled monomers, respectively. A discussion of the origin of the factor of 2 in the association reaction between labeled and unlabeled monomers is given at the end of this section.

The differential equations that describe the time-dependent concentrations of dimers and monomers are:

$$-\frac{dD_{LL}}{dt} = k_d D_{LL} - k_a M_L^2 \quad \text{(S4)}$$

$$-\frac{dD_{LU}(t)}{dt} = k_d D_{LU} - 2k_a M_L M_U \quad \text{(S5)}$$

$$-\frac{dD_{UU}}{dt} = k_d D_{UU} - k_a M_U^2 \quad \text{(S6)}$$

The equilibrium dissociation constant (K_d) relates the dissociation and association rate constants and the equilibrium concentrations of monomers and dimers:

$$K_d = \frac{k_a}{k_d} = \frac{(M_L + M_U)^2}{D_{UU} + D_{LL} + D_{LU}} \quad \text{(S7)}$$

The factor of two in Eq. S5 (whose origin is discussed in detail below) may seem counter-intuitive as it appears to contradict the fact that labeled and unlabeled monomers are assumed to have the same biochemical properties. However, we note that this factor of 2 is necessary for Eqs. S4-S6 to be consistent with equation S7. In equilibrium, $\frac{dD_{Total}}{dt} = \frac{dD_{UU}}{dt} + \frac{dD_{LL}}{dt} + \frac{dD_{LU}}{dt} = 0$, and the sum of eqs. S4-S6 would not be zero without the factor of two in Eq. S5.

In addition to the differential equations above, two algebraic equations relate the concentrations of labeled and unlabeled species due to mass conservation (recall that L_o and U_o are expressed in terms of protein dimers):

$$L_0 = D_{LL} + \frac{M_L}{2} + \frac{D_{LU}}{2} \quad \text{(S8)}$$

$$U_0 = D_{UU} + \frac{M_U}{2} + \frac{D_{LU}}{2} \quad \text{(S9)}$$

The system of equations S4-S6 and S8-S9 can be solved numerically using appropriate initial conditions:

$\mathcal{D}_{LL}(0) = \mathcal{L}_0$, $\mathcal{D}_{LL}(0) = \mathcal{U}_0$, $\mathcal{D}_{LL}(0) = \mathcal{M}_L(0) = \mathcal{M}_L(0) = 0$

Figure S3 contains the solution of this system of equations using the following inputs: K_d = 100 pM, ka = 5 *105 M-1 s-1, L_0 = 0.2 μM and U_0 = 1 μM. The dissociation constant is an upper limit of the value we reported in the previous work1 while the association rate constant is in the range of typical protein-protein association rate constants reported in the literature[85,86]. Results show that the system is expected to equilibrate over many hours, as we observed experimentally. Note that the

concentrations of monomers are negligible at all times because all concentrations are much greater than K_d. Of particular interest is the time-dependent behavior of D_{LL} (doubly-labeled dimers), which we measure as a quenched component in the fluorescence decay of the TMR probes. As shown in the right panel, the function $D_{LL}(d)$ obtained from solving the differential equations above (symbols) is indistinguishable from the exponential function defined in Eq. S10 (solid line)

$$y(t) = (L_0 - D_{LL}^{eq})e^{-k_d t} + D_{LL}^{eq} \quad \text{(S10)}$$

The equilibrium concentration of doubly-labeled dimers is given by equation S2. We note that although the amplitude and asymptote of this function depend on factors such as labeling efficiency that may vary among different protein preps, the exponential term depends only on the dissociation rate constant of the dimer.

In other words, the concentration of doubly-labeled dimers relaxes from its initial to its equilibrium value in an exponential fashion with a relaxation time $\tau = 1/k_d$, which in turn equals the intrinsic lifetime of the dimer. Therefore, we conclude that the subunit exchange experiments presented in this manuscript are a direct measure of k_d. As stated in the manuscript, this is true because the concentrations of dimeric protein are much greater than K_d, and therefore the rate at which two monomers associate to form a dimer is much greater than the rate at which a dimer dissociates to form two monomers. The concentrations of monomers are therefore negligible at all times, and the rate limiting step in subunit exchange reaction is the spontaneous dissociation of the protein dimer.

Numerical solution of the system of Equations S4-S6 and S8-S9 using K_d = 100 pM, k_a

$= 5 * 10^5\ M^{-1}\ s^{-1}$, $L_0 = 0.2\ \mu M$ and $U_0 = 1\ \mu M$. Left: Concentrations of all species in solution. The concentrations of monomers are negligible at all times. Right: Concentration of doubly-labeled dimer (D_{LL}). Disks are the results of the simulation, and the solid line is the function defined in Eq. S10 (not a fit). This shows that the time-dependent behavior of D_{LL} is well-described by Eq. S10, or in other words, decays exponentially with a relaxation time that equals $1/k_d$

As mentioned above, the factor of 2 in Eq. S5 may be counter-intuitive because it seems to contradict the fact that labeled and unlabeled monomers are assumed to have the same biochemical properties. Before, we presented mathematical arguments that support the need for this factor in Eq. S5. We now discuss physical arguments to explain its origin.

The rate of association between two protein monomers is proportional to the number of monomer- monomer encounters per unit time. Consider a sample containing equal amounts of monomers of type A and type B. A and B are biochemically identical except for a label that makes them experimentally distinguishable. Counting relative frequencies of forming A-A, B-B, A-B and B-A dimers is analogous to classical problems of drawing balls from urns in probability theory. The probability that a monomer A encounters another monomer of A to form an A-A dimer is the same as the probability that a monomer of B encounters another monomer of B to form a B-B dimer. The probability that a mixed A/B dimer is formed, however, is the probability of forming an A-B or a B-A dimer, which is twice the probability of forming an A-A or B-B dimer. In other words, the number of A/B encounters (A + B or B + A) per unit

time is twice the number of A + A encounters, which results in a factor of two in the association rate constant. This is analogous to the treatment of gas phase reactions in collision theory (which can be found in any introductory physical chemistry textbook), where a factor of ½ is included when considering like- molecules (A + A vs A +B) to avoid counting collisions twice. Mathematically, we can rewrite Eq. S5 distinguishing the cases A-B and B-A:

$$-\frac{dD_{AB}(t)}{dt} = k_d D_{AB} - k_a M_A M_B \quad \text{(S11)}$$

$$-\frac{dD_{BA}(t)}{dt} = k_d D_{BA} - k_a M_A M_B \quad \text{(S12)}$$

The association rate constants in these equations are the same as in the association reaction between two monomers of A and two monomers of B because A and B are biochemically indistinguishable.

The concentration of mixed dimers is $D_{\text{mixed}} = D_{AA} + D_{AA}$, and adding Eqs. S11 and S12, we obtain Eq. S13.

$$-\frac{dD_{mixed}(t)}{dt} = k_d D_{mixed} - 2\, k_a M_A M_B \quad \text{(S13)}$$

Calculation of K_d and error estimation

The data of Figure 3.6 in the manuscript was obtained using a formalism previously developed by Kanno and Levitus[46]. If the equilibrium between dimers and monomers is described by a single dissociation constant K_d, this constant can be expressed in terms of the degree of dissociation ($\alpha = C_M/C_0$) and the total protein concentration (C_0, expressed in terms of monomers):

$$K_d = \frac{2\alpha^2 C_0}{1-\alpha} \quad \text{(S14)}$$

The measured apparent diffusion time (τ_{app}) can be expressed as:[4]

$$\tau_{app}^2 - [1 - 2\frac{\alpha}{1+(1-\alpha)f}](\tau_2 - \tau_1)\tau_{app} - \tau_1\tau_2 = 0 \quad \text{(S15)}$$

where $\tau_{1,2}$ are the diffusion times of the monomer and dimer, respectively, and f is the labeling efficiency.

Given the slow timescales for dissociation, it is reasonable to assume that τ_2 equals the apparent diffusion time measured immediately after dilution, τ_{app} (t = 0). Furthermore, our results suggest that can τ_2 be well approximated by $2^{-1/3}$, which gives

$$\tau_{app}^2 - [1 - 2\frac{\alpha}{1+(1-\alpha)f}](1 - 2^{-1/3})\tau_2\tau_{app} - 2^{-1/3}\tau_2^2 = 0 \quad \text{(S16)}$$

Eq. S16, therefore, allows the determination of the degree of dissociation (and therefore K_{eq}) from the experimentally determined τ_{app}. To estimate the uncertainty in the equilibrium constant, K_{eq} was treated as a function of the variables τ_{app} and τ_2, and ΔK_{eq} was computed as:

$$\Delta K_{eq} = [(\frac{\partial k_{eq}}{\partial \tau_{app}})^2(\Delta\tau_{app})^2 + (\frac{\partial k_{eq}}{\partial \tau_2})^2(\Delta\tau_2)^2]^{1/2} \quad \text{(S17)}$$

where $\Delta\tau_{app}$ and $\Delta\tau_2$ are the uncertainties in τ_{app} and τ_2, respectively. The error bars shown in Figure 3.6 were calculated as,

$$\Delta log K_{eq} = \frac{1}{ln10 K_{eq}}\Delta K_{eq} \quad \text{(S18)}$$

The data plotted in Figure 3.6 in the manuscript were obtained using the apparent diffusion values plotted in Figure 3.2A for β-I305C-TMR assuming f = 1. Error bars were computed, assuming that $\Delta\tau_2$ and $\Delta\tau_{app}$ are the standard deviations of the mean values obtained from the five measurements shown in figure S1. The value of f (labeling efficiency) affects the determination of K_{eq} (Eq. S15), but as shown in the figure below,

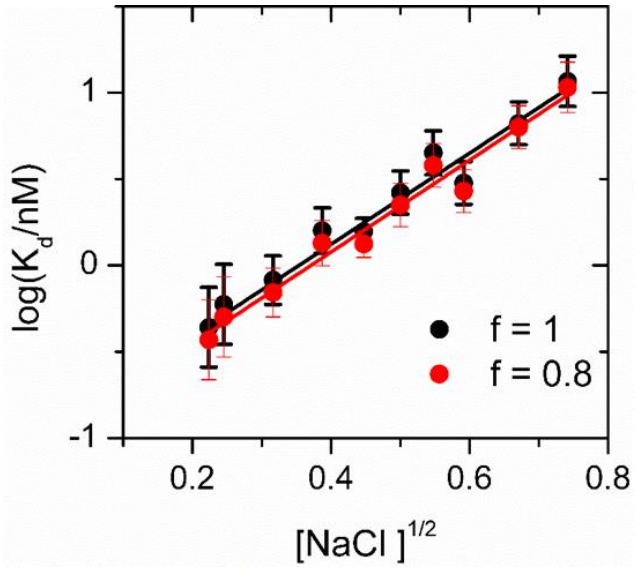

the effect in the data plotted in Figure 3.6 is negligible. Therefore, any uncertainties in our determinations of the labeling efficiency do not affect our conclusion.